Spring 2022

Corrosion protection mechanisms of trivalent chromium based passivations on γ-ZnNi coated Al6061-T6 alloy

Kevin Foster

CORROSION PROTECTION MECHANISMS OF TRIVALENT CHROMIUM BASED PASSIVATIONS ON γ-ZnNi COATED AL6061-T6 ALLOY

by

KEVIN LEE FOSTER

A DISSERTATION

Presented to the Graduate Faculty of the

MISSOURI UNIVERSITY OF SCIENCE AND TECHNOLOGY

In Partial Fulfillment of the Requirements for the Degree

DOCTOR OF PHILOSOPHY

in

METALLURGICAL ENGINEERING

2022

Approved by:

William G. Fahrenholtz, Advisor
Matthew O'Keefe
Michael S. Moats
Ronald J. O'Malley
Jay Switzer

PUBLICATION DISSERTATION OPTION

This dissertation consists of the following four articles, formatted in the style used by the Missouri University of Science and Technology:

Paper I, found on pages 21–51, has been published in *Thin Solid Films*.

Paper II, found on pages 52–81, has been published in *ACS Applied Materials and Interfaces.*

Paper III, found on pages 82–106, has been submitted to *Metallurgical Transactions A.*

Paper IV, found on pages 107-134, is intended for submission to *Materials Chemistry and Physics*.

ABSTRACT

The role of cobalt in trivalent chromium passivations (TCPs) to improve corrosion resistance of γ-ZnNi coated steel and aluminum is based on its effect on hexavalent chromium content in the passive layer. Investigations of both a cobalt-containing and cobalt-free TCP on SAE 1008 steel indicated that both passivations protect well for up to 1000 hours in neutral salt spray exposure (SSE). A repetition on Al 6061-T6 alloy indicated that TCP performed much better than cobalt-free TCP implicating the underlying substrate. Optical and electron micrographs indicated physical changes such as crack thickness, crack density, passivation porosity, and passivation thickness existed between the TCP and cobalt-free TCPs but had contradictory results on corrosion performance. Electrochemical differences between the TCPs on both substrates were consistent and scribed specimens on the Al 6061-T6 specimens showed active protection from TCP and not cobalt-free TCP indicating a chemical rather than physical difference. Confounding factors of electroless nickel (EN) between the substrate and γ-ZnNi coating and heat treatments led to Al 6061-T6 panels that were heat treated and steel panels with EN layers. The EN layer had no significant effect and heat treatments had inconsistent performance. Direct measurements of Cr(VI) content found some correlation between the amount of Cr(VI) and corrosion performance. XPS analysis of the surface Cr(VI) content revealed that Cr(VI) is needed for corrosion protection but that there must be an interaction with physical aspects of the coating to explain the inconsistent results. The TCPs were found to perform better because the divalent cobalt in TCPs facilitated production of Cr(VI) during corrosion.

ACKNOWLEDGMENTS

First, I would like to thank my advisors, Dr. William Fahrenholtz and Dr. Matthew O'Keefe for their guidance, patience, support, and understanding over the duration of the project. Both of them continuously pushed me to improve, reflect, and focus on the important aspects of the project.

I would like to thank Dr. Tarek Nahlawi and Mr. Felix Almodovar at Dipsol of America for their part creating the test specimens, discussing aspects of the research and papers, and welcoming me to their headquarters in Livonia, MI.

I would like to thank the other members of my committee: Dr. Michael Moats, Dr. Ronald O'Malley, and Dr. Jay Switzer for being available and willing to discuss any aspect of the project and to guide me to a better understanding of my research.

I would like to thank my wife, Margaret Foster, for tolerating the late nights and inconsistent hours, for continuously nudging and encouraging me to keep on going, and for always being there for me. I would also like to thank my parents, James and Karen Foster, as well as my sister, Jamie, for being flexible, understanding, and insisting that I put my research first while working around my schedule.

I would like to thank Mr. Steve Gaydos, Mr. Dave Zika, Dr. Wei-Ting Chen, Dr. Xiaoqing He, Dr. Eric Bohannan, Mr. Brian Porter, Mr. Fred Eickelmann, Dr. Clarissa Wisner, and my friends Mason Olson, Lance Little, Florian Verbruggen, and Jack Riley for their help and support over all this time. I would like to acknowledge that this project was funded by the Strategic Environmental Research and Development Program (SERDP) through contract WP18-F2-1439.

TABLE OF CONTENTS

Page

LIST OF ILLUSTRATIONS

SECTION Page

PAPER IV

LIST OF TABLES

1. INTRODUCTION

Trivalent chromium passivations (TCPs) have been proposed as environmentally friendly alternatives to chromate conversion coatings (CCCs) for corrosion protection dating back to the 1950s. However, only more recently with the passage of REACH legislation in the European Union and tightening restrictions by the EPA in the United States have TCPs been implemented as commercial alternatives. TCPs are used on aluminum and aluminum alloys such as Al 6061-T6, Al 7075-T6, and Al 2024-T3, but also on steel, galvanized steel, and zinc alloy coatings. Despite their increasing use, TCPs are not yet approved as CCC alternatives for all applications such as low electrical resistance passivating treatment for ZnNi alloy coated Al 6061 mil-spec electrical connectors.

One of the factors that hold back TCP approval for electrical connector applications are concerns that the TCPs will not be able to both mitigate corrosion and maintain low electrical contact resistance during environmental exposure. Passivating treatments on electrical connectors are evaluated by the United States Department of Defense per MIL-DTL-81706B that requires an initial resistance of <5 mΩ/cm^2 and a resistance of <10 mΩ/cm^2 after one week of salt spray exposure. The electrical contact resistance of TCPs has not been reported in the literature.

Another factor that delays wider implementation of TCPs is the inconsistency of the literature surrounding TCPs. Literature evaluation of TCPs is complicated by the different categories of TCPs that are present with passivating baths varying significantly in chemistry, precursor salts, and processing parameters leading to TCPs that can fall into

categories like thick or thin, porous or dense, post-treated or as-deposited. This is further complicated by several papers studying proprietary coatings where chemistry is undefined, evaluating corrosion performance using electrochemical means but no environmental exposure. Observations such as improved corrosion performance with cobalt additions to the passivating bath and limited active protection have been reported for TCPs, but the underlying mechanisms have not been explained. The wide range of variability reported for corrosion performance makes it difficult to predict how well a TCP formulation will perform on a particular substrate or as part of a specific coating system.

A lack of fundamental understanding of the corrosion protection mechanism of TCPs hinders widespread implementation as an alternative to CCCs. The general idea behind TCPs as CCC alternatives is that chromate-based coatings protect the substrate by reducing Cr(VI) to Cr(III) at active cathodic sites, which promotes deposition of an insoluble Cr(III) oxide that prevents corrosion activity. TCP deposition processes are designed to coat an insoluble Cr(III) oxide across the whole surface, thus precluding the need for hexavalent chromium to protect the surface. However, TCPs tend to be structurally amorphous, incorporate ions from the substrate during deposition, and also contain cobalt when it is present in the passivating bath, which indicate that TCPs are much more complex than just an insoluble Cr(III) oxide layer. While many studies show the clear benefit of cobalt additions, the mechanism by which it improves corrosion performance has not been determined. Additionally, other studies have detected hexavalent chromium in TCPs, implying that TCPs may protect because of the presence of hexavalent chromium.

To address the literature inconsistencies and to investigate the mechanism behind TCP corrosion protection, a cobalt-containing and a cobalt-free TCP were each investigated under different conditions to answer four research questions: What difference in corrosion performance does cobalt cause for TCPs on γ-ZnNi coated SAE 1008 steel? What difference in corrosion performance does cobalt cause for TCPs on γ-ZnNi coated Al 6061-T6 alloy? Does the corrosion performance of TCPs depend upon Cr(VI) in the passive layer or heat treatment of the passivation? Does placing an electroless nickel layer underneath the ZnNi coating affect the corrosion performance of TCPs on SAE 1008 steel? Answering these questions will determine if cobalt in the deposition bath results in deposition of chromates in the TCP layer or acts to promote oxidation of Cr(VI) in aqueous environment while also determining if there is any contribution to the literature inconsistencies caused by the substrate and not just the TCP coating.

2. LITERATURE REVIEW

2.1. SUBSTRATES AND ANTI-CORROSION PLATING

2.1.1. SAE 1008 Steel. Steel is produced in different alloyed forms to maximize or minimize a variety of material properties. Historically, the American Iron and Steel Institute (AISI) and Society of Automotive Engineers (now SAE International) developed standards for differentiating between different steel alloys. In 1995, AISI allowed SAE to take over future maintenance of the standards used to produce different steel grades leading to the specifications used today that classify different alloys using a designation of SAE XXXX where the X's are numbers that give information about the alloy[1]. The first number is the primary alloying element, the second denotes a sub-classification of the first number, and the last two represent carbon content in hundredths of a percent[2].

SAE 1008 steel is a low-carbon steel alloy commonly used in extruded, cold upset, and cold pressed parts. It has a chemical composition given in Table 2.1 that only restricts the amount of carbon, manganese, phosphorus, and sulfur in the steel. This alloy has seen widespread use in the automotive industry to produce structural components for decades. Automotive applications expose metals to natural corrosive environments and so SAE 1008 steel is commonly galvanized with sacrificial zinc or zinc-alloy plating to protect against corrosion.

2.1.2. Aluminum 6061-T6. Aluminum alloys are classified according to a system set up by the H35 committee of the American National Standards Institute (ANSI) and follows a 4 or 5-digit classification similar to the SAE steel grading system in the case of wrought alloys. For wrought aluminum, the first digit represents the major

alloying elements, the second represents variation on a particular alloy, and the last two digits identify the alloy within the series[3]. The alloy designations are typically followed with a temper designation that takes the form of a hyphen followed by a letter indicating the type of tempering, followed by numbers classifying processing within that temper category. The alloys are also limited to have no more elements than 15 wt% with the rest of the weight being aluminum.

6061 is one of the most common of magnesium and silicon alloys of aluminum that serves a general purpose role and has a chemical composition shown in Table 2.1. The alloy is easily machined, welded, and precipitation hardened which contributes to its widespread use. The degree of precipitation hardening is affected by the temper and the designation of -T6 represents a piece that was solution heat treated and artificially aged in order to achieve the greatest precipitation hardening. The alloy can have metal coatings applied to protect it from corrosion with several different types available such as cadmium, nickel, and zinc.

Table 2.1. Alloy chemical composition to meet standards for SAE 1008 and Al6061.

	Composition wt%										
Alloy	**C**	**Mn**	**P**	**S**	**Fe**	**Si**	**Cu**	**Mg**	**Cr**	**Zn**	**Other**
SAE1008	0.1	0.3-0.5	0.04	0.05	rem	-	-	-	-	-	-
Al6061	-	0.15	-	-	0.7	0.4-0.8	0.15-0.4	0.8-1.2	0.04-0.35	0.25	<0.15

2.1.3. Electroless Nickel Plating. First invented in 1946 by Brenner and Riddell, electroless plating allows deposition of many metals such as Ni, Co, Pd, Au, or Ag without an external electrical source[4]. The deposition is an autocatalytic process wherein

a substrate is dipped in a chemical bath with salts of the metal to be plated and a reductant that results in nucleation and growth of the plating on the substrate. This growth is then continued as the deposited metal catalyzes further deposition of the metal which results in a linear growth rate with time after a continuous film has covered the entire surface. This allows for precise control of the film thickness[5].

Nickel was the metal that led to the discovery and invention of electroless plating and was first plated as a Ni-P alloy on steel in a bath that contained hypophosphites. Since that time, many advancements have been made and now electroless deposition of nickel can occur on a variety of substrates including insulators, polymers, and metals with excellent control of a variety of properties such as hardness, density, conductivity, or corrosion resistance[6]. While many applications utilize control of the plating hardness or wear resistance, it can be used on aluminum 6061-T6 alloy to provide a strongly adhered surface that allows for electro-depositing of ZnNi coatings.

2.1.4. Cadmium and γ-ZnNi Coatings. Electroplated cadmium has many properties that lead to its widespread historical use such as its corrosion resistance (1000 hours until rust in ASTM B117), high electrical conductivity (1.46×10^7 S/m), lubricity (~0.5), hardness (~240, Knoop), and ability to be applied as a thin (< 25 μm) layer.[7–10] In the United States, cadmium was considered an anticipated human carcinogen since the 1980s and in 2000 the National Institutes of Health (NIH) declared cadmium a known human carcinogen while some studies associate cadmium with kidney damage and diabetes.[11–14] The toxic and carcinogenic nature of cadmium and its cyanide containing plating process has lead the United States and the European Union to pass regulations limiting the exposure of workers and wildlife to cadmium with a call for alternatives.[15–17]

Several commercially available alternatives to cadmium exist and include gold, tin, ZnCo, ZnFe, SnZn, and ZnNi. Gold plating has excellent corrosion resistance and conductivity, but suffers from a brittle phase that forms when plated on aluminum, high cost, and it is typically deposited with a cyanide containing electroplating bath.[18] Tin plating offers some corrosion resistance (24 hours to rust in 5% salt spray), excellent solderability, and is very cost-effective; however, issues have arisen with tin "whiskers" and the corrosion resistance is not as high as the zinc alloys.[19–21] ZnCo and ZnFe alloys with 10-20 wt% Co or ~0.75wt% Fe show good corrosion performance, lubricity, and low cost, but inconsistent corrosion performance at temperatures above 250 ºF remains an issue.[22–27] SnZn coatings with 20-30 wt% Zn have shown comparable corrosion resistance (400 hours to red rust in salt spray) and lubricity to cadmium coatings but have difficulty controlling Zn in plating baths to ensure consistent anti-corrosion performance.[28–30]

Electroplated ZnNi coatings have similar anti-corrosion and tribological properties to cadmium, exceeding cadmium performance in some cases.[30] The primary phase of interest is γ-ZnNi which lies between 14 and 23 wt% Ni on the binary phase diagram shown in Figure 2.1.[31] In electrodeposited ZnNi the phases follow a non-equilibrium progression where the γ-phase starts to form at Ni contents as low as 13 wt% and the δ-phase is never observed.[32] Many ZnNi coatings studied were in the range of 5-15 wt% Ni, which explains some variability in corrosion performance including 4 and 96 hours to 6 and 640 hours for white and red rust, respectively.[30, 33–36] The corrosion resistance maximum at around 13-15 wt% nickel was correlated with cracks in the ZnNi coating with coatings exhibiting small closely spaced cracks offering greater corrosion

resistance than wider cracks.[37] ZnNi coatings are typically passivated with a conversion coating after electroplating. The most commonly used passivation is a hexavalent chromium (chromate) layer that significantly improves corrosion protection.[38–40]

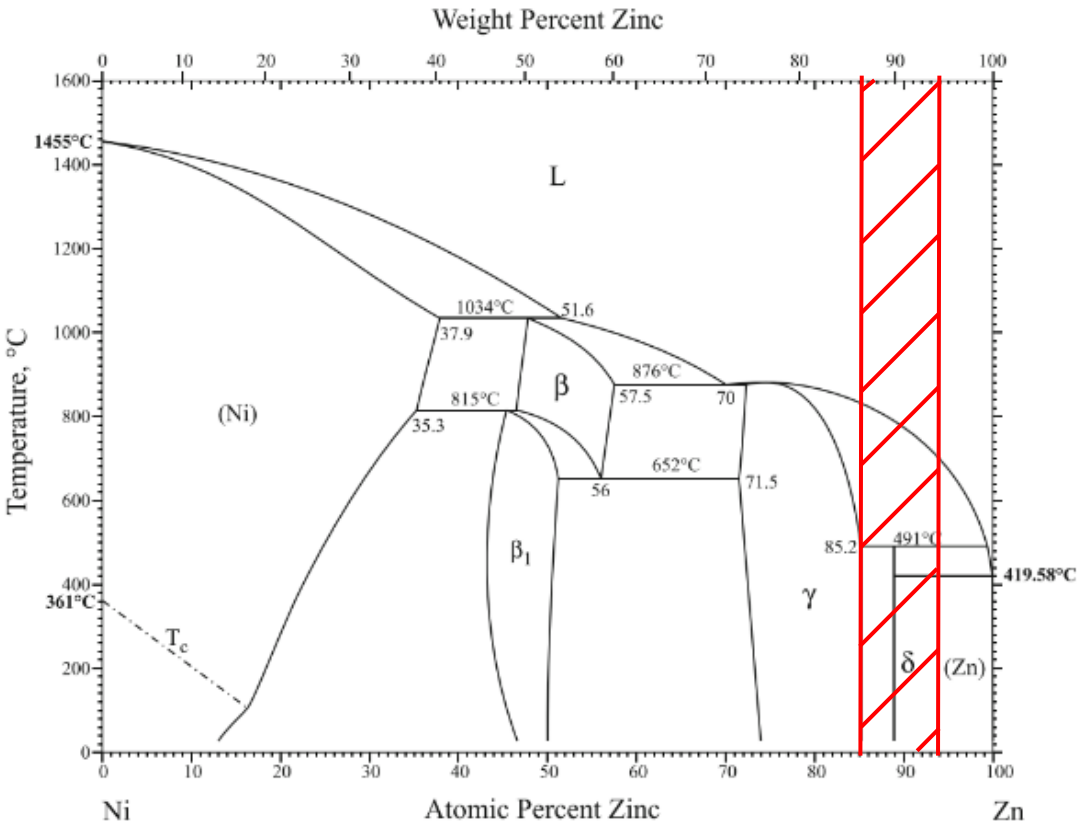

Figure 2.1. Binary phase diagram of the Nickel-Zinc system from H. Okamoto.31 Red patterned area represents typical commercial ZnNi coating composition (12-20%wt Ni).

2.2. HEXAVALENT CHROMATE PASSIVATIONS

Chromate conversion coatings (CCC) have been long used to passivate anti-corrosion coatings of many metallic materials, including cadmium and ZnNi.[7, 8, 40–42] Formation of a CCC on a given metallic (M) substrate is governed by five chemical reactions shown in equations 1 to 5:

$$M \rightarrow M^{2+} + 2e^{-} \quad (1)$$

$$2H^{+} + 2e^{-} \rightarrow H_2 \quad (2)$$

$$Cr^{6+} + 3e^{-} \rightarrow Cr^{3+} \quad (3)$$

$$M^{2+} + 2OH^{-} \rightarrow M(OH)_2 \quad (4)$$

$$2Cr(OH)_3 + CrO_4{}^{2-} + 2H^{+} \rightarrow Cr(OH)_3 \cdot CrOH \cdot CrO_4 + 2H_2O \quad (5)$$

Equations 1 and 2 happen simultaneously with a local increase in pH leading to reduction of Cr(VI) and precipitation of metal hydroxides as shown in equations 3 and 4. Lastly, the Cr(III) and Cr(VI) species precipitate out into a chromate film that consolidates with remaining metal oxide and precipitated metal hydroxide on the substrate surface.[42]

CCCs have shown superior corrosion performance on several different substrates and actively protect against damage as from a scratch or scribe.[43–46] The active protection of non-passivated surfaces is related to reduction of Cr(VI) to Cr(III) at the exposed surfaces.[47] Unfortunately, CCCs are associated with negative health consequences and are being phased out by legal regulations in Europe and the United States.[17, 48, 49]

Many non-toxic alternatives to CCCs have been identified including molybdate, zirconium-based, and trivalent chromium compounds although all systems fail to match the anti-corrosion properties of CCCs.[42] Molybdate and zirconium conversion coatings can provide corrosion protection in place of CCCs but are found to be inferior.[50–53] Trivalent chromium passivation (TCP) systems offer the most promise as a viable alternative as their corrosion performance can match or exceed CCCs on undamaged samples with some degree of active protection.[54]

2.3. TRIVALENT CHROMIUM PASSIVATIONS

Trivalent chromium passivations date back to the 1950s but were not widely adopted until more recent restrictions on CCCs were passed.[17, 55] Deposition of TCP is achieved by skipping reduction of Cr^{6+} to deposit a $Cr(OH)_3$ layer and instead deposit the layer directly.[56–60] TCPs show some evidence of self-healing capability, but only slightly which is a disadvantage of TCPs compared with CCCs. TCPs do have the advantage that they can retain corrosion protective properties after heating whereas CCCs can lose up to 90% of their corrosion protection after exposure to temperatures >100°C.[58]

The variability of TCP coatings can be explained by differences related to bath chemistry, substrate, and bath parameters. For bath chemistry, TCPs are deposited in an acidic solution with a pH ≤ 5 with a precursor Cr^{3+} salt, an oxidizer, and usually a transition metal ion such as Co, Ni, or Fe, although these may be a post-treatment.[61–64] Bath chemistries can also vary with the choice of chromate precursor and acid, or with complexing agents that are sometimes used such as oxalic acid or ammonium bifluoride.[60, 65] These changes result in differences in corrosion performance through changes in the microstructure of the TCP layer, likely via altered bath kinetics.[60, 66]

The substrate and bath parameters also affect corrosion resistance by altering the deposition process through oxidation of the metal substrate, evolution of hydrogen at the substrate surface, and co-deposition of Cr/metal oxides and hydroxides.[62, 66–68] Key bath parameters to control this process include bath pH, temperature, sample immersion time, concentration of Cr^{3+} precursor, concentration of substrate metal ions already present, and presence of a complexing agent.[67–75] Despite the literature variabilities, some general

trends that are observed place TCPs into two general categories: first generation and second generation.[59]

First generation passivations are defined by their thickness which is typically <100 nm and tend to have a dense single-layered structure that may or may not be porous.[76] Second generation passivations tend to be in the range of 300-500 nm, potentially up to 1000 nm, and almost always contain a two or three layered structure with a dense uniform surface layer 20-50 nm thick, a bulk porous layer, and an optional dense layer near the substrate interface.[59, 66, 77] These passivations also tend to have better corrosion performance, attributed to the increased thickness.

2.4. HEAT TREATMENTS

A few studies have investigated trivalent chromium passivations that have undergone heat treatment post-deposition, and even fewer that have investigated the effects of heat treatments on the passivations themselves. The treatment temperatures tend to range from 90-150°C with times ranging from 30 minutes to several hours but do not significantly degrade the corrosion resistance they provide in contrast to the effect of heat treatment on CCCs.[56, 58, 75, 78] A study by Li and Swain found that aging and heating TCPs provides chemical and physical changes of dehydration and increased hydrophobicity that can benefit corrosion performance to a point, after which further aging and heating is detrimental.[78] A different investigation tied visual changes caused by heat treatments to water filled porosity and dissolved oxygen as performing the heat treatment in a nitrogen atmosphere does not produce the same changes.[79] The ability for

TCPs to retain most of their anti-corrosion properties after exposure to elevated temperatures is one advantage TCPs hold over CCCs.

2.5. MECHANISMS OF CORROSION

Corrosion is an electrochemical process wherein a metal substrate will undergo rusting or degradation due to the oxidation or reduction of chemical species at active sites on the surface. Four processes are necessary for corrosion to occur:

1. An anodic reaction (usually oxidation of the metal surface)
2. A cathodic reaction (reduction of dissolved ions)
3. A metallic pathway connecting anodic and cathodic surface sites (for electron conduction from anodic to cathodic sites)
4. An electrolyte (to provide and collect dissolved ions)

Inhibition of corrosion can be achieved by inhibiting any one of these processes. A passivation layer such as TCP works by attempting to inhibit the fourth process by acting as a direct physical barrier between the electrolyte and the surface of the alloy.[80]

Corrosion can be uniform or localized wherein the localized corrosion can be one of three categories: pitting, crevice, or stress corrosion cracking. Uniform corrosion represents distributed loss of material from anodic and cathodic sites spontaneously moving across the surface. Pitting and crevice corrosion results from the active sites becoming localized on the surface and focusing material loss only to a fixed area. Stress corrosion cracking is a result of an applied stress speeding up a corrosive reaction. Uniform corrosion is preferred to localized as it is more readily controlled and occurs at a predictable rate.[81]

Another type of corrosion related to this project is galvanic corrosion. Galvanic corrosion takes place spontaneously when two different metals with different electromotive potentials are placed into contact in an electrolyte where one metal acts as an anode and the other a cathode. The metal with the more negative potential on the emf series acts as the anode and has a driving force for corrosion measured via Equations 6 and 7.

$$E^{\circ}_{cell} \rightarrow E^{\circ}_{cathode} - E^{\circ}_{anode} \quad (6)$$

$$\Delta G^{\circ}_{cell} \rightarrow -nFE^{\circ}_{cell} \quad (7)$$

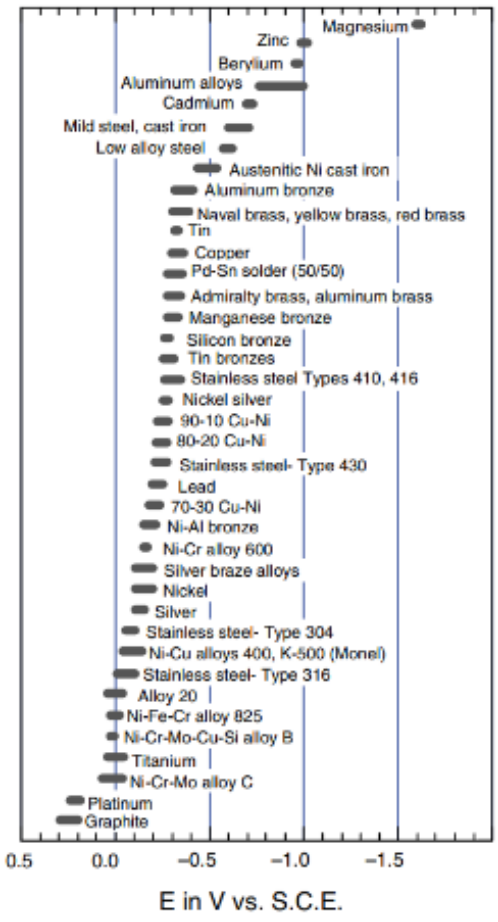

Figure 2.2. The galvanic series in seawater from LaQue[83]

The emf series is defined with a metal in an aqueous environment containing its own dissolved ions at unit activity. Hence, the emf series cannot be used to predict the anode or cathode in non-aqueous environments or in aqueous solutions with different dissolved ions. The galvanic series was empirically determined to overcome this limitation. Figure 2.2 shows the galvanic series as determined for a seawater environment.[82]

Galvanic corrosion does allow for cathodic and anodic protection to be used beneficially. Cathodic protection happens by placing a metal into contact with a more anodic metal so that the anodic metal sacrificially corrodes and protects the more cathodic metal.[82] Anodic protection occurs when the metal to be protected acts as the anode in a galvanic couple due to an external power supply that controls the cell potential and keeps the metal in a passive thermodynamic region.[84]

Typically, γ-ZnNi coatings contain many crevices that penetrate through the coating to the underlying substrate. These coatings protect the underlying metal by cathodic protection. The CCCs and TCPs passivate a γ-ZnNi coating by preventing electrolyte contact with the surface and underlying substrate. The self-healing mechanisms of CCCs and TCPs protect the underlying substrate by precipitating Cr^{3+} species onto the cathodic sites where pH is locally lower, slowing the cathodic reaction.

2.6. CHACTERIZATION OF PASSIVE FILMS

2.6.1. Physical Characterization. Electron microscopy is one of the most prevalent techniques used to physically characterize TCPs. In the case of thick coatings, scanning electron microscopy (SEM) is used to measure the thickness and examine

morphology within the layer. For thin coatings, SEM is often used to look for the presence of cracks or pores on the surface as well as to visually compare the roughness of the surface pre- and post-deposition. When paired with energy dispersion spectroscopy (EDS), it has been used to simultaneously examine chemical composition of the passive layer but only on thick coatings.[44, 71, 77, 85, 86] Transmission electron microscopy (TEM) is used more rarely but allows for accurate measurement of thin TCP thickness and verification of the amorphous or crystalline nature of the deposited layer.[54, 87–89] Even more rarely, atomic force microscopy (AFM) is used to investigate surface roughness and ellipsometry is used to determine layer thickness.[90, 91]

2.6.2. Chemical Characterization. Due to the thin nature of the TCP layers, most chemical characterization relies on X-ray photoelectron spectroscopy (XPS) to determine layer composition. Other techniques used include glow discharge optical emission spectroscopy, auger electron spectroscopy, Raman spectroscopy, and inductively coupled plasma optical emission spectroscopy.[61, 92] Due to the nature of multiplet splitting in Cr XPS spectra and the fact that TCPs are made up of mixtures of Cr oxides, hydroxides and Zn, multiple chemical characterization methods need to be used to accurately describe the valence state of the Cr present. Unfortunately, only a few studies have confirmed their XPS findings with multiple analytical methods.[54, 88, 92] When investigating specifically the content of Cr(VI), another analytical method based upon 1,5 diphenylcarbazide (DPC) can be used.

Using UV/Vis spectrophotometry a reaction between DPC and Cr(VI) in solution can be quantitatively determined. DPC is oxidized by Cr(VI) to form 1,5 diphenylcarbazone and Cr(III) which then forms a complex with Cr(III) to create a pink

color in acidic solutions. This pink color has a peak absorbance at ~540 nm that can be quantitatively measured given a set of known standards has also been measured. The method does suffer from interferences with Fe, Mo, and V, but the absorbance directly from these species is orders of magnitude less sensitive than Cr and thus amounts in the 10-100 µg/mL region can be tolerated without concern. Fe(II) ions create a bigger problem as they can reduce the Cr(VI) thus generating a false negative requiring the use of a buffer such as NaF to ensure accurate measurement.[93, 94]

2.6.3. Electrochemical Characterization. Several electrochemical techniques can be used to characterize coated specimens and their corrosion resistance including open circuit potential (OCP), cyclic potentiodynamic polarization (CPDP), and electrochemical impedance spectroscopy (EIS). OCPs are determined by placing the specimen as the anode in a three electrode setup and measuring the potential while waiting for the specimen to equilibrate with an example give in Figure 2.3. The measured potential represents the point at which no current is flowing in the sample and is the maximum potential difference the cell would see without an applied voltage or current.[95] Comparisons between OCPs in the same electrolyte allows for determination of which specimens would function as the anode in a galvanic couple or which specimen has a greater driving force for corrosion. In the case of coatings and passivations, it can indicate a reduction in driving force for corrosion or confirm that a coating is/is not acting sacrificially.

CPDP is done after measuring OCP and begins at a voltage below the OCP. A potential is applied to the cell and sweeps at a slow rate, usually around 0.1667 mV/s, and continues above the OCP to a point where the scan is then repeated in reverse.[96]

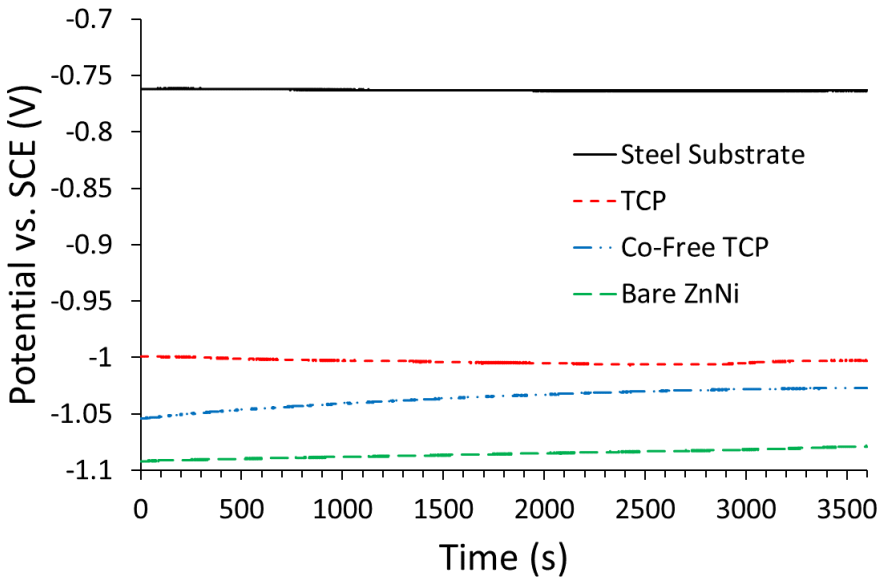

Figure 2.3. Open circuit potentials of steel samples in 0.6 M NaCl + 0.6 M $NH_4(SO4)_2$.

This serves as a technique to get information from both an anodic and cathodic polarization simultaneously with the understanding that cathodic reactions can affect the subsequent anodic polarization. The CPDP can also show if a region of passivity exists above the OCP and can identify the presence of pitting corrosion. Figure 2.4 shows a theoretical curve for a sample demonstrating many possible features visible from a CPDP. A Tafel approximation can be performed at the corrosion potential to estimate the corrosion current, i_{corr}, and the polarization resistance, R_p, which can be compared between specimens to determine if a coating or passivating treatment is reducing the rate of corrosion.

Electrochemical impedance spectroscopy is a technique often used in corrosion studies because of the amount of information that can be indirectly obtained. Information

can be gathered by visual inspection of changes in the Nyquist and Bode plots to get semi-quantitative comparisons between different specimens.

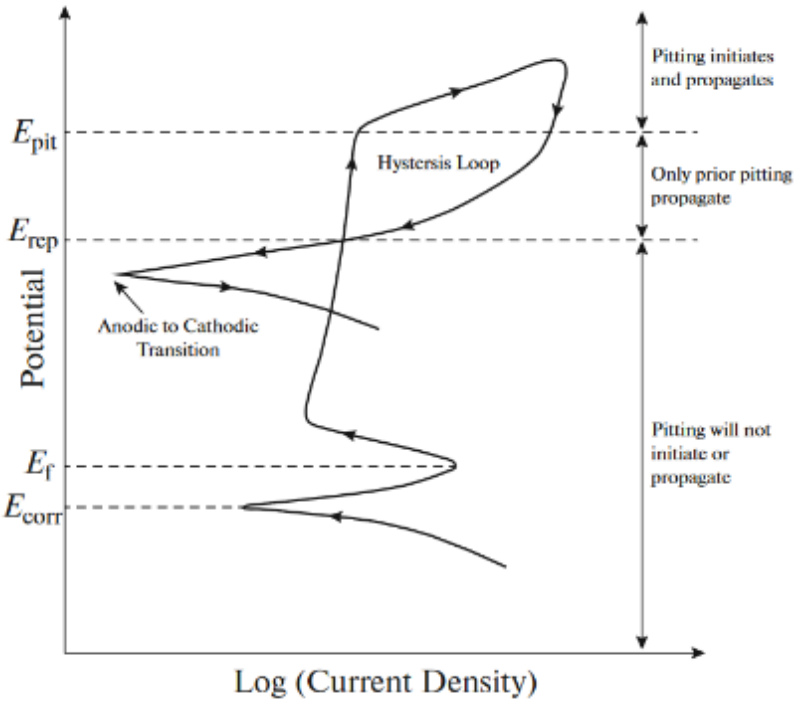

Figure 2.4. Theoretical CPDP curve showing notable features related to pitting, passivation, and surface breakdown. Image from Ezmailzadeh et al.[97]

Quantitative information can be obtained through equivalent circuit modeling of the active mechanisms present and then attributed to physical processes via experimentation. Using this quantitative and semi-quantitative data, aspects of the corrosion process and coating morphology can be inferred. EIS data can also detect changes in the surface such as growth of new phases and can be used to compare susceptibility to corrosion of different treatments.

For equivalent circuit modeling to be valid the data must satisfy the Kramers-Kronig relationships for complex quantities which allow real data to be constructed from imaginary data and vice versa. The requirements placed on data are linearity, causality, and stability. Stability is ensured when the perturbation or amplitude of the applied signal does not change as the experiment is run. Linearity is satisfied if the data have a linear response to the applied perturbations. Lastly, causality is satisfied if a response to the perturbation does not occur prior to the perturbation.[98]

An equivalent circuit model will always satisfy the Kramers-Kronig relationships as the circuits are mathematical models that are always linear, stable, and causal. For real data, stability and causality can be considered satisfied and it is the requirement of linearity that fails due to non-stationary effects. Non-stationarity is the result of gas evolution, a chemical reaction, or instrumental artifacts that cause time-dependent noise greatest in the low frequency region where sampling times are long. Satisfaction of the Kramers-Kronig relationships is usually verified analytically by separating impedance data into real and imaginary parts, transforming them, and then recombining to see if the original data is recreated.[98] For corrosion studies, if the original data cannot be recreated, then the data is not valid and either the experiment must be redesigned to slow down corrosion of the studied material, or the lower frequencies studied during EIS must be dropped until stationarity is ensured in the remaining data.

The last consideration when using equivalent circuit modeling of EIS data to investigate a surface is the model fit itself. There are an infinite number of electrical circuits that will provide a valid fit to experimentally gathered EIS data which necessitates knowledge of the surface, coating, or passivation being studied and

confirmation of results via different analytical methods. Emphasis must be placed on ensuring the results are physical and real by limiting the number of circuit components to only those that can be justified via chemical or morphological evidence from other characterization methods. Only after such careful analysis is taken to ensure that results are physically real can once use EIS data as evidence to support their research conclusions.

PAPER

I. CHARACTERIZATION OF COBALT CONTAINING AND COBALT-FREE TRIVALENT CHROMIUM PASSIVATIONS ON γ-ZnNi COATED STEEL SUBSTRATES

Kevin Foster[a], James Claypool[a], William G. Fahrenholtz[a], and Matthew O'Keefe[a]
[a]Missouri University of Science & Technology
401 W. 16th St.
101 Straumanis-James Hall
Rolla, MO, 65409, United States

Tarek Nahlawi[b] and Felix Almodovar[b]
[b]Dipsol of America
34005 Schoolcraft Rd.
Livonia, MI, 48150, United States

Corresponding: Kevin Foster, klfmkd@mst.edu, 417-860-0460,
436 Hickory St., Steelville, MO 65565, United States

Other Emails: James – jbcgyf@mst.edu, William – billf@mst.edu, Matthew – mjokeefe@mst.edu, Tarek – tnahlawi@dipsolamerica.com, Felix – falmodovar@dipsolamerica.com

ABSTRACT

The corrosion performance was studied for standard trivalent chromium passivations and cobalt-free trivalent chromium passivations on steel substrates. The steel substrates were either polished or unpolished and coated with γ-phase ZnNi prior to passivation. For unpolished substrates, cobalt-free specimens had 50 ± 8 cracks/mm, a thickness of 69 ± 4 nm, and notable porosity compared to cobalt-containing passivations which had no cracks, a thickness of 40 ± 5 nm, and no porosity. For polished substrates, cobalt-free passivations had 50 ± 3 cracks/mm, a thickness of 38 ± 2 nm, and notable

porosity compared to cobalt-containing passivations with 16 ± 2 cracks/mm, thickness of 48 ± 2 nm, and no porosity. After 1000 hours of salt-spray exposure, cobalt-free passivations had visible white rust on 4% of the surface area while cobalt-containing passivations had 22% of the surface area covered by white rust. The thickness of both passivations increased on both polished and unpolished specimens after salt spray exposure. Electrochemical testing showed that the cobalt-free passivation had the least change before and after salt spray exposure. The difference in corrosion performance was attributed to the greater porosity in the cobalt-free passivations influencing the amount of corrosion inhibiting species present.

Keywords: Trivalent chromium passivation; Zinc-nickel coating; Corrosion; Steel, Transmission electron microscopy; Cobalt

1. INTRODUCTION

Electroplated cadmium has been used to protect materials such as steel or aluminum from corrosion for decades[1,2]. Unfortunately, cadmium is carcinogenic, which has led to regulations that limit cadmium exposure and necessitated alternative plating technologies[3–7]. Electroplated zinc and zinc alloys are potential replacements for cadmium-based platings and are widely used in the steel and automotive industries[8–11]. One zinc alloy that is a viable alternative to Cd is the γ-phase of ZnNi[11–16]. Similar to galvanization, ZnNi coatings act as a sacrificial anode to cathodically protect the underlying substrate through galvanic coupling. To slow the corrosion and extend the

lifetime, passivations can be employed in addition to the sacrificial coatings. One of the most effective passivations is based on hexavalent chromium, which can exhibit active corrosion inhibition that protects portions of the exposed surface where the passivation has been damaged or removed[17–19]. Unfortunately, hexavalent chromium is also carcinogenic and regulations have been passed to limit usage in the United States and the European Union[20,21]. These regulations necessitated development of alternative passivation technologies.

Trivalent chromium passivations (TCPs) have been demonstrated as viable alternatives to hexavalent chromium. The Cr(III) species that are predominant in TCPs are formed naturally as part of the corrosion response of hexavalent chromium coatings as described by Equations 1-3[22] and consisting of metal dissolution, hydrogen evolution, and subsequent reduction of Cr(VI) from locally increased pH. While TCPs may or may not exhibit active corrosion protection[23], the performance of TCPs exceeds the corrosion protection of hexavalent chromium coatings in some cases such as the impedance work provided by Di Sarli et al.,[24] the corrosion work by Foster et al.[25], and the comparisons between Cr(VI) and Cr(III) made by Zaki[26]. Additions of cobalt have been shown to improve the corrosion performance of TCPs during salt spray testing[27,28]; however, regulations in the European Union limiting cobalt exposure have led to the development of TCP deposition processes that do not use cobalt.

$$M \rightarrow M^{2+} + 2e^{-} \quad (1)$$

$$2H^{+} + 2e^{-} \rightarrow H_2 \quad (2)$$

$$Cr^{6+} + 3e^{-} \rightarrow Cr^{3+} \quad (3)$$

Even though additions of cobalt to TCPs has been shown to improve corrosion performance, there is significant variation in the amount of time it takes for a TCP layer to exhibit white rust on ZnNi coatings. Reported times vary from ~120 hours[29] to ~450 hours[26] for TCPs that are produced using only slightly different materials or deposition parameters. This makes it clear that while cobalt can improve a TCP, it is not sufficient to create a long lasting passivating layer and that other factors may be more important to producing an excellent TCP. This leads to a question of how cobalt additions affect the TCP layer to improve the corrosion performance and how they ultimately contribute to the protection of the underlying substrate.

The goal of this research was to characterize two TCPs, one with cobalt and one without, on electroplated γ-phase ZnNi coated SAE 1008 steel substrates to determine what changes to the TCP layer caused by cobalt could influence the corrosion performance of trivalent chromium passivated samples. Since the ZnNi coating can also influence the corrosion performance of the TCP, some specimens were polished before TCP deposition to limit the effects of surface roughness on the passivation.

2. PROCEDURE

2.1. SPECIMEN PREPARATION

SAE 1008 steel substrates were prepared in two separate batches. One batch had dimensions of 10 cm by 2.5 cm by 0.2 cm and the other 5.1 cm by 2.5 cm by 0.1 cm. Half of the specimens were polished and half were left unpolished. All specimens were prepared for electroplating by five minutes of alkaline cleaning in an aqueous solution

containing 90 mL/L of Dipsol 523-SC (alkaline cleaning solution) at 55°C and sixty seconds of surface activation in an aqueous solution containing 40 wt% HCl + 60 g/L of Dipsol 971-SC (acid activator) at ambient temperature. Electroplating was conducted at 300 A/cm2 for twenty-five minutes in the Dipsol IZ-C17+ Zn / Ni deposition bath (proprietary electroplating solution). The resulting ZnNi coating contained approximately 80/20 wt% Zn/Ni and consisted of Ni5Zn21 and NiZn3 γ-phase stoichiometries.

The ZnNi plated panels were then either polished or left as-plated prior to being passivated with TCP or Co-Free TCP. Grinding and polishing was done on a wheel (Buehler Ecomet III) at 500 RPM with each step performed until no scratches from the previous step were visible. Grinding steps used water as the lubricant and went in order from 80 and 120 grit paper with alumina abrasives to 180, 240, 320, 400, 600, 800, and 1200 grit paper with SiC abrasives. Specimens were then polished using 1.0 µm and 0.3 µm alumina suspensions (Buehler MicroPolish) on a polishing cloth (Buehler MicroFloc) with an aqueous lubricant (MetaDi Fluid). Each polishing step was conducted for 30 seconds. Between each grinding or polishing step, specimens were rinsed with soapy water, ultrasonically cleaned in ethanol for 3 mins, and then dried with a heat gun.

Both as-deposited and polished ZnNi-plated specimens were passivated according to the following procedure:

1. 1mL/L HCl acid activation for 15 seconds with two 30 second DI water rinses
2. Passivation of the Dipsol IZ-264 TCP (proprietary passivating bath) or the cobalt-free modified IZ-264 TCP (proprietary passivating bath) via chemical bath deposition for 90 seconds

3. 25 second drain followed by 30 second DI water rinse
4. Hot rinsed in DI water for 30 seconds
5. Air dried
6. Heat treated at 191°C for 23 hours in air

2.2. SALT SPRAY EXPOSURE

There were six specimens for every tested condition with two set aside and used for testing at 0 hours of salt spray exposure (SSE), while the remaining four were placed in a salt spray chamber (Cyclic Corrosion Tester, Q-Fog) set up for ASTM B117[30]. After 500 hours of SSE two of the four specimens were removed and characterized and after 1000 hours of SSE the last two specimens were removed and characterized. After SSE, specimens were rinsed in DI water until no more salt product was removed or 30 seconds, whichever was longest, and then air dried for 24 hours. Dried specimens had contact resistance measured consistent with MIL-DTL-81706B[31] specifications of 200 pounds of force per square inch using copper electrodes with 10 measurements taken per specimen using a source measure unit (2450 Sourcemeter, Keithley 1.00 Amp, Power Line Cycles = 10, 4-wire resistance measurement mode) prior to further characterization.

2.3. IMAGING

Images after SSE were taken of specimens using a camera or a printer/scanner. Specimens were also imaged using optical microscopy with a digital optical microscope (KH-8700, Hirox). Some specimens were sectioned using a shear cutter and a low speed saw (Isomet 11-1280-160, Buehler) for X-ray photoelectron spectrometry (XPS; Axis

165, Kratos, Al anode, dwell time = 500 ms, spot size = 120 µm, no sputtering used) or scanning and transmission electron microscopies (SEM and TEM, respectively). The amount of corrosion product was measured as the percentage of the panel area that was covered using computerized image analysis (ImageJ; National Institute of Health) to trace the regions where corrosion product was visible and dividing that by the total area of the specimen in pixels from the specimen pictures. Corrosion product from an unpassivated ZnNi specimen after 1000 hours SSE was analyzed via X-ray diffraction (XRD; X'Pert Pro, Panalytical, Cu K_α = 1.540598 Å, fixed slit = 0.38 mm, data angle = 5.015° - 89.975° 2θ, step size = 0.03°). Computerized image analysis was also used to count the cracks per mm by utilizing a method similar to ASTM E112-13[32] to find the lineal mean intercept of the cracks. Lastly, crack widths were measured using computerized image analysis by taking thirty measurements of randomly selected cracks in SEM images across all images of a sample and averaging.

SEM was done on either a RAITH e-Line PLUS or a Hitachi S-4700 while TEM liftouts were produced using a gallium focused ion beam on an FEI Scios with the following procedure. A representative section of the surface was located and had platinum deposited in a 15 µm by 1.5 µm rectangle with the electron beam at 5 kV and 1.4 nA beam current to a thickness of 200 nm. This was followed by a Pt deposition on the same spot with the ion beam at 30 kV and 0.28 nA to a thickness of 1.5 µm. A cross-section pattern was then used in a 20 µm by 12 µm rectangle to a depth of ~6 µm with the ion beam at 30 kV and 21 nA and then repeated on the other side. Cleaning cross-sections were used to further mill both sides from the edge of the platinum to 1.5 µm into the milled trough at a current of 6.5 nA. A U-shaped cut was made into the cross-section

to almost separate it from the substrate and a tungsten probe welded onto one corner of the liftout with platinum. The liftout was then removed and welded onto a Cu TEM grid post and thinned to electron transparency by tilting +/- 2° by using 2.8 nA beam currents for bulk removal followed by 0.46 nA currents for the final thinning. The last step consisted of a 28 pA cleaning of each side at a 7° tilt for two minutes. TEM images were gathered using a Tecnai F20 scanning TEM (STEM).

Passivation thicknesses were measuring using computerized image analysis on TEM liftout images where 30 lines were drawn perpendicular on a random part of the passivation with the measurements averaged across all lines. When multiple images were available, the 30 lines were split across the available images and averaged the same way.

2.4. ELECTROCHEMICAL CHACTERIZATION

Electrochemical characterization took place in 250 mL of a 0.6 M NaCl (Fisher Scientific, Granular USP/FCC) + 0.6 M $NH_4(SO_4)_2$ (Fisher Scientific, Certified ACS) electrolyte. The electrolyte was placed in a flat cell and used a saturated calomel reference electrode (+0.244 V vs. SHE at 25°C). Electrochemical testing was performed using a potentiostat/galvanostat (Model 273A, Princeton Applied Research) and a frequency response analyzer (SI 1255 HF, Solartron Instruments). Open circuit potentials (OCPs) were measured first for 3600 seconds followed by cyclic potentiodynamic polarizations (CPDP). CPDPs were performed by sweeping from -0.3 V to 0.8 V and back to -0.3 V vs. OCP at a rate of 0.1667 mV/second. Each specimen had electrochemical testing performed three times on three different areas. The OCP and CPDP data were analyzed using CView (3.5h, Scribner Associates) to perform Tafel

analysis at the corrosion potential. All values were averaged across the multiple trials done for each sample.

3. RESULTS

3.1. PASSIVATION COMPOSITION

The passivations were primarily composed of chromium, zinc, and oxygen as summarized in Table 1 and shown in Figure 1. The most abundant elements detected were oxygen and carbon followed by chromium. Most of the carbon and some of the oxygen were expected to be due to adventitious carbon present on surfaces[18,23]. The TCP contained 10.6 at% Cr and the Co-free TCP contained 8.2 at% Cr. Zinc was also detected with 3.3 at% in TCP and 6.5 at% in Co-Free TCP. The TCP contained 0.6 at% Co. All other elements had concentrations less than 1.0 at% and are not discussed further. The Co-Free TCP had no detectable level of cobalt but contained nearly twice as much zinc (6.5 at%) as the TCP (3.3 at%). Zinc is known to incorporate into the TCP layer during the deposition process in an amount based upon the bath kinetics[33]. The chemical baths for each passivation were different and the Cr to Zn deposition ratio between the passivations indicated that the passivations had differences in addition to the presence or absence of cobalt.

3.2. AS-DEPOSITED PASSIVATIONS

The passivations deposited on polished substrates had a similar visual appearance with the TCP having a purple appearance while the Co-Free had a purple-blue appearance with some yellow. For unpolished substrates, the Co-Free TCP was light

blue with a yellow tint while the TCP was brown as seen in the 0 hour columns of Figure 2. Closer examination (Parts a) and b) of Figures 3 and 4) revealed that cracks were apparent on the surface of TCP on polished and unpolished substrates as well as on Co-Free TCP on polished substrates. Cracks were less frequent on TCP with 16 ± 2 cracks/mm while Co-Free TCP had 50 ± 3 cracks/mm. In the unpolished case, no cracks were apparent on TCP, but Co-Free TCP had about the same crack density of 49 ± 8 cracks/mm, indicating similar starting conditions for polished and unpolished Co-Free specimens. The cracks were 0.8 ± 0.3 μm wide on unpolished Co-Free, 0.8 ± 0.1 μm wide on polished Co-Free, and 0.3 ± 0.1 μm wide on polished TCP. Cracks were both wider and more numerous on the Co-Free specimens.

Thicknesses of the passivations were determined using TEM images such as those seen in Figures 5 and 6 where measured values were 69 ± 4 nm for Co-Free TCP on polished substrates and 40 ± 5 nm for TCP on polished substrates. Co-Free passivations on unpolished substrates were 38 ± 2 nm thick and TCP passivations on unpolished substrates were 49 ± 2 nm thick. The Co-Free passivations were initially thicker than the TCPs on polished substrates while the reverse was true of the unpolished samples. All passivations were <100 nm thick, which is similar to the “thin” type trivalent chromium based passivation[19,29] as opposed to the “thick” type seen in some studies[24,29].

3.3. VISUAL INSPECTION AFTER SSE

After SSE, the Co-Free passivations showed less corrosion than the TCPs regardless of whether the substrates were polished, but the difference in corrosion was greater between the unpolished specimens. Figure 2 shows the progression of corrosion

build up from 0 to 1000 hours. The images visually reinforce that the Co-Free passivation performs better than the TCP, which indicates that some aspect of the passivation is beneficial to corrosion performance. The polished TCP showed ~6% corrosion product coverage after 500 h SSE and ~15% corrosion product coverage after 1000 h SSE. For comparison, the Co-Free passivation had ~5% corrosion product coverage at 500 h and ~1% corrosion product coverage at 1000 h. The unpolished specimens followed a similar trend with TCP showing ~4% corrosion produce coverage at 500 h and ~22% at 1000 h, which was more than Co-Free with ~2% at 500 h and ~4% at 1000 h. The high variability in corrosion performance can be attributed to only having two specimens for most conditions with only one specimen for Co-Free 1000 h polished or unpolished, although the results demonstrate the large range of corrosion behavior, which is consistent with other studies.

3.4. OPTICAL MICROSCOPY AND CRACK MEASUREMENTS

The progression of surface appearance during SSE is shown in Figures 3 (polished substrates) and 4 (unpolished substrates). Very little corrosion product was observed for either of the passivations on polished specimens, but some staining was observed for the cobalt-free passivation after SSE. Numerous cracks were visible across the surface of both polished passivations with Co-Free passivations having 55 ± 4 cracks/mm after 500 hours SSE and 77 ± 8 cracks/mm after 1000 hours SSE, much more than TCP with 16 ± 4 cracks/mm after 500 hours SSE and 30 ± 3 cracks/mm after 1000 hours SSE. The unpolished cobalt-free passivation had fewer cracks than the polished specimen with 39 ± 15 cracks/mm after 500 hours SSE and 35 ± 10 cracks/mm after 1000

hours SSE, while the unpolished TCP had no visible cracks until 1000 hours of SSE after which it had 34 ± 10 cracks/mm. The specimens followed a trend of increasing cracks with increasing SSE time except for Co-Free passivations on unpolished substrates, which had the opposite behavior, although those specimens had much greater variability leaving open the possibility of sampling error.

Like the results from visible examination, very little corrosion product was observed on all the panel surfaces, except for some localized regions on TCPs on polished and unpolished substrates. The corrosion product that was visible was clustered around cracks and pores on the surfaces, suggesting that the cracks acted as corrosion initiation sites. Corrosion extent does not correlate with crack width and density but only with the presence of cracks and flaws, likely a result of heterogeneous nucleation requiring less energy for a corrosion site to form. This would also explain why unpolished samples showed more visible corrosion product than polished as an unpolished surface has more grooves and valleys for nuclei to form heterogeneously.

3.5. CRACK WIDTHS AND CORROSION PRODUCTS

Inspection using SEM (Figures 7 and 8) shows intergranular crevices visible at high magnifications. After 1000 hours of SSE, corrosion products on the Co-Free passivations on unpolished substrates were only visible near or inside of the cracks. In contrast, the TCP on unpolished specimens had a uniform layer of corrosion product across its surface with increasing amounts of corrosion product located near the small cracks and pores. The passivated polished specimens had only debris visible on the surfaces with a little corrosion product visible within the cracks and pores. Only the

unpassivated ZnNi panels had enough corrosion produce for XRD analysis. This analysis (Figure 9) of the corrosion product showed most peaks fit from zinc hydroxide chloride hydrate ($Zn_5(OH)_8Cl_2 \bullet H_2O$) with some zinc carbonate hydroxide hydrate ($Zn_4CO_3(OH)_6 \bullet H_2O$) and some of the underlying ZnNi substrate visible ($NiZn_3$).

The cracks on the unpolished Co-Free TCP specimens had an average width of 0.8 ± 0.2 µm and were about three times larger than the cracks in the TCP on unpolished specimens that had average widths of 0.2 ± 0.1 µm. Passivations on polished specimens had cracks that were 1.4 ± 0.5 µm wide for Co-Free TCP and 0.3 ± 0.1 µm wide for TCP.

3.6. PASSIVATION STRUCTURE AND THICKNESS

Passivations remained amorphous but increased in thickness during SSE. Fast Fourier transforms of TEM images (Figure 10) confirmed that all of the passivations were amorphous both before and after SSE. All passivations ranged from ~40-80 nm thick after SSE with the polished Co-Free specimens at 59 ± 2 nm, unpolished Co-Free at 77 ± 4 nm, polished TCP at 52 ± 2 nm, and unpolished TCP at 61 ± 23 nm. All passivated specimens examined showed and increase in thickness after SSE, with the greatest change for Co-Free passivations on polished substrates with the least change for TCP on polished substrates. The most notable morphological difference between the two passivations was the much larger amount of porosity in the cobalt-free TCP layer compared to the TCP (Figures 5 and 6). Every cobalt-free TCP specimen had a clearly visible porous layer while some TCP specimens had moderate porosity and others did not. Passivations on polished substrates showed lower average thicknesses and variability compared to passivations on unpolished substrates, but otherwise had the same

morphological features. This change in thickness correlates with the visible corrosion as the Co-Free passivations on polished substrates performed worse than the passivations on unpolished substrates, consistent with the lower thickness in the passivations on polished substrates. The TCP on polished substrates performed better, which was consistent with the differences in thickness between the specimens.

3.7. ELECTROCHEMICAL CHARACTERIZATION

Electrochemical results are summarized in Figures 11 and 12 starting with OCP and CPDP before and after SSE. OCPs are listed in Table 2 where the averaged values for polished and unpolished Co-Free TCP decreased from about -1.030 V to approximately -0.992 V and TCP decreased from about -1.017 V to approximately -0.980 V. None of the specimens had potentials near the measured potential for exposed steel, which is -0.763 V ± 0.001 V, and only the unpassivated ZnNi surface showed a notable change in potential after SSE with an increase of approximately 210 mV.

The CPDP curves allowed comparison of the TCP and Co-Free TCP to each other as well as to unpassivated ZnNi. The forward sweep of the cobalt-free TCP revealed an initial corrosion potential comparable to ZnNi, which increased by 33 mV after SSE. The TCP was not initially as similar to bare ZnNi as Co-Free and showed an increase of 71 mV in the corrosion potential after SSE. During testing, gas evolution was observed from the cathodic sweep to the corrosion potential value, where the evolution ceased, until around -0.8 V where gas evolution began again. At -0.6 V on the forward sweep, the ZnNi coating lost adherence to and separated from the underlying steel substrate.

Beyond this, further reactions to the CPDP were from the substrate in the absence of the passivated ZnNi coating.

Tafel analysis of the unpolished TCP passivation (Table 3) showed a decrease in anodic slope (β_a) with SSE from 99 ± 4 mV at 0 hours to 72 ± 2 mV at 1000 hours. A similar trend was seen for the cathodic slope (β_c) that went from 178 ± 37 mV at 0 hours to 154 ± 20 mV at 1000 hours. The corrosion current density (i_{corr}) increased gradually going from 0.49 ± 0.07 x 10^4 mA/cm^2 to 0.81 ± 0.09 x 10^4 mA/cm^2 after 1000 hours SSE. The polarization resistance decreased from 500 ± 90 Ω*cm^2 at 0 hours to 226 ± 62 Ω*cm^2 after 1000 hours.

The Co-Free TCP showed the opposite trend for both the anodic and cathodic slopes going from 100 ± 1 mV to 124 ± 1 mV after 1000 hours for the anodic, and 151 ± 13 mV to 193 ± 6 mV for the cathodic. Co-Free initially had a corrosion current density of 0.49 ± 0.05 x 10^4 mA/cm^2 then showed an increase at 500 hours to 2.44 ± 3.07 x 10^4 mA/cm^2 before decreasing to 0.86 ± 0.03 x 10^4 mA/cm^2. The polarization resistance of Co-Free was initially 483 ± 43 Ω*cm^2 but decreased to 392 ± 5 Ω*cm^2 after 1000 hours SSE.

Unpassivated ZnNi showed a greater increase in anodic slope with 84 ± 3 mV at 0 hours and 266 mV at 1000 hours. The cathodic slope increased from 176 ± 12 mV at 0 hours to 200 mV at 1000 hours. Current density was initially low at 0.81 ± 0.03 x 10^4 mA/cm^2 but increased to 2.05 x 10^4 mA/cm^2 after 1000 hours. The polarization resistance decreased with SSE initially being 319 ± 0 Ω*cm^2 and becoming 218 Ω*cm^2 after 1000 hours. These results show that both passivations compared favorably against unpassivated ZnNi in terms of corrosion current density and polarization resistance and

that the Co-Free TCP exhibited the greatest polarization resistance between the two passivations which correlated with the observed corrosion performance

4. DISCUSSION

While several differences exist between TCP and the Co-Free TCP passivations such as composition, crack density, crack width, layer thickness, and porosity, these differences do not correlate with the observed corrosion performance after SSE. Cho et al.[34] stated that corrosion build up within the cracks can impede further corrosion and allow samples to appear stable for a time before the corrosion product grows and causes crack propagation, which allows corrosion to proceed again. This model leads to the expectation that little to no corrosion should be observed while the corrosion product acts as a barrier until some critical exposure time at which the barrier fails and allows corrosion to proceed rapidly. The specimens studied here did not show such a transition as corrosion buildup was slow and no critical exposure time was observed for the transition to more rapid corrosion. This behavior could indicate that the specimens were not exposed to the salt spray long enough to reach that critical time but considering most TCP passivated samples report white rust starting at 120-400 hours, 1000 hours of exposure should have been long enough to reach any such threshold. The other observations that led to a different conclusion than that of Cho et al. were that: 1) the number of cracks did not correlate with the observed corrosion on the panels such as the unpolished TCP at 1000 hours having the most visible corrosion but no cracks at 0 or 500 hours; and 2) crack width correlating to corrosion in the opposite direction to what the

model would suggest as the smaller cracks on TCP samples should have led to more corrosion product on the surface as opposed to around the cracks and pores since the narrower space of the cracks would produce a greater diffusional barrier.

Layer thickness correlated to corrosion performance with the thicker Co-Free passivations generally having less corrosion product than the thinner TCPs. The thickness of the passivation alone does not explain the observed results as thickness should not affect the corrosion rate inside cracks where interior surfaces are not passivated. Because the Co-Free passivation had the highest crack density and the least amount of corrosion, another mechanism must be at work. Hesamedini and Bund[35] found that the pores in TCP contained water which, when dried in ambient atmosphere, can lead to oxidation of Cr(III) to Cr(VI) above pH 3 through equations 4-6 and reduction of oxygen in the aqueous solution. Oxidation of Cr(VI) through this mechanism could give TCPs some level of active corrosion protection[23]. With the observed increase in porosity of the Co-Free passivation and lack of significant corrosion in the numerous cracks on the Co-Free passivations, this mechanism could possibly inhibit further corrosion within the cracks of the Co-Free passivation leading to the observed improved corrosion performance in salt spray compared to TCP.

$$HCrO_4^- + 7H^+ + 3e^- \rightleftharpoons Cr^{3+} + 4H_2O \qquad E^0 = +1.38 \qquad (4)$$

$$Cr_2O_7^{2-} + 14H^+ + 6e^- \rightleftharpoons 2Cr^{3+} + 7H_2O \qquad E^0 = +1.386 \qquad (5)$$

$$O_2 + 4H^+ + 4e^- \rightleftharpoons 2H_2O \qquad E^0 = +1.23 \qquad (6)$$

If total chromium or cobalt were beneficial to corrosion protection, then TCP would have been expected to perform better during SSE since it has a chromium to zinc ratio close to 3.2:1 compared to 1.25:1 for Co-Free passivation. Using a similar argument as that for layer thickness, the composition of the passivation layer in terms of Cr:Zn ratio, cobalt content, or total chromium should not be able to protect regions of the surface that the passivation does not cover, unless the passivations exhibit active corrosion protection. Likewise, if Cr(III) in the passivations is oxidized to Cr(VI) as part of an active protection mechanism, then increasing total chromium content should lead to a greater concentration of Cr(VI) ions which would lead to a longer period of active protection as it would take longer to deplete the Cr(VI). If this were the case, then TCP should have performed better than Co-Free passivation. However, if the water-filled porosity promotes oxidation of Cr(III) to Cr(VI), then the Co-Free passivation would benefit since the TCP produced as part of this study had almost no porosity. It is not the thickness, morphology of cracks, or elemental composition of the passivations that leads the Co-Free passivation to protect better than the TCP, but the amount of Cr(VI) species produced in the TCP layer which could be influenced by the amount of porosity.

The electrochemical data showed a gradual increase in corrosion current and decrease in polarization resistance from 0 hours SSE to 1000 hours SSE for both TCP and Co-Free passivations if the 500 hour Co-Free data is treated as spurious due to the large variability. The similar trends observed along with the closeness of the corrosion potentials suggests that something similar happened in both passive layers. The anodic slopes observed followed differing trends with the TCP specimen showing a reduction in anodic slope with SSE while Co-Free showed an increase in anodic slope with SSE. This

difference is posited to be the difference in porosity between the TCP and Co-Free TCP layers and how that progressed with increased SSE time.

TCP began with few pores, did not develop new pores, contained cobalt, became less stable (decreased anodic slope combined with increased i_{corr}) with SSE, and developed more corrosion while Co-Free TCP began with many pores, exhibited fewer pores after SSE, did not contain cobalt, became more stable with SSE, and developed less corrosion. Interpretation of this data as a whole in light of Cr(VI) species likely being present in TCP layers[23] suggests that cobalt led to an increased initial content of Cr(VI) that was consumed during SSE leading to a reduction in corrosion protection as exposure time increased while Co-Free TCP exhibited protection from oxidation of Cr(III) to Cr(VI) in porosity close to the metal surface from local pH increases that then precipitated and filled in the pores. This would suggest that Co-Free TCP could protect the underlying substrate from corrosion as long as there is some porosity close to the metal surface that allows for Cr(VI) to be oxidized and then reduced in a protective way and that cobalt-containing TCPs may benefit from processing changes that would promote an inner layer of porosity near the metal surface with a solid layer on the outermost portion of the TCP. Directly measuring the Cr(VI) content in TCPs and correlating that with changes in porosity would be needed to confirm such a mechanism.

5. CONCLUSION

This study investigated the effect of cobalt additions on the corrosion performance of trivalent chromium passivations for ZnNi coatings by characterizing a

conventional cobalt-containing TCP and a version of the same TCP modified to contain no cobalt. The limited amount of observed corrosion across all specimens was found primarily localized to the cracks and pores in the passivations. Neither the layer thickness nor passivation composition were sufficient to explain the differences in corrosion performance. The observed differences in corrosion behavior correlated with the increased porosity of the cobalt-free passivations, which is presumed to promote oxidation of Cr(III) to Cr(VI) when the passivations are dried after deposition. If this hypothesis is true, then the corrosion performance of TCP could be improved by intentionally increasing the amount of porosity in the passivation layer. Since the effect of the layer thickness cannot be separated from the compositional differences between the passivations, further research is needed where thickness or composition would be independently varied while other factors are controlled and the amount of Cr(VI) species present in the passivations measured to be certain of the role of cobalt additions to TCPs.

ACKNOWLEDGEMENTS

This research was funded by the Strategic Environmental Research and Development Program (SERDP) through contract WP18-F2-1439. The authors wish to acknowledge the guidance and support of Dr. Robin Nissan at SERDP along with Steve Gaydos and Dave Zika at Boeing. A special thanks is extended to Dr. Xiaoqing He who produced TEM liftouts at the University of Missouri-Columbia for the project and to Dr. Wei-Ting Chen for operating and assisting with the TEM analysis.

Funding: This work was supported by the Strategic Environmental Research and Development Program (SERDP) contract WP18-F2-1439

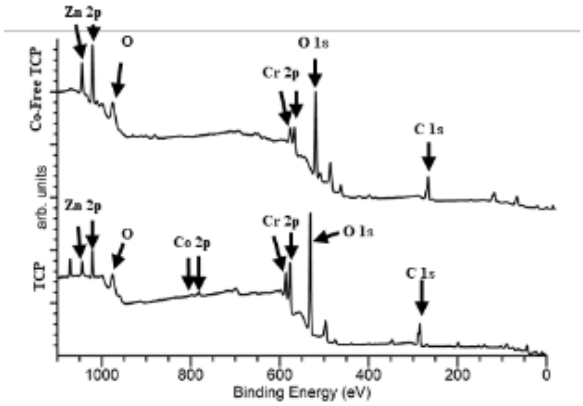

Figure 1. XPS spectra of both TCP and Co-Free TCP showing the lack of cobalt in Co-Free TCP with similar Zn, O, and Cr.

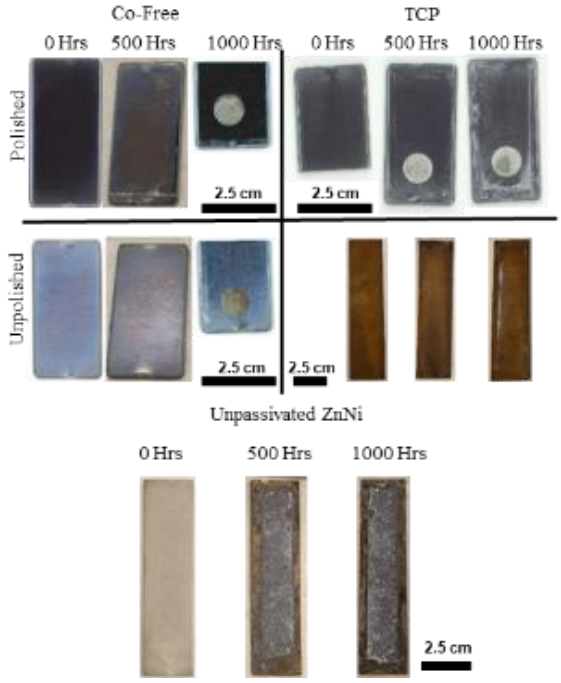

Figure 2. Appearance of different passivated specimens before and after salt spray exposure with unpassivated ZnNi for comparison.

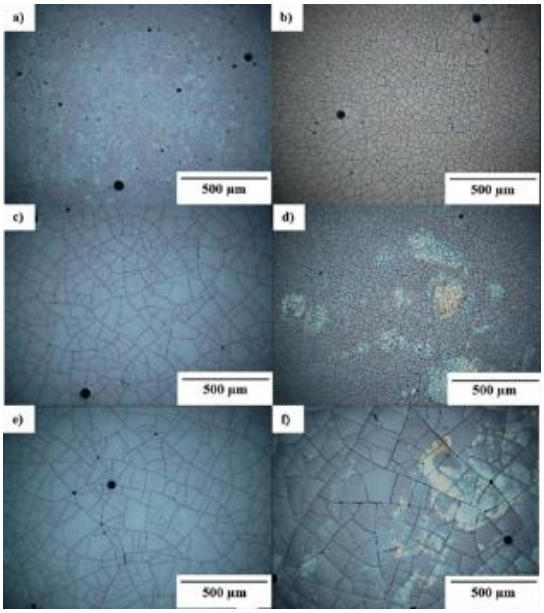

Figure 3. Polished steel samples showing a) TCP at 0 hours SSE, b) cobalt-free TCP (CoF) at 0 hours SSE, c) TCP at 500 hours, d) CoF at 500 hours, e) TCP at 1000 hours, and f) CoF at 1000 hours.

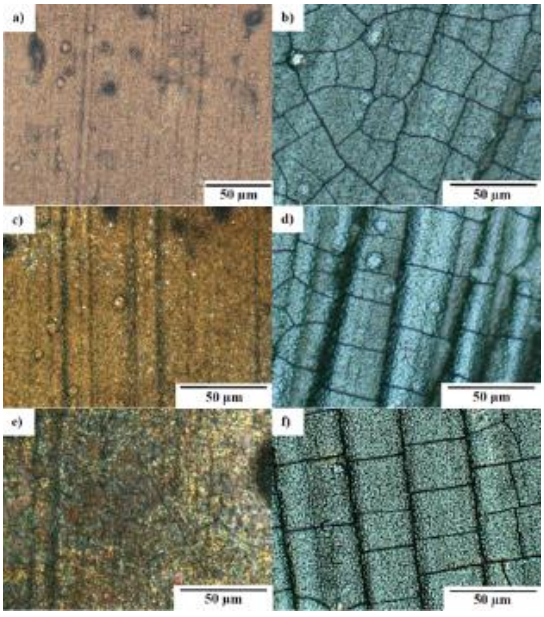

Figure 4. Unpolished steel samples showing a) TCP at 0 hours SSE, b) cobalt-free TCP (CoF) at 0 hours SSE, c) TCP at 500 hours, d) CoF at 500 hours, e) TCP at 1000 hours, and f) CoF at 1000 hours.

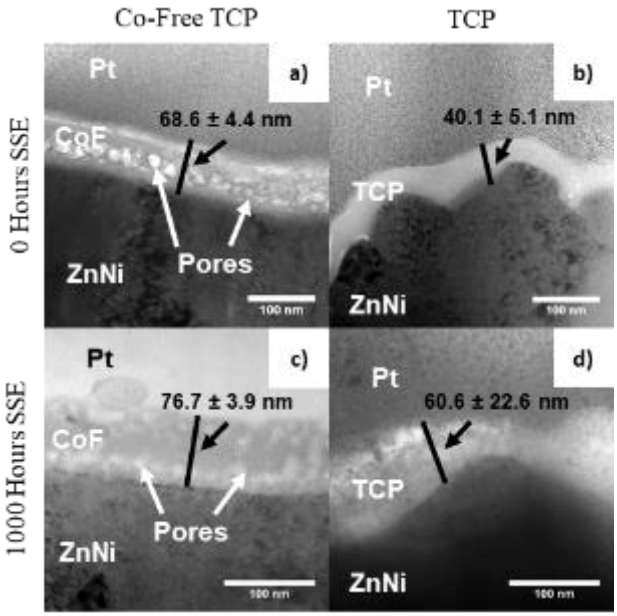

Figure 5. TEM images showing morphology and thicknesses of the unpolished cobalt-free TCP (a and c) and TCP layers (b and d) before and after salt spray exposure.

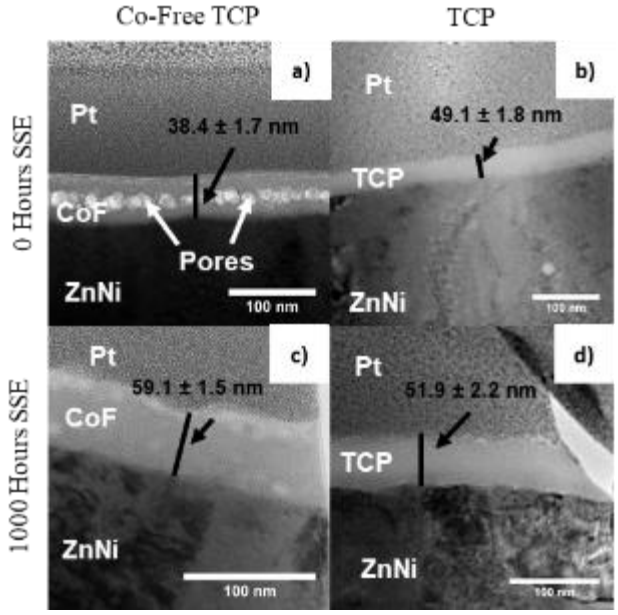

Figure 6. TEM images showing morphology and thickness of polished cobalt-free TCP (a and c) and TCP (b and d) layers before and after salt spray exposure.

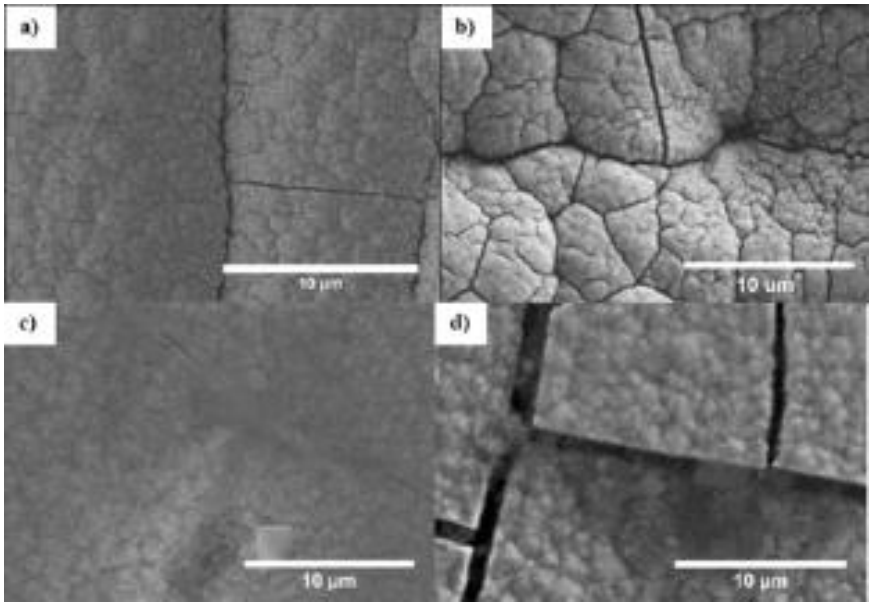

Figure 7. SEM images showing unpolished samples for: a) TCP at 0 hours SSE, b) CoF at 0 hours SSE, c) TCP at 1000 hours, and d) CoF at 1000 hours.

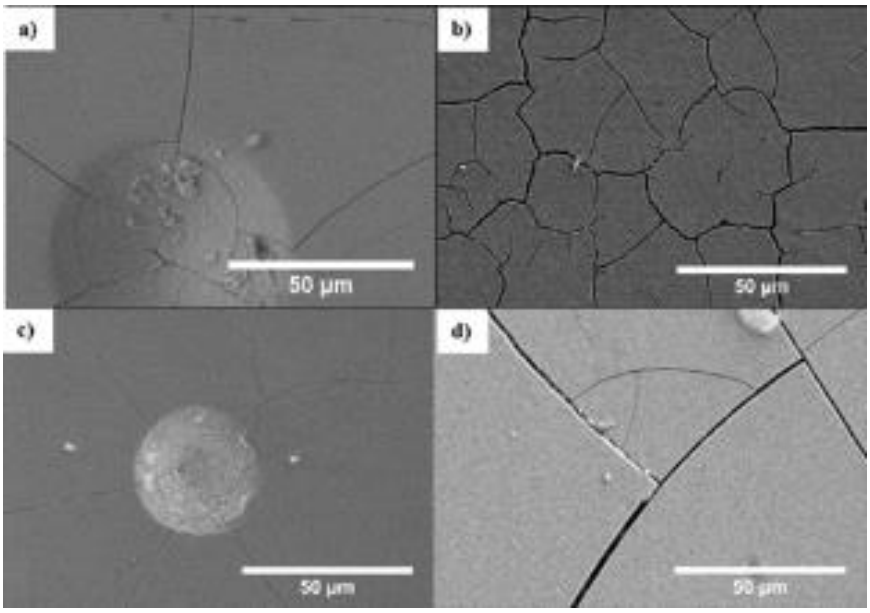

Figure 8. SEM images showing polished samples for: a) TCP at 0 hours SSE, b) CoF at 0 hours SSE, c) TCP at 1000 hours, and d) CoF at 1000 hours.

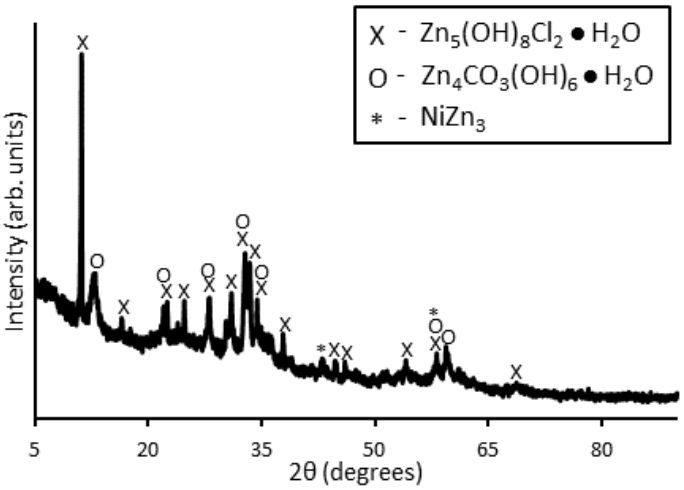

Figure 9. XRD analysis of the 1000 hour SSE ZnNi corrosion product showing zinc hydroxide chloride hydrate (X), zinc carbonate hydroxide hydrate (O), and some underlying ZnNi substrate.

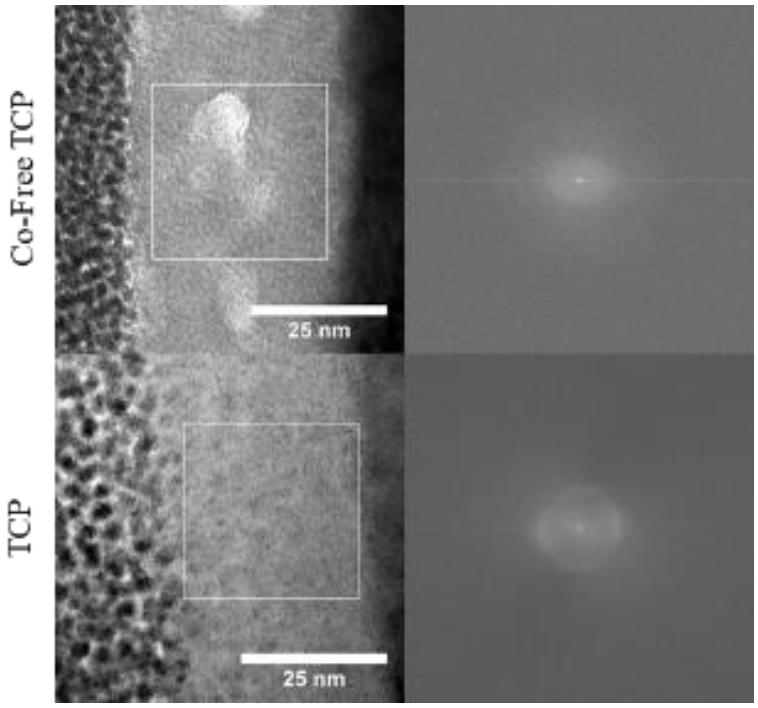

Figure 10. TEM images showing representative regions of passivation analyzed via FFT (shown right) indicating amorphous nature.

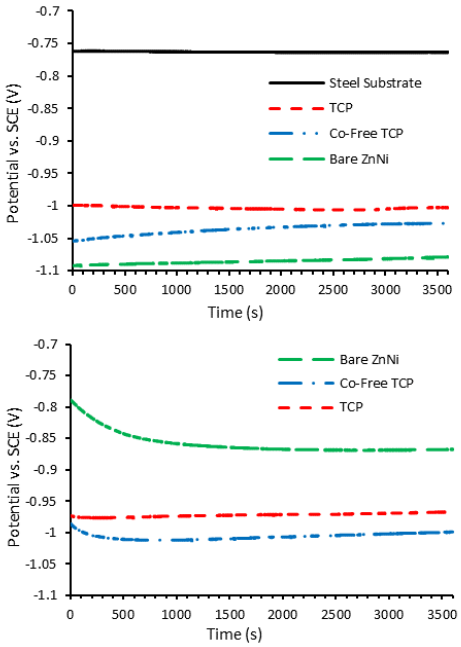

Figure 11. OCP graphs before and after 1000 hours of salt spray exposure.

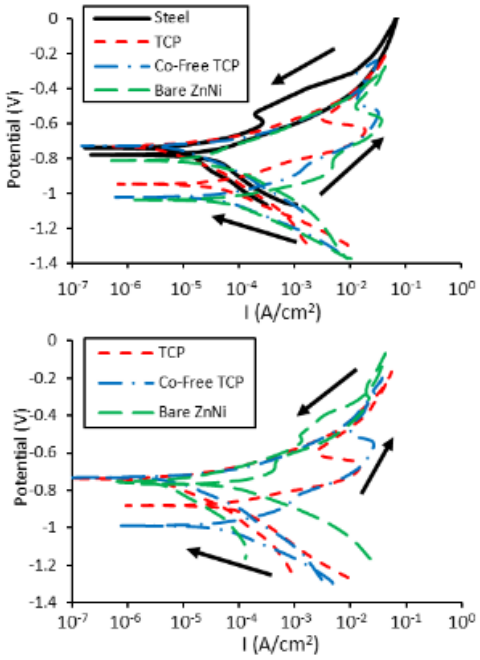

Figure 12. CPDP graphs before and after 1000 hours of salt spray exposure.

Table 1. XPS quantified data of elements > 0.5 at% in both passivations.

	TCP (At%)	Co-Free TCP (At%)
Cr	11	8
O	49	43
Zn	3	7
C	33	
N	1	1.0
Co	1	-

Table 2. Open circuit potentials of polished and unpolished TCP and cobalt-free TCP before and after 1000 hours of salt spray exposure.

	Pol. CoF	Pol. TCP	Unpol. CoF	Unpol. TCP	Bare ZnNi
0 Hrs					
SSE (V_{SCE})	-1.03	-1.02	-1.03	-1.01	-1.08
SD	0.01	0.01	0.01	0.03	0.00
1000 Hrs					
SSE (V_{SCE})	-0.99	-1.01	-1.00	-0.96	-0.87
SD	0.03	0.00	0.00	0.01	-

Table 3. Tafel parameters from analysis of CPDP data for unpolished TCP, Co-Free TCP, and unpassivated ZnNi specimens. ZnNi 1000 hours has no standard deviation (SD) because there was only one test performed.

	TCP			Co-Free			ZnNi		
Hours SSE	0	500	1000	0	500	1000	0	500	1000
β_a (mV)	99	70	72	100	141	124	84	197	266
SD	4	17	2	1	40	1	3	1	-
β_c (mV)	178	152	154	151	220	193	176	157	200
SD	37	49	20	13	89	6	12	8	-
i_{corr} (mA/cm^2) x10^4	0.49	0.51	0.81	0.49	2.44	0.86	0.81	1.54	2.05
SD x10^4	0.07	0.15	0.09	0.05	3.07	0.03	0.04	0.05	-
E_{corr} (V)	-0.93	-0.89	-0.88	-1.01	-0.99	-0.99	-1.03	-0.77	-0.77
SD	0.03	0.02	0.01	0.01	0.03	0.00	0.01	0.00	-
R_p (Ω*cm^2)	500	287	226	483	487	392	319	236	218
SD	90	94	62	43	562	5	0	13	-

REFERENCES

[1] D.M. Johnson, Zinc and cadmium passivating bath, US2559878A, 1951. U.S.A. Patent.

[2] C.M. Cotell, J.A. Sprague, F.A. Smidt, eds., Cadmium Plating, in: Surface Engineering, ASM International, 1994: pp. 215–226. https://doi.org/10.31399/asm.hb.v05.a0001247.

[3] Aquatic Life Ambient Water Quality Criteria - Cadmium 2016, (2016). https://www.epa.gov/sites/production/files/2016-03/documents/cadmium-final-report-2016.pdf.

[4] OSHA Brief - Medical Evaluation of Renal Effects of Cadmium Exposures, (n.d.). https://www.osha.gov/Publications/OSHA_3675.pdf (accessed October 22, 2020).

[5] J. Huff, R.M. Lunn, M.P. Waalkes, L. Tomatis, P.F. Infante, Cadmium-induced cancers in animals and in humans, Int J Occup Environ Health. 13 (2007) 202–212. https://doi.org/10.1179/oeh.2007.13.2.202.

[6] L. Järup, Cadmium overload and toxicity, Nephrology Dialysis Transplantation. 17 (2002) 35–39. https://doi.org/10.1093/ndt/17.suppl_2.35.

[7] National Toxicology Program, Cadmium and Cadmium Compounds, National Institute of Environmental Health and Safety, Triangle Park, NC, 2016. https://ntp.niehs.nih.gov/ntp/roc/content/profiles/cadmium.pdf (accessed October 22, 2020).

[8] A.R. Moreira, Z. Panossian, N.L. De Almeida, N.G. Berry, G.S. Pimenta, M.T.P. Paes, Replacers to Cadmium Coating for Corrosion Protection, in: NACE International, NACE International, Salt Lake City, UT, 2012: p. 11. https://store.nace.org/replacers-to-cadmium-coating-for-corrosion-protection (accessed October 22, 2020).

[9] D.A. Shifler, R.K. Conrad, A.D. Sheetz, Environmental Evaluation of a Cadmium Replacement Coating for Use in a Marine Environment, in: NACE International, 2003. https://www.onepetro.org/conference-paper/NACE-03248 (accessed October 22, 2020).

[10] W. Tian, F.Q. Xie, X.Q. Wu, Z.Z. Yang, Study on corrosion resistance of electroplating zinc–nickel alloy coatings, Surface and Interface Analysis. 41 (2009) 251–254. https://doi.org/10.1002/sia.3017.

[11] A.M. Alfantazi, U. Erb, Corrosion Properties of Pulse-Plated Zinc-Nickel Alloy Coatings, CORROSION. 52 (1996) 880–888. https://doi.org/10.5006/1.3292081.

[12] Bruet-Hotellaz, J.P. Bonino, A. Rousset, Marolleau, E. Chauveau, Structure of zinc–nickel alloyelectrodeposits, Journal of Materials Science. 34 (1999) 881–886. https://doi.org/10.1023/A:1004553803788.

[13] H. Conrad, J. Corbett, T.D. Golden, Electrochemical Deposition of γ-Phase Zinc-Nickel Alloys from Alkaline Solution, J. Electrochem. Soc. 159 (2011) C29. https://doi.org/10.1149/2.027201jes.

[14] R. Fratesi, G. Roventi, Corrosion resistance of Zn-Ni alloy coatings in industrial production, Surface and Coatings Technology. 82 (1996) 158–164. https://doi.org/10.1016/0257-8972(95)02668-1.

[15] C. Müller, M. Sarret, E. García, Heat treatment effect on the corrosion behaviour of black passivated ZnNi alloys, Corrosion Science. 47 (2005) 307–321. https://doi.org/10.1016/j.corsci.2004.04.004.

[16] S.K. Rajagopalan, Characterization of Electrodeposited Zn-Ni Alloy Coatings As A Replacement For Electrodeposited Zn and Cd Coatings, Ph. D. thesis, McGill University, 2012.

[17] M.W. Kendig, A.J. Davenport, H.S. Isaacs, The mechanism of corrosion inhibition by chromate conversion coatings from x-ray absorption near edge spectroscopy (Xanes), Corrosion Science. 34 (1993) 41–49. https://doi.org/10.1016/0010-938X(93)90257-H.

[18] G. Lu, E. Ada, G. Zangari, Investigations of the effect of chromate conversion coatings on the corrosion resistance of Ni-based alloys, Electrochimica Acta. 49 (2004) 1461–1473. https://doi.org/10.1016/S0013-4686(03)00928-9.

[19] P. Pokorny, P. Tej, P. Szelag, Chromate conversion coatings and their current application, Metalurgija. 55 (2016) 253–256.

[20] Environmental Protection Agency, Toxicological Review of Hexavlent Chromium, (1998). https://cfpub.epa.gov/ncea/iris/iris_documents/documents/toxreviews/0144tr.pdf (accessed October 22, 2020).

[21] Directive 2000/53/EC of the European Parliament and of the Council of 18 September 2000 on end-of life vehicles, Queen's Printer of Acts of Parliament, n.d. https://www.legislation.gov.uk/eudr/2000/53/contents (accessed October 22, 2020).

[22] G.D. Wilcox, Replacing Chromates for the Passivation of Zinc Surfaces, Transactions of the IMF. 81 (2003) B13–B15. https://doi.org/10.1080/00202967.2003.11871474.

[23] Y. Guo, G.S. Frankel, Active Corrosion Inhibition of AA2024-T3 by Trivalent Chrome Process Treatment, CORROSION. 68 (2012) 045002-1-045002–10. https://doi.org/10.5006/0010-9312-68-4-3.

[24] A.R. Di Sarli, J.D. Culcasi, C.R. Tomachuk, C.I. Elsner, J.M. Ferreira-Jr, I. Costa, A conversion layer based on trivalent chromium and cobalt for the corrosion protection of electrogalvanized steel, Surface and Coatings Technology. 258 (2014) 426–436. https://doi.org/10.1016/j.surfcoat.2014.08.057.

[25] K. Foster, J. Claypool, W.G. Fahrenholtz, M. O'Keefe, T. Nahlawi, F. Almodovar, Characterization of Cobalt-Containing and Cobalt-free Trivalent Chromium Passivation Layers on γ-ZnNi-Coated Al6061-T6 Substrates, ACS Appl. Mater. Interfaces. 13 (2021) 4535–4544. https://doi.org/10.1021/acsami.0c20015.

[26] N. Zaki, Trivalent Chrome Conversion Coating For Zinc and Zinc Alloys, Metal Finish. 105 (2007) 425-425.

[27] S. Hesamedini, G. Ecke, A. Bund, Structure and Formation of Trivalent Chromium Conversion Coatings Containing Cobalt on Zinc Plated Steel, J. Electrochem. Soc. 165 (2018) C657–C669. https://doi.org/10.1149/2.0951810jes.

[28] B. Ramezanzadeh, M. m. Attar, Effects of Co(II) and Ni(II) on the Surface Morphology and Anticorrosion Performance of the Steel Samples Pretreated by Cr(III) Conversion Coating, CORROSION. 68 (2012) 015008–1. https://doi.org/10.5006/1.3676629.

[29] A. Gardner, J. Scharf, High Performance Alternative to Hexavalent Chromium Passivation of Plated Zinc and Zinc Alloys, SAE International, Warrendale, PA, 2001. https://doi.org/10.4271/2001-01-0644.

[30] American Society for Testing and Materials, ASTMB117-19 Standard Practice for Operating Salt Spray (Fog) Apparatus, (2019). https://compass-astm-org.libproxy.mst.edu/download/B117.14142.pdf (accessed October 22, 2020).

[31] MIL-DTL-81706B Chemical Conversion Materials For Coating Aluminum and Aluminum Alloys, (2004).

[32] E04 Committee, Test Methods for Determining Average Grain Size, ASTM International, n.d. https://doi.org/10.1520/E0112-13.

[33] P. Preikschat, R. Jansen, P. Hulser, Chromate-free conversion layer and process for producing the same, US6287704B1, 2001. U.S.A. Patent.

[34] K. Cho, V. Shankar Rao, H. Kwon, Microstructure and electrochemical characterization of trivalent chromium based conversion coating on zinc, Electrochimica Acta. 52 (2007) 4449–4456. https://doi.org/10.1016/j.electacta.2006.12.032.

[35] S. Hesamedini, A. Bund, Formation of Cr(VI) in cobalt containing Cr(III)-based treatment solution, Surface and Coatings Technology. 334 (2018) 444–449. https://doi.org/10.1016/j.surfcoat.2017.12.006.

II. CHARACTERIZATION OF COBALT CONTAINING AND COBALT-FREE TRIVALENT CHROMIUM PASSIVATION ON γ-ZnNi COATED Al6061-T6 SUBSTRATES

Kevin Foster*Ξ, James ClaypoolΞ, William G.FahrenholtzΞ, Matthew O'KeefeΞ, Tarek NahlawiΛ and Felix AlmodovarΛ

Missouri University of Science & Technology Ξ
401 W. 16th St.
101 Straumanis-James Hall
Rolla, MO, 65409

Dipsol of America Λ
34005 Schoolcraft Rd.
Livonia, MI, 48150

ABSTRACT

The corrosion performance and electrical contact resistance was investigated for a trivalent chromium passivation and a cobalt-free version of that same passivation on γ-ZnNi coated Al 6061-T6. Both passivations had similar surface morphology, were amorphous, had similar thicknesses, and contained pores within the passivation layer. The cobalt-containing passivation initially had an exchange current density of 9.5 X 10^{-4} A/cm^2 and a polarization resistance of 290 Ω/cm^2. The cobalt-free passivation initially had an exchange current density of 10.6 X 10^{-4} A/cm^2, and a polarization resistance of 116 Ω/cm^2. After 500 hours of exposure to neutral salt spray, the cobalt-containing passivation showed no visible corrosion, had an exchange current density of 2.9 X 10^{-4} A/cm^2, and a polarization resistance of 136 Ω/cm^2. The cobalt-free passivation showed uniform corrosion, had an exchange current density of 5.2 X 10^{-4} A/cm^2, and a

polarization resistance of 80 Ω/cm^2. After 500 hours of exposure to neutral salt spray on specimens with scribes down to the Al substrate, the cobalt-free passivations were uniformly corroded, but scribed specimens with the cobalt-containing passivations were only partially corroded. Both the cobalt-containing and cobalt-free passivations were found to be viable alternatives to hexavalent chromium per the requirements of MIL-DTL-81706 with cobalt-containing offering protection comparable to hexavalent chromium and cobalt-free offering less. The presence of cobalt in the TCP was found to improve corrosion performance and suggested that an intermediate species such as cobalt is beneficial to the oxidation of Cr(III) to Cr(VI).

Keywords: TCP, trivalent chromium passivation, corrosion protection, Al6061-T6, hexavalent chrome, contact resistance, MIL-DTL-38999, MIL-DTL-81706, cobalt

1. INTRODUCTION

Cadmium coatings have long been used to protect various metals from corrosion[1,2]. The carcinogenic[3–5], teratogenic[6], toxicological[7–9], and environmental[10] effects related to the use of cadmium led to a search for alternative coatings that were less toxic. Many alternatives were investigated and found to be viable replacements, including γ-ZnNi coatings[11–13]. ZnNi coatings protect the underlying metal in a manner similar to galvanization by acting as a sacrificial anode. While ZnNi coatings alone offer some corrosion resistance, these coatings are often passivated to increase the functional lifespan of the coated components.

Hexavalent chromium is an anti-corrosion passivation that can be used to protect sacrificial coatings due to its active corrosion inhibition mechanism that allows protection of damaged areas of the passivation or flaws in passivation after deposition[14–16]. While hexavalent chromium is an excellent passivation, it is also a human carcinogen[17,18] and toxicological[19,20] environmental contaminant. These negative health effects prompted regulatory agencies in the United States and European Union to limit usage and industrial exposure to hexavalent chromium resulting in a need for alternative passivations[21,22]. One potential alternative passivation is based on trivalent chromium.

Investigations into trivalent chromium passivations (TCPs) have shown excellent anti-corrosion performance on many substrates[23–28] including ZnNi alloys[29–31]. TCPs utilize Cr(III) compounds for corrosion protection, which are the same as the products formed when hexavalent chromium passivations react to protect damaged portions of the passivation. TCPs may also generate some Cr(VI) species during deposition or use, although a lesser degree of active corrosion protection has been demonstrated for TCPs compared to chromate conversion coatings[25,32,33]. Many different chemical solutions can be used to deposit TCPs, but solutions that contain cobalt lead to improved corrosion performance of TCPs in salt spray testing[34,35]. Despite the improvement seen by additions of cobalt, a hexavalent chromium alternative that does not contain cobalt is needed since the European Union already has some industrial restrictions on cobalt with an expectation that even stricter regulations will be passed in the future[36].

Improvement in corrosion performance of TCPs that contain cobalt has not been consistently reported. Many studies test corrosion performance of passivated test coupons by measuring the time it takes until white rust is observed on passivated ZnNi

coatings, which varies from ~120 hours[37] to ~450 hours[30] for TCPs. Since some TCPs without cobalt additions outperformed other TCPs with cobalt additions, a cobalt-free TCP could be produced that would exhibit comparable performance to a cobalt-containing TCP. Previous work on ZnNi coated SAE 1008 steel substrates showed that a cobalt-free TCP performed just as well as a cobalt containing TCP[38].

The goal of this research was to characterize the corrosion performance and electrical contact resistance of a cobalt-containing and cobalt-free TCP on γ-phase ZnNi coated Al 6061-T6 substrates. The TCP passivations were compared against a commercial hexavalent chromium passivation to see if they could be considered a viable alternative.

2. EXPERIMENTAL

2.1. SPECIMEN PREPATATION

Test coupons that were 254 mm by 76 mm by 1 mm were sectioned from a sheet of Al6061-T6 as per MIL-DTL-81706B[39]. The sectioned panels were sent to a commercial vendor for deposition of an electroless nickel layer that was nominally ~5 µm thick. Next, panels were immersed for five minutes in an aqueous solution containing 90 mL/L of an alkaline cleaner (523-SC, Dipsol of America) at 55°C then immersed for 60 s in an aqueous solution containing 40 wt% HCl and 60 g/L of a surface activator (971-SC, Dipsol of America) at ambient temperature. A commercial γ-ZnNi coating (IZ-C17+, Dipsol of America) was deposited by electroplating at 300 A/cm2 for twenty-five minutes. Panels were then either left unpassivated (bare) or passivated with

one of three coatings, a trivalent chromium passivation (TCP; IZ-264, Dipsol of America), an experimental cobalt-free version of the TCP (Co-Free; modified IZ-264, Dipsol of America), or a hexavalent chromium conversion coating (HexCr; IZ-258, Dipsol of America). Depositions of passivations began with surface activation by immersion for 15s in an aqueous solution containing 1 mL/L HCl followed by two rinses of 30 s each in deionized (DI) water. Panels were then immersed in the deposition bath for 90 s, drained for 25 s, followed by a 30 s rinse in DI water, a 30 s rinse in 71-82 °C DI water, and drying at ambient temperature in ambient atmosphere. Prior to testing, specimens were rinsed with acetone followed by DI water and allowed to dry for 24 hours. Some panels were scribed with an "X" to a depth of ~10 μm through the middle of the panel using a 1/16" diameter endmill and a computerized numerical control machine (Model 5400, Sherline Products Inc.).

2.2. CHARACTERIZATION

Electrical contact resistance was measured using a custom-built apparatus consistent with MIL-DTL-81706B. The apparatus has a 1 in^2 copper top electrode and a 2.4 in^2 copper bottom electrode. Prior to measurements, the copper electrodes were polished with 240 grit SiC paper (50-10015, Allied High Tech Products) for 30 seconds then rinsed with soapy water and ultrasonically cleaned in ethanol (90.4%, Fisher Scientific). The electrodes were then dried with a heat gun and allowed to sit for 24 hours prior to any measurements being taken. The power source for the resistance measurements was a source measure unit (2450 Sourcemeter, Keithley 1.00 Amp, Power Line Cycles = 10, 4-wire resistance measurement mode). Measurements were

made at 10 points on the panel surface in the order and locations specified in MIL-DTL-81706B.

Salt spray exposure (SSE) was performed in a chamber (Cyclic Corrosion Tester, Q-Fog) according to ASTM B117 with sodium hydroxide (10.0 N, Alfa Aesar) or hydrochloric acid (36.5%, Fisher Scientific) added to maintain neutral pH[40]. Panels were exposed to salt spray for 0, 168, 336, 500, or 1000 hours. Each passivation had three panels for 0 hours exposure and one scribed panel at all other conditions except for HexCr, which only had two panels at 0 hours and had no panels at 1000 hours because three panels from the original set were not of acceptable quality. After undergoing SSE for the pre-determined amounts of time, panels were removed from the chamber and rinsed in DI water with light abrasion provided by a nitrile glove covered hand for either 30 seconds or until no salt was being removed from the surface, whichever was longer.

2.3. IMAGING

Specimens were imaged before and after SSE using a printer/scanner and a digital optical microscope (KH-8700, Hirox). Computerized image analysis (ImageJ, 1.52a; National Institute of Health) was used to determine the fraction of the panel area covered by corrosion product on unscribed specimens by tracing the regions where corrosion product was visible and dividing that by the total exposed area of the specimen. For scribed specimens, computerized image analysis traced the corroded areas on the X-shaped scribes and divided the measured area by the total area of the scribe to determine the extent of corrosion in scribed areas. The area density of cracks was determined utilizing a method similar to ASTM E112-13 calculating the lineal mean intercept with

computerized image analysis[41]. Electron microscopy specimens approximately 1 cm by 1 cm for electron microscopy were cut from larger panels using a shear cutter and a low speed saw (Isomet 11-1280-160, Buehler). Scanning electron microscopy (SEM) was performed on two different instruments (S-4700, Hitachi or e-Line plus, RAITH). Corrosion product from a Co-Free TCP specimen after 1000 hours SSE was analyzed via X-ray diffraction (XRD; X'Pert Pro, Panalytical, Cu Kα = 1.540598 Å, fixed slit = 0.38 mm).

Liftouts for transmission electron microscopy (TEM) were produced using focused ion beam (FIB) milling (Scios, FEI) with a gallium source. A scanning TEM (STEM; F20, Tecnai) was used to image liftout specimens. Liftouts were produced by choosing a representative section of the surface and depositing platinum in a 15 µm by 1.5 µm rectangle with the electron beam at 5 kV and 1.4 nA beam current to a thickness of 200 nm. The ion beam was then used at 30 kV and 0.28 nA beam current to deposit platinum to a thickness of 1.5 µm. A 20 µm by 12 µm rectangle cross-section pattern was then milled to a depth of ~6 µm with the ion beam at 30 kV and 21 nA and then repeated on the other side. The sample was further milled from the edge of the platinum to 1.5 µm away from the platinum on both sides at a current of 6.5 nA. A U-shaped cut was made to almost separate the cross-section and a tungsten probe welded onto one corner at the top with platinum. The liftout was removed by finishing the cut and welded onto a Cu TEM grid post and thinned to electron transparency by tilting +/- 2° by using 2.8 nA beam currents for bulk removal followed by 0.46 nA currents for the final thinning. The last step consisted of a 28 pA cleaning of each side at a 7° tilt for two minutes.

Computerized image analysis was used to measure passivation thickness by drawing 30 lines perpendicular to the passivation on randomly selected parts of the images and averaged over all images. Passivation morphology was characterized using computerized image analysis by performing a fast Fourier transform on a section of the image that only contained the passivation layer.

2.4. ELECTEROCHEMICAL CHARACTERIZATION

A flat cell with a saturated calomel reference electrode (+0.244 V vs. SHE at 25°C) and 250mL of 0.6 M NaCl (Fisher Scientific, Granular USP/FCC) + 0.6 M $NH_4(SO_4)_2$ (Fisher Scientific, Certified ACS) pH 5.3 electrolyte was used for all electrochemical testing. A potentiostat/galvanostat (Model 273A, Princeton Applied Research) and a frequency response analyzer (SI 1255 HF, Solartron Instruments) supplied the electrical signal for all electrochemical testing. Electrochemical tests were performed in order of open circuit potential (OCP) measured for 4000 seconds, followed by five replicates of electrochemical impedance spectroscopy (EIS) from 105 to 10-2 Hz at an amplitude of ±10 mV vs. OCP, and finished with a potentiodynamic polarization (PDP) ranging from -0.3 V to 0.8 V and back to -0.3 V vs. OCP at a rate of 0.1667 mV/second. Each specimen had electrochemical testing performed three times on three different areas to assess repeatability. OCP and PDP data were analyzed using CView (3.5h, Scribner Associates) software to perform Tafel analysis at the corrosion potential and correlating the data with observations of the flat cell made during the PDP. EIS data was analyzed using ZView (3.5h, Scribner Associates) to fit equivalent circuit models

and validate data using a Kramers-Kronig fit. Values obtained were averaged across data obtained from each electrochemical test for each analyzed specimen.

3. RESULTS

3.1. APPEARANCE

The first aspect of the test specimens examined was the physical appearance after different SSE times. Initially, test panels showed a mostly uniform appearance throughout the interior sections of the panel while edges of the panels took on a darker coloration that corresponded with increased open porosity left behind by gas evolution during electroplating the ZnNi coating. The bare ZnNi panels had a light grey color, TCP panels had a light blue appearance, Co-Free panels had a darker grey/light brown appearance, and the HexCr panels had a dark brown appearance (Figure 1). Upon SSE (Figure 2), bare ZnNi specimens were completely covered in white corrosion product, no change in the appearance was noted for TCP after 1000 hours, Co-Free specimens exhibited 39% corrosion coverage at 168 hours and complete uniform corrosion by 336 hours, and the HexCr panels showed a steady change in color towards more gray at every step of SSE but no visible corrosion. Examination of Figures 1 and 2 demonstrates the degree to which the HexCr panels change color and the difference in appearance between the corrosion product present on the Co-Free vs. bare ZnNi specimens. For the unscribed condition, TCP and HexCr offer excellent resistance to corrosion while Co-Free begins to corrode at 168 hours and is then uniformly corroded at every condition after 168 hours, although much less corroded than unpassivated ZnNi.

When scribed panels underwent SSE, all panels except HexCr experienced at least some degree of corrosion. Figure 3 shows how scribes affected the corrosion of all passivated panels while Figure 4 shows representative optical micrographs of the scribed sections demonstrating commonly observed features on all passivations. TCP had moderate and increasing amounts of severe localized corrosion with areas of uniform corrosion within the scribe ranging from surface area coverages of 20% for 168 hours, 43% for 336 hours, 51% for 500 hours, and 84% for 1000 hours of salt spray. TCP showed mixed corrosion results across all SSE conditions with the areas of severe localized corrosion marked by dark brown and white corrosion product visible within the scribe, areas of a thin brown colored corrosion product, and areas where the metal was still shiny and uncorroded. TCP also showed cracks around some of the corroded spots within and outside of the scribe. Co-Free showed complete, 100% surface area corrosion coverage of the scribed area at all levels of SSE with more severe corrosion within the scribe compared with the passivated panel surface. Scribed HexCr panels initially looked free of corrosion, but under microscopic inspection, small areas of corrosion product were scattered throughout the scribe with increasing coverage of 11% corrosion coverage area at 168 hours, 16% at 336 hours, and 24% at 500 hours.

3.2. ELECTRICAL CONTACT RESISTANCE

Comparisons of the electrical contact resistance of each specimen before and after SSE showed TCP and HexCr maintained low resistance until 1000 hours SSE while Co-Free maintained low resistance only until 168 hours SSE. Presented in Table 1 and shown in Figure 5, unpassivated ZnNi had an average contact resistance of 0.063 ± 0.035

mΩ prior to SSE but had the greatest electrical contact resistance after 168 hours of SSE at 310 ± 470 Ω. With a standard deviation nearly 150% larger than the measured average, the contact resistance measurements of heavily corroded samples were unreliable. TCP showed the best contact resistance during corrosion with an initial resistance of 0.5 ± 0.2 mΩ and a final resistance after 1000 hours SSE of 1.1 ± 0.3 mΩ. Co-Free had an initial resistance of 0.5 ± 0.1 mΩ and only had a slight increase in average resistance after 168 hours SSE to 1.2 ± 1.2 mΩ but with a large increase in variability that began to make the measurements unreliable. After 336 hours, average values and standard deviations both increased into the single ohm range representing an increase of three orders of magnitude. HexCr had an average initial resistance of 6.4 ± 3.3 mΩ but decreased after 168 hours of hours SSE to 3.0 ± 1.5 mΩ and after 336 hours of SSE to 2.8 ± 1.0 mΩ, but then increased after 500 hours of SSE to 4.2 ± 2.1 mΩ.

3.3. MORPHOLOGY

Examination via optical microscopy of the specimen surfaces before and after SSE showed that Co-Free passivations initially had some cracks present that could only be seen on ZnNi after corrosion had taken place. Figure 6 shows the initial state of the passivations, which consists primarily of differences in color and cracks in Co-Free that look similar to the cracks near the scribed locations of the TCP panels in Figure 4. Measurement of the cracks in Co-Free showed the density was about 32 per mm. After SSE, TCP had no discernable changes on the unscribed specimens for all conditions while Co-Free specimens had a thin transparent layer of corrosion product across much of the surface with isolated spots of crystalline platelets after 168 hours (Figure 7).

Unpassivated ZnNi at all SSE times and Co-Free at times beyond 168 hours were completely covered in a thick layer of corrosion product where some cracks could be seen underneath the corrosion product on the ZnNi specimens. HexCr specimens showed a change in color with some pores and removed portions of the ZnNi coating leaving discolored streaks.

Scanning electron microscopy images showed little difference between ZnNi, TCP, and Co-Free surfaces prior to SSE. The features in the corrosion product on Co-Free after SSE were much larger than the underlying ZnNi features. Figure 8 shows that prior to SSE the ZnNi coating had the roughest/most angular surface features while TCP had the smoothest surface features. The cracks that were visible on the Co-Free optical micrographs were not easily visible on the SEM images as the cracks generally followed along the intergranular boundaries of the ZnNi coating. HexCr was found to have a rough surface with cracks going visibly down into the passivation layer. After SSE, the TCP specimens showed little difference aside from the presence of sub-micron structures sparsely scattered across the surface believed to be salt that did not wash away during the DI water rinse. The corroded Co-Free surface developed structures about five times larger than the ZnNi nodules that originally comprised the surface which exhibited a large amount of roughness and porosity.

Transmission electron microscopy images of the TCP and Co-Free specimens taken before and after SSE showed that both passivations had similar thickness and porosity prior to SSE. In Figure 9 the average measured thickness for TCP was 82 ± 20 nm before SSE and 74 ± 4 nm after 1000 hours. No signs of corrosion product were observed at any SSE time for any of the TCP specimens. Internal porosity, which was

also present in a previous study of the same passivations on 1008 steel substrates[38], can be seen throughout the passivation and consistently decreased after 1000 hours SSE. The thickness of Co-Free was 72 ± 5 nm before SSE and exhibited corrosion product growth until the passivation was completely replaced by an approximately 6 µm thick layer of by 1000 hours SSE that left no trace of the Co-Free passivation. Co-Free showed similar initial internal porosity to the TCP. Both passivations were determined to be amorphous according to a fast Fourier transform of diffraction patterns done on sections completely contained within the passivation layer.

X-ray diffraction was utilized to investigate the corrosion product scraped from a Co-Free TCP after 1000 hours of SSE. Analysis of the spectrum (Figure 10) indicated that the corrosion product consisted of zinc carbonate hydroxide hydrate ($Zn_4CO_3(OH)_6 \bullet H_2O$), zinc chloride hydroxide hydrate ($Zn_5(OH)_8Cl_2 \bullet H_2O$), and a small amount of the underlying ZnNi substrate (Ni_5Zn_{21}). These findings were consistent with the corrosion product of unpassivated ZnNi seen in a previous study[38] by the authors.

3.4. ELECTROCHEMICAL CHARACTERIZATION

OCPs of the passivations were compared after different SSE times and showed a general trend of Co-Free having the most noble potential followed by HexCr and then TCP. The top half of Figure 11 shows that before any SSE all passivations had OCPs more noble than the 1.09 V OCP of unpassivated ZnNi indicating that none of the passivations would initially provide galvanic protection to the underlying coating. Of these initial values, Co-Free had the most noble at -0.97 ± 0.02 V, HexCr had -0.98 ± 0.02 V, and TCP had -1.04 ± 0.02 V. As SSE time was increased, Co-Free showed no

change in OCP, the OCP for TCP increased until 336 hours to -0.98 ± 0.01 V, then decreased to -1.01 ± 0.01 V at 500 hours, while HexCr increased until -0.93 ± 0.03 V at 336 hours, then decreased to -1.00 ± 0.01 V at 500 hours. Unpassivated ZnNi showed the largest change during SSE increasing to -0.92 ± 0.01 V after 500 hours.

EIS scans showed a large degree of variability across repetitions of the same samples. Validation via the Kramers-Kronig relations indicated that the data were not valid over some portions of the frequency range tested but fit properly in the 10^0 - 10^5 Hz range. For valid regions, variability resulted in model fits of parameters with relative errors in excess of 100% and as such the data were not considered reliable in those regions and excluded from analysis.

Tafel analysis of the PDP data for the passivations before and after SSE indicated that TCP underwent a greater reduction in exchange current density than Co-Free. TCP polarization resistance remained higher than Co-Free at all SSE times while HexCr was consistently high at every exposure time. All passivations as well as the unpassivated ZnNi exhibited a higher Tafel slope (β_a and β_c) on the cathodic vs. the anodic side (Table 2). The exchange current density, i_o, for Co-Free was 10.6 x 10^{-4}A/cm^2 before SSE and 5.2 x10^{-4}A/cm^2 after 500 hours SSE while TCP had 9.5x10^{-4} A/cm^2 before SSE and 2.9x10^{-4} A/cm^2 after SSE. The polarization resistance, Rp, was initially highest on bare ZnNi at a value of 583 Ω/cm^2 with HexCr having the next highest at 382 Ω/cm^2, TCP at 290 Ω/cm^2, and Co-Free with the lowest at 116 Ω/cm^2. After 500 hours of SSE, ZnNi resistance decreased to 76 Ω/cm^2, TCP decreased to 136 Ω/cm^2, Co-Free decreased to 80 Ω/cm^2, and HexCr increased to 644 Ω/cm^2.

4. DISCUSSION

A previous study by Cho et al. showed that chromium-containing corrosion product depositing in the cracks of trivalent chromium conversion coatings could inhibit corrosion for 50 hours via anodic polarization testing and electrochemical impedance spectroscopy[42]. They found that microcracks in the conversion coating were the sites that held the chromium-containing corrosion product until the corrosion product grew large enough to cause the cracks to propagate to the substrate and lead to sudden, heavy corrosion. A few differences exist between the study by Cho et al. and the current work as Cho et al. studied TCP that contained cobalt and was 3 to 12 times thicker than the TCP layer reported here. Since the present passivations were so much thinner but the corrosive environment was similar, the same chromium-containing corrosion product should still be formed whether cracks are present or not and would comprise a larger relative volume of the passivation compared with Cho et al.

One of the differences between the Co-Free and TCP passivations was cracks into the ZnNi layer that were present on the Co-Free but not on the TCP. The cracks may seem like an obvious difference that would be responsible for the decreased corrosion resistance of the Co-Free compared to the TCP; however, the previous study on steel substrates found that neither crack density nor crack width correlated with the corrosion performance of these two passivations on ZnNi coated SAE 1008 steel substrates[38]. Furthermore, the chromium-containing corrosion product cited by Cho et al. could be what is initially formed from the Co-Free passivation layer that then fractures and allows growth of zinc carbonate hydroxide hydrate and zinc chloride hydroxide hydrate over the

entire surface. This result would explain why the Co-Free samples have corrosion that appears different from the unpassivated ZnNi and does not appear to originate from the cracks. The last observation regarding cracks in the passivations is that HexCr showed many more cracks than Co-Free but also had corrosion performance comparable to or exceeding that of TCP. Since HexCr is known to inhibit corrosion through leaching of Cr(VI) ions from the coating into solution that deposit on sites of active corrosion and halt progression via reduction to Cr(III), the cracks could benefit the corrosion inhibition mechanism by providing a greater surface area for Cr(VI) to dissolve and migrate to corrosion sites[43]. For these reasons, cracks alone are not responsible for the difference in corrosion performance.

The exchange current density and polarization resistance of Co-Free and TCP were different before and after SSE. Both passivations start with similar exchange current densities, but as the SSE time increased, the exchange current density of the TCP decreased more than Co-Free, suggesting that any changes to the surface or formation of corrosion product reduces current flow more in cobalt containing TCP passivation than in the Co-Free passivation. While both passivations have a decrease in polarization resistance after SSE, TCP always had a higher polarization resistance and less visible corrosion than Co-Free. This indicates that the presence of cobalt in the passivation results in a process that leads to a more corrosion resistant film.

Bare ZnNi had the lowest exchange current density and highest polarization resistance of all specimens initially. After SSE, when a large amount of corrosion product was visible, bare ZnNi had the highest current density and lowest polarization resistance of all the specimens, reinforcing that passivation of the electroplated ZnNi

coating prevents visible corrosion of the surface. HexCr started with a lower exchange current density and higher polarization resistance among the passivations and showed little change with SSE. Since the lowest current density and highest polarization resistance of unpassivated ZnNi lead to the formation of large amounts of corrosion product, the HexCr, TCP, and Co-Free passivations have exchange reaction(s) that happen at a greater rate than ZnNi corrosion but does not produce visible corrosion product.

The work of Hesamedini and Bund examined the oxidation of Cr(III) to Cr(VI) in TCPs related to fluid filled internal porosity within the passivation layer[33]. They reported that water filled porosity within the TCPs on Zn-coated steel heated in an oxygen containing environment can result in oxidation of chromium species to the Cr(VI) valence state. They concluded that the amount of oxidation was independent of the presence of cobalt but depended upon the amount of porosity in a TCP, with more pores promoting more oxidation through consumption of water. More Cr(VI) in a TCP allows it to exhibit similar active corrosion protection as usually seen in HexCr, such as observed in Guo and Frankel, and could explain the limited corrosion in the TCP scribed specimens after SSE in this study[25]. The scribed sample results where the Co-Free failed to protect the scribe and the TCP partially protected the scribe implies active corrosion protection and that some of the exchange current density measured in TCP could be from Cr(III) to Cr(VI) oxidation while the Co-Free exchange current density is caused by formation of corrosion product. These results suggest that Cr(III) to Cr(VI) oxidation depends upon cobalt contained in the passivation and not the porosity present in the passivation while Hesamedini and Bund argue the opposite. However, when the Co-Free

and TCP passivation were applied to ZnNi coated steel substrates in the previous investigation, similar results to those from Hesamedini and Bund were obtained. This suggests that oxidation of Cr(III) to Cr(VI) can be affected by an interaction with the underlying substrate.

Three differences were observed among the specimens prepared for the previous study of ZnNi coated SAE 1008 steel substrates and the present study: 1) substrate; 2) the presence of a ~5 µm layer of electroless nickel between the ZnNi and substrate; and 3) heat treatment. Because the aluminum substrate is beneath an electroless nickel layer, the substrate is not be expected to have a direct effect on corrosion of the ZnNi coating surface, although it is possible that the electroless nickel could interact with the corrosive solution at areas where porosity or cracks in the ZnNi would allow the solution to reach the electroless nickel layer. Since no localized corrosion was observed at cracks on Co-Free and with nickel being more noble than zinc, exposure of nickel is not expected to promote reaction of the ZnNi coating during corrosion. Another consideration is that the low hydrogen embrittlement heat treatment that was performed on the steel specimens in the previous study, but not the aluminum specimens in the present study, could play a role through the oxidation mechanism reported by Hesamedini and Bund. More research is needed to confirm this hypothesis. Given the data gathered in the present study, the presence of cobalt influences the corrosion performance of the TCPs by being a beneficial component in the oxidation of Cr(III) to Cr(VI). Since the work of Hesamedini and Bund as well as the previous study done by the authors both used steel substrates and found TCP corrosion resistance to be independent of Co in the coating, it is apparent that oxidation of Cr(III) to Cr(VI) should depend upon an intermediate

species that can be provided by steel substrates or cobalt, and as such TCPs on non-ferrous substrates have corrosion performance improved by cobalt additions.

To answer the question of whether TCPs can be viable alternatives to commercial HexCr for corrosion protection depends upon the requirements of MIL-DTL-8170639. A viable alternative must have an electrical contact resistance of <5 mΩ after passivation and <10 mΩ after 168 hours of SSE. Both the Co-Free and TCP were found to have electrical contact resistances lower than HexCr up to 168 hours of SSE and as such are considered viable alternatives although the extended SSE times and scribed samples tests show that the cobalt-containing TCP offers the best protection.

5. CONCLUSIONS

Both cobalt free and cobalt containing TCPs were viable alternatives to HexCr for ZnNi coated Al 6061-T6 based on the results of this study. The TCP offered a level of corrosion protection comparable to HexCr while the Co-Free offered less protection and had little evidence of active protection. The corrosion test results and electrochemical data suggest that Co additions improve TCP coatings, which is potentially through production of Cr(VI) species as evidenced by the limited active protection displayed by the TCP. Future work will focus on the role of the ZnNi coating, substrate, electroless nickel layer, and heat treatments on corrosion performance as well as measurement of the Cr(VI) content in test specimens to determine whether oxidation of Cr(III) to Cr(VI) is taking place.

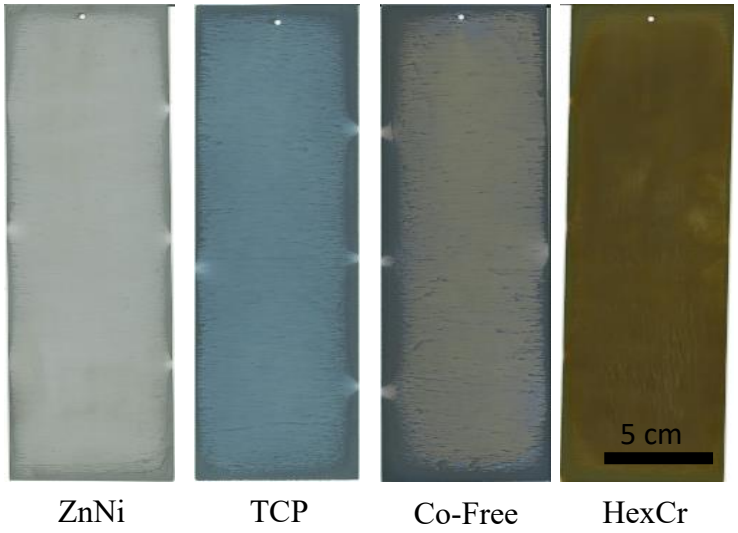

Figure 1. Test specimens as received after acetone cleaning but prior to any testing.

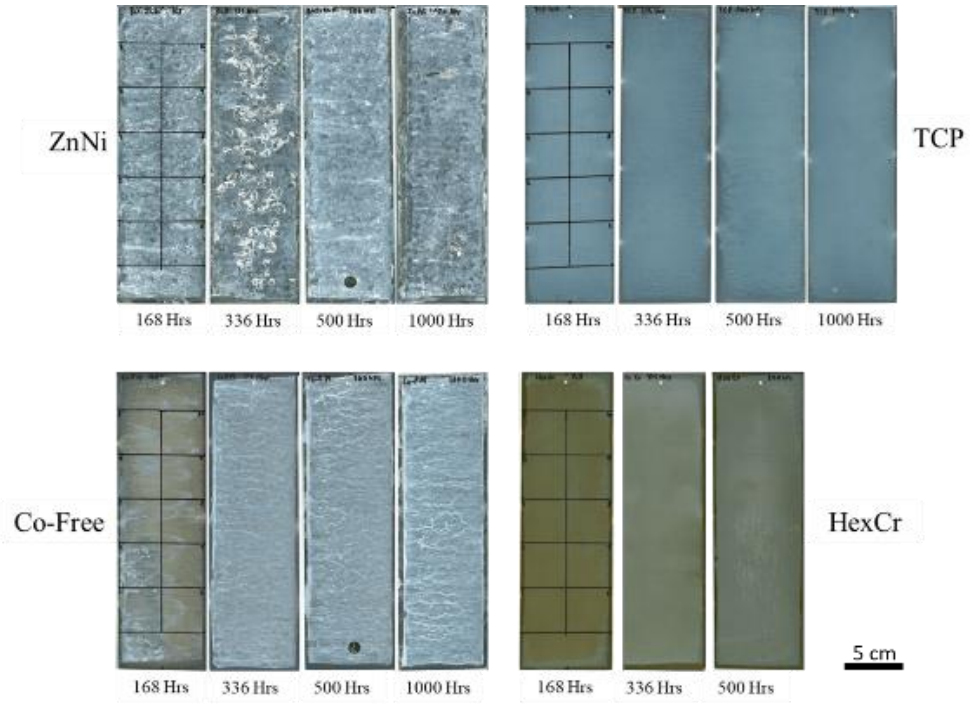

Figure 2. Progression of corrosion with increasing salt spray exposure time for all passivation conditions. Markings on 168 hour SSE panels show where electrical contact resistance measurements were made. Dark circles on bottom of ZnNi and Co-Free 500 hour panels are initial electrochemical tests taken before pictures.

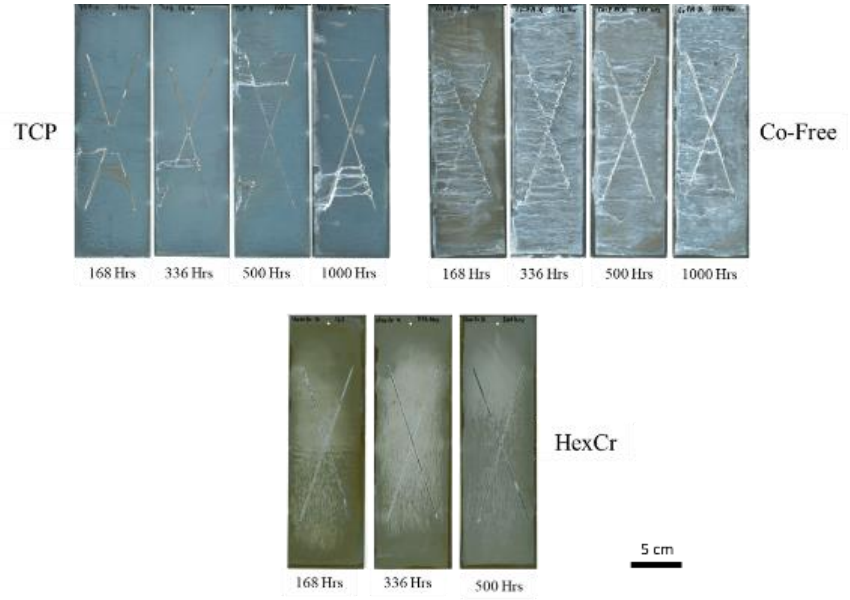

Figure 3. Scribed samples showing corrosion progression of the different passivations at different levels of SSE. Non-metallic spots within scribe of HexCr panels are thin layers of corrosion product that effectively prevent further corrosion.

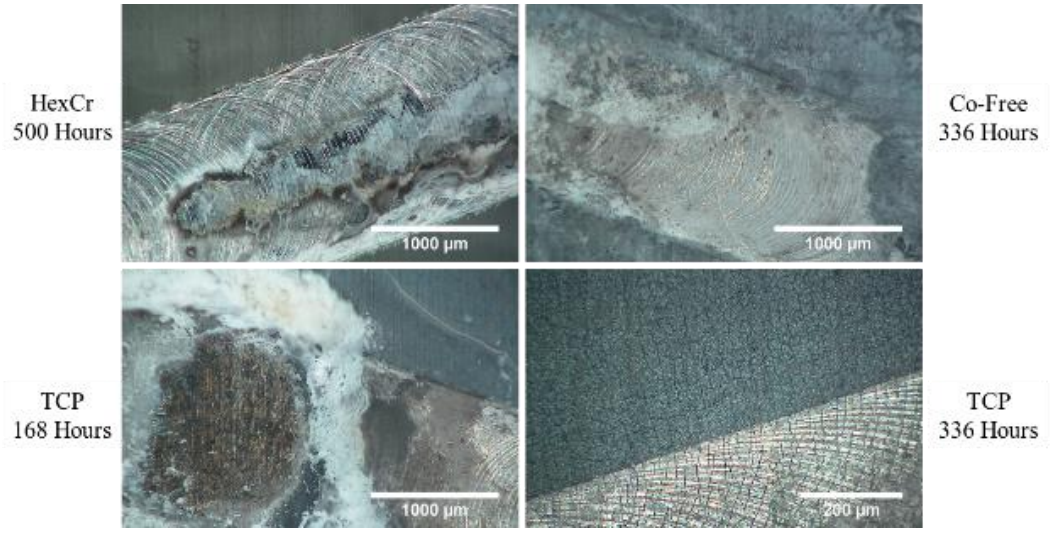

Figure 4. Optical micrographs of specimen scribes to examine active corrosion protection showing shiny metal and corroded patch on HexCr, typical corrosion within a Co-Free scribe, sites of localized and uniform corrosion as well as an uncorroded patch on TCP at 168 hours SSE, as well as the cracks that were observed near some corroded spots on TCP at 336 hours SSE.

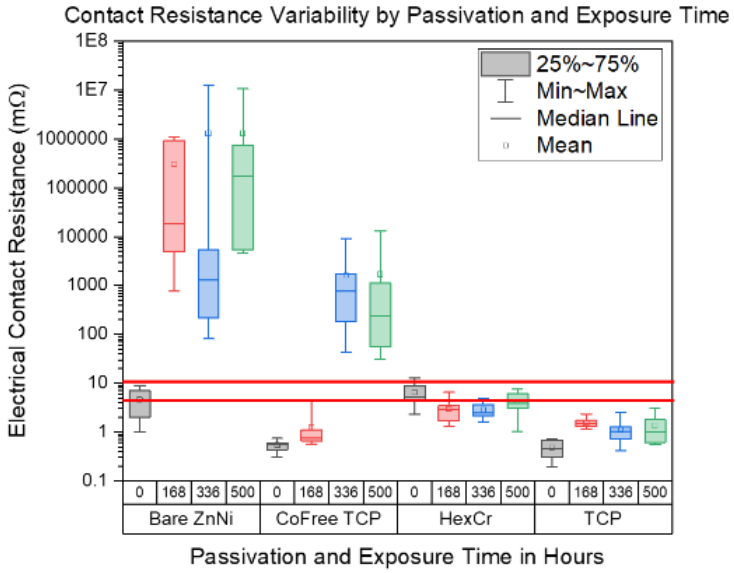

Figure 5. Electrical contact resistance of all samples before and after SSE with total measured range and the difference between medians and means visible to demonstrate variability. Lines marked 0 hours and 168 hours represent resistance requirements to approve passivations from MIL-DTL-81706B.

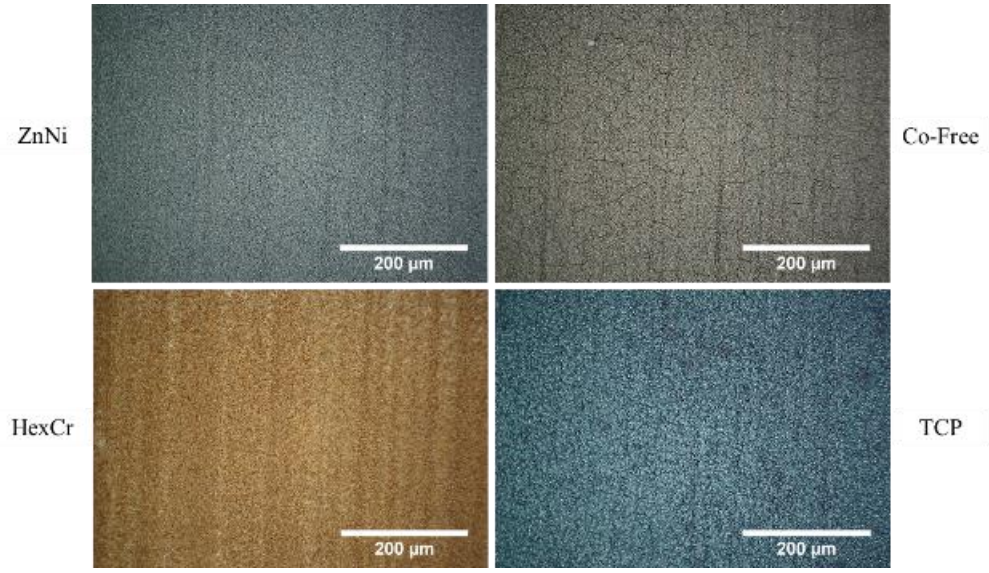

Figure 6. Optical microscopy images of each specimen prior to any SSE. Aside from color changes and the presence of cracks on Co-Free there is little difference between the specimens.

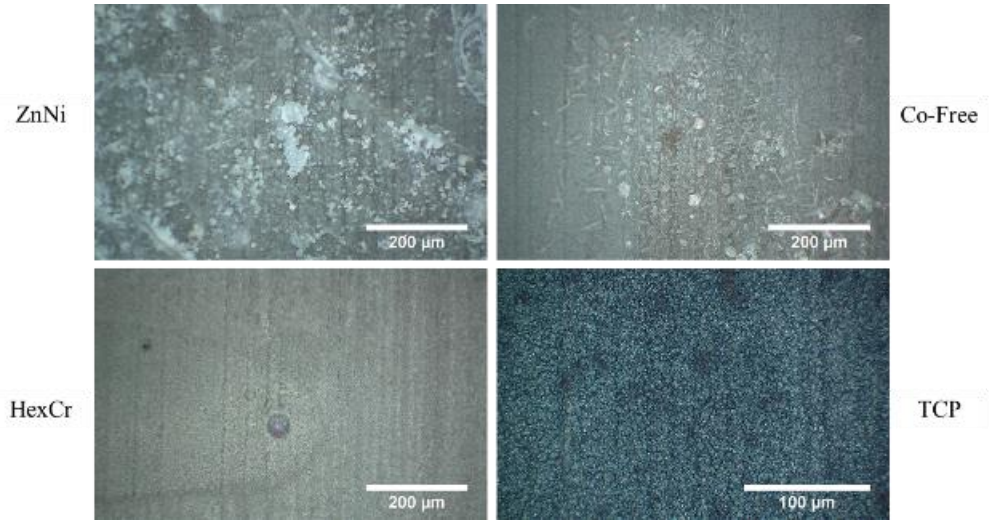

Figure 7. Selected images of specimens after SSE showing no change in TCP, platelet crystals on Co-Free, pore activity on HexCr, and new cracks underneath the corrosion product of bare ZnNi.

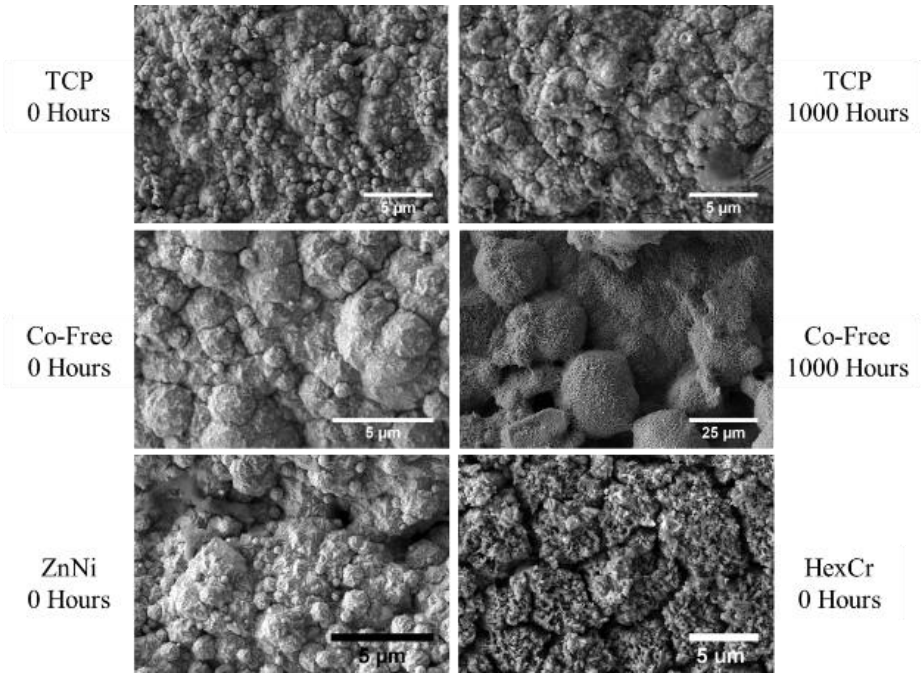

Figure 8. SEM images of the different specimens showing the observed differences between them. The left column compares TCP, Co-Free, and ZnNi prior to SSE while the right column shows the relative lack of change in TCP after 1000 hours SSE compared with Co-Free. HexCr had a surface different from all the other samples, most notably is had many large, deep cracks.

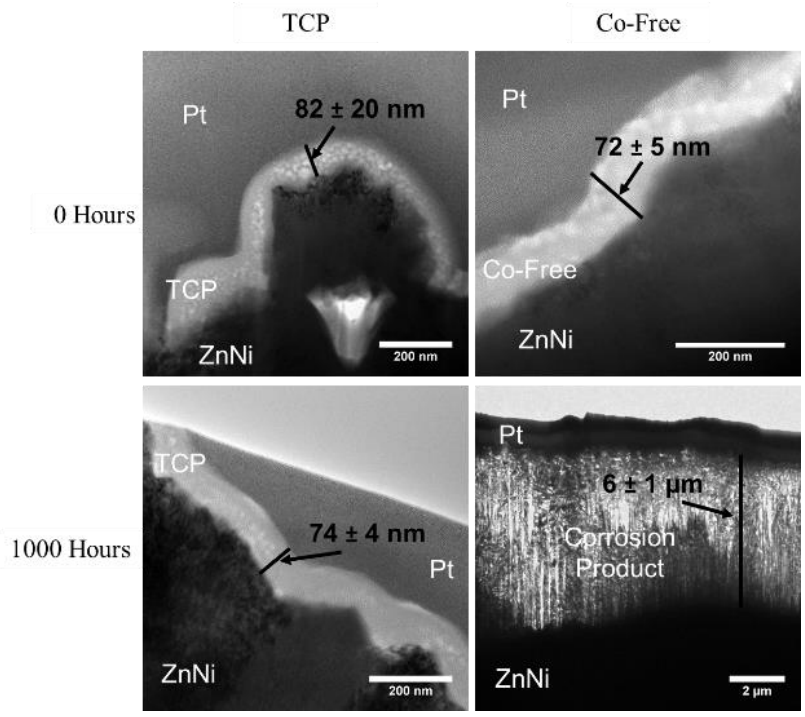

Figure 9. TEM images from TCP and Co-Free liftouts showing the nature of the passivations layers before and after SSE as well as the measured thicknesses at each condition.

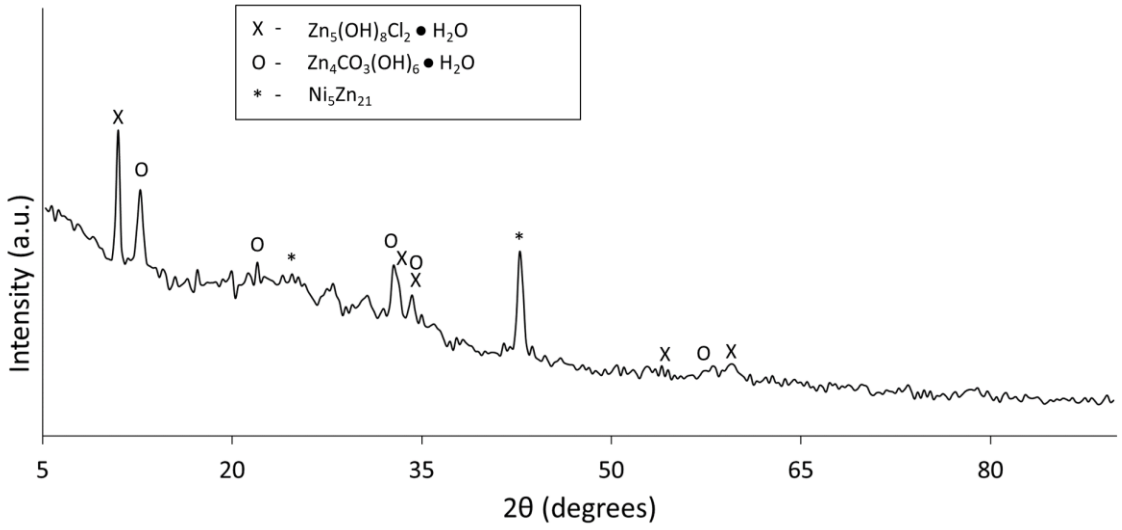

Figure 10. XRD spectrum of corrosion product from a Co-Free TCP sample after 1000 hours of SSE showing the zinc chloride hydroxide hydrate (X), zinc carbonate hydroxide hydrate (O), and a small amount of the underlying ZnNi substrate (*).

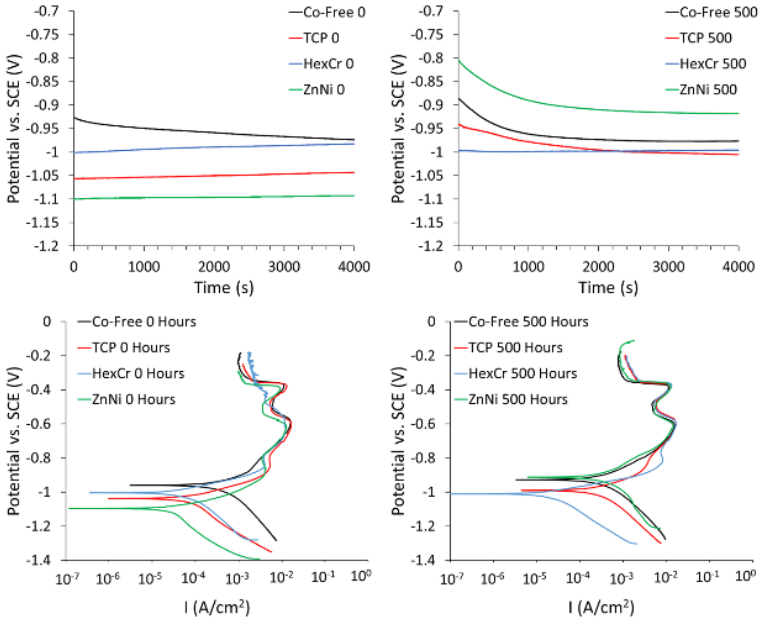

Figure 11. Graphs of OCPs (top) and PDP (bottom) curves comparing all passivations with bare ZnNi before and after SSE exposure.

Table 1. Electrical Contact Resistance Averages and Standard Deviations for all Passivations

		Surface			
SSE Time		Bare ZnNi	TCP	Co-Free	HexCr
0 Hours	Average, mΩ	0.06	0.47	0.54	6.38
	Std. Dev, mΩ	0.04	0.20	0.13	3.26
168 Hours	Average, mΩ	310000	1.50	1.23	2.97
	Std. Dev, mΩ	470000	0.34	1.17	1.55
336 Hours	Average, mΩ	1300000	1.09	1600	2.84
	Std. Dev, mΩ	4100000	0.60	2700	1.01
500 Hours	Average, mΩ	1300000	1.35	1700	4.18
	Std. Dev, mΩ	3300000	0.85	4100	2.07
1000 Hours	Average, mΩ	47000000	1.13	140	-
	Std. Dev, mΩ	50000000	0.30	220	-

Table 2. Tafel Analysis Parameter Values for All Specimens Before and After SSE

	Co-Free 0	TCP 0	HexCr 0	ZnNi 0	Co-Free 500	TCP 500	HexCr 500	ZnNi 500
β_a (mV)	237	136	88	69	157	120	69	277
β_c (mV)	491	336	176	195	256	284	217	422
I_o x 10^4 (A/cm^2)	10.59	9.45	0.63	0.22	5.15	2.88	0.65	9.27
E_o (V)	-0.974	-1.011	-1.031	-1.097	-0.915	-1.001	-1.010	-0.913
R_p (Ω/cm^2)	116	290	382	583	80	136	644	76

CORRESPONDING AUTHOR

Kevin Foster, Missouri University of Science and Technology, klfmkd@mst.edu, 417-860-0460, 401 W. 16th St., Rolla, MO, 65409-1170

AUTHOR CONTRIBUTIONS

The manuscript was written through contributions of all authors. All authors have given approval to the final version of the manuscript. ‡These authors contributed equally. (match statement to author names with a symbol)

FUNDING SOURCES

Authors Foster, Claypool, O'Keefe, Fahrenholtz, Nahlawi, and Almodovar received funding from the Strategic Environmental Research and Development Program (SERDP) through contract WP18-F2-1439.

ACKNOWLEDGMENTS

The authors wish to acknowledge the guidance and support of Dr. Robin Nissan at SERDP along with Steve Gaydos and Dave Zika at Boeing. A special thanks is extended to Dr. Xiaoqing He who produced TEM liftouts at the University of Missouri-Columbia for the project and to Dr. Wei-Ting Chen for operating and assisting with the TEM analysis.

ABBREVIATIONS

DI, deionized; SSE, salt spray exposure; TCP, trivalent chromium passivation; Co-Free, cobalt-free trivalent chromium passivation; HexCr, hexavalent chromate passivation; SEM, scanning electron microscopy; TEM, transmission electron microscopy; OCP, open circuit potential; SHE, standard hydrogen electrode; SCE, saturated calomel electrode; PDP, cyclic potentiodynamic polarization; EIS, electrochemical impedance spectroscopy.

REFERENCES

(1) Johnson, D. M. Zinc And Cadmium Passivating Bath 2559878, **1951**

(2) Cadmium Plating In Surface Engineering; Cotell, C. M.; Sprague, J. A.; Smidt, F. A.; Eds.; ASM International, **1994**; 215–226

(3) Waalkes, M. P. Cadmium Carcinogenesis Mutat. Res. **2003**, 533, 107–120

(4) Huff, J.; Lunn, R. M.; Waalkes, M. P.; Tomatis, L.; Infante, P. F. Cadmium-Induced Cancers in Animals and in Humans Int. J. Occup. Environ. Health **2007**, 13, 202–212

(5) Medical Evaluation of Renal Effects of Cadmium Exposures Occupational Safety and Health Administration

(6) Ferm, V. H.; Carpenter, S. J. Teratogenic Effect of Cadmium and Its Inhibition by Zinc Nature **1967**, 216, 1123–1123

(7) Zhu, Q.; Li, X.; Ge, R.S. Toxicological Effects of Cadmium on Mammalian Testis Front. Genet. **2020**, 11, 527

(8) Edwards, J. R.; Prozialeck, W. C. Cadmium, Diabetes and Chronic Kidney Disease Toxicol. Appl. Pharmacol. **2009**, 238, 289–293

(9) Järup, L. Cadmium Overload and Toxicity Nephrol. Dial. Transplant. **2002**, 17, 35–39

(10) Aquatic Life Ambient Water Quality Criteria - Cadmium 2016; EPA 820-R-16-002 U.S. Environmental Protection Agency, **2016**; 721

(11) Eliaz, N.; Venkatakrishna, K.; Hegde, A. C. Electroplating and Characterization of Zn–Ni, Zn–Co and Zn–Ni–Co Alloys Surf. Coat. Technol. **2010**, 205, 1969–1978

(12) Rajagopalan, S. K. Characterization of Electrodeposited Zn-Ni Alloy Coatings As A Replacement For Electrodeposited Zn and Cd Coatings McGill University, **2012**

(13) Shifler, D. A.; Conrad, R. K.; Sheetz, A. D.; Archer, H. L. Environmental Evaluation of a Cadmium Replacement Coating for Use in a Marine Environment 18

(14) Kendig, M. W.; Davenport, A. J.; Isaacs, H. S. The Mechanism of Corrosion Inhibition by Chromate Conversion Coatings from X-Ray Absorption near Edge Spectroscopy (XANES) Corros. Sci. **1993**, 34 , 41–49

(15) Kendig, M.; Jeanjaquet, S.; Addison, R.; Waldrop, J. Role of Hexavalent Chromium in the Inhibition of Corrosion of Aluminum Alloys Surf. Coat. Technol. **2001**, 140, 58–66

(16) Xia, L.; Akiyama, E.; Frankel, G.; McCreery, R. Storage and Release of Soluble Hexavalent Chromium from Chromate Conversion Coatings Equilibrium Aspects of Cr VI Concentration J. Electrochem. Soc. **2000**, 147, 2556

(17) Benova, D.; Hadjidekova, V.; Hristova, R.; Nikolova, T.; Boulanova, M.; Georgieva, I.; Grigorova, M.; Popov, T.; Panev, T.; Georgieva, R.; Natarajan, A. T.; Darroudi, F.; Nilsson, R. Cytogenetic Effects of Hexavalent Chromium in Bulgarian Chromium Platers Mutat. Res. Toxicol. Environ. Mutagen. **2002**, 514, 29–38

(18) Pellerin C; Booker S M. Reflections on Hexavalent Chromium: Health Hazards of an Industrial Heavyweight Environ. Health Perspect. **2000**, 108, A402–A407

(19) Ray, R. R. Review Article. Adverse Hematological Effects of Hexavalent Chromium: An Overview Interdiscip. Toxicol. **2016**, 9, 55–65

(20) Mishra, S.; Bharagava, R. N. Toxic and Genotoxic Effects of Hexavalent Chromium in Environment and Its Bioremediation Strategies J. Environ. Sci. Health Part C **2016**, 34, 1–32

(21) 1910.1026 - Chromium (VI) | Occupational Safety and Health Administration

(22) Smith, R. Regulation (EC) No 764/2008 of the European Parliament and of the Council. In Core EU Legislation; Macmillan Education UK: London, **2015**, 183–186

(23) Berger, R.; Bexell, U.; Mikael Grehk, T.; Hörnström, S.-E. A Comparative Study of the Corrosion Protective Properties of Chromium and Chromium Free Passivation Methods Surf. Coat. Technol. **2007**, 202, 391–397

(24) Di Sarli, A. R.; Culcasi, J. D.; Tomachuk, C. R.; Elsner, C. I.; Ferreira-Jr, J. M.; Costa, I. A Conversion Layer Based on Trivalent Chromium and Cobalt for the Corrosion Protection of Electrogalvanized Steel Surf. Coat. Technol. **2014**, 258, 426–436

(25) Guo, Y.; Frankel, G. S. Active Corrosion Inhibition of AA2024-T3 by Trivalent Chrome Process Treatment Corrosion **2012**, 68, 045002-1-045002–045010

(26) Kawaguchi, H.; Funatsumaru, O.; Sugawara, H.; Sumiya, H.; Iwade, T.; Yamamoto, T.; Koike, T.; Kashio, R. Development of Trivalent Chromium Passivation for Zn Plating with High Corrosion Resistance after Heating SAE Int. J. Mater. Manuf. **2016**, 9, 833–838

(27) Bellezze, T.; Roventi, G.; Fratesi, R. Electrochemical Study on the Corrosion Resistance of Cr III-Based Conversion Layers on Zinc Coatings Surf. Coat. Technol. **2002**, 155, 221–230

(28) Bhatt, H. Trivalent Chromium Conversion Coating for Corrosion Protection of Aluminum Surface 12

(29) Boin, C. Black Passivation Films without Hexavalent Chromium on Top of Electroplated Layers of Zinc and Zinc Alloys **2007**, 2007-01–2593

(30) Zaki, N. Trivalent Chrome Conversion Coating For Zinc and Zinc Alloys 11

(31) Gardner, A.; Scharf, J. Trivalent Passivation of Plated Zinc and Zinc Alloys—Alternatives to Hexavalent Based Systems Trans. IMF **2003**, 81, B107–B110

(32) Iyer, A.; Willis, W.; Frueh, S.; Nickerson, W.; Fowler, A.; Barnes, J.; Hagos, L.; Escarsega, J.; La Scala, J.; Suib, S. L. Characterization of NAVAIR Trivalent Chromium Process (TCP) Coatings and Solutions Plat. Surf. Finish. **2010**, 32–42

(33) Hesamedini, S.; Bund, A. Formation of Cr(VI) in Cobalt Containing Cr(III)-Based Treatment Solution Surf. Coat. Technol. **2018**, 334, 444–449

(34) Hesamedini, S.; Ecke, G.; Bund, A. Structure and Formation of Trivalent Chromium Conversion Coatings Containing Cobalt on Zinc Plated Steel J. Electrochem. Soc. **2018**, 165, C657–C669

(35) Ramezanzadeh, B.; Attar, M. M. Effects of Co(II) and Ni(II) on the Surface Morphology and Anticorrosion Performance of the Steel Samples Pretreated by Cr(III) Conversion Coating Corrosion **2012**, 68, 015008–1

(36) Cobalt - legislation-obligation - ECHA

(37) Gardner, A.; Scharf, J. High Performance Alternative to Hexavalent Chromium Passivation of Plated Zinc and Zinc Alloys **2001**, 2001-01–0644

(38) Foster, K.; Claypool, J.; Fahrenholtz, W.; O'Keefe, M.; Nahlawi, T.; Almodovar, F. Characterization of Cobalt Containing and Cobalt-Free Trivalent Chromium Passivations on Γ-ZnNi Coated Steel Substrates [Submitted] **2020**

(39) MIL-DTL-81706B Chemical Conversion Materials For Coating Aluminum and Aluminum Alloys Department of Defense **2004**

(40) G01 Committee. Practice for Operating Salt Spray (Fog) Apparatus ASTM International

(41) E04 Committee. Test Methods for Determining Average Grain Size ASTM International

(42) Cho, K.; Shankar Rao, V.; Kwon, H. Microstructure and Electrochemical Characterization of Trivalent Chromium Based Conversion Coating on Zinc Electrochimica Acta **2007**, 52, 4449–4456

(43) Zhao, J.; Frankel, G.; McCreery, R. L. Corrosion Protection of Untreated AA-2024-T3 in Chloride Solution by a Chromate Conversion Coating Monitored with Raman Spectroscopy J. Electrochem. Soc. **1998**, 145, 2258–2264

III. EFFECT OF HEAT TREATMENT ON THE CHROMATE CONTENT AND PERFORMANCE OF TRIVALENT CHROMIUM PASSIVATIONS ON γ-ZnNi

Kevin Foster*Ξ, James ClaypoolΞ, William G.FahrenholtzΞ, Matthew O'KeefeΞ, Tarek NahlawiΛ and Felix AlmodovarΛ

Missouri University of Science & Technology Ξ
401 W. 16th St.
101 Straumanis-James Hall
Rolla, MO, 65409

Dipsol of America Λ
34005 Schoolcraft Rd.
Livonia, MI, 48150

ABSTRACT

The effects of heat treatment and Cr(VI) content on the corrosion performance of trivalent chromium passivations on electroplated γ-ZnNi were examined. Prior to any heat treatment, conventional trivalent chromium passivations had a Cr(VI) content of ~0.35 µg/mL while Co-free trivalent chromium passivations had Cr(VI) contents of less than 0.01 µg/mL. After heat treatment at 80°C, the Cr(VI) content decreased to 0.13 µg/mL for trivalent chromium passivations but increased to 0.06 µg/mL for the Co-free passivations. Heat treatment at 191ºC decreased the detected Cr(VI) to 0.10 µg/mL for trivalent chromium passivations but increased the Cr(VI) content to 0.05 µg/mL for the Co-free trivalent chromium passivations. A positive increase in electrochemical open circuit potential values to ~-0.83-0.84 V was measured for both passivations after heat treatment at 191°C. The corrosion performance of all passivations was found to improve

as the Cr(VI) content increased. Corrosion resistance of trivalent chromium passivations depends upon the amount of Cr(VI) present, which can be altered by the composition of the deposition solution or heat treatment of the coatings.

Keywords: TCP, trivalent chromium passivation, hexavalent chromium, corrosion

1. INTRODUCTION

Various metals can be protected from corrosion by combinations of protective sacrificial coatings and passivating treatments. Among passivating treatments, hexavalent chromium stands out for its excellent corrosion resistance and active corrosion inhibition, which can protect surfaces exposed by damage[1–4]. Unfortunately, hexavalent chromium is toxic[5,6], an environmental contaminant[7], and a carcinogen[8,9]. These negative effects of hexavalent chromium are the primary motivation for research into alternative passivations that remains active today[10,11]. One such alternative passivation is based on trivalent chromium.

Trivalent chromium passivations (TCPs) have excellent corrosion resistance on many different substrates[12–16]. While some evidence shows that TCPs can offer active protection[13,17–19], TCPs do not perform as well as hexavalent chromium coatings in some cases. Cobalt is a common additive in TCP deposition baths. The addition of cobalt produces passivations that perform well in corrosive environments [20,21]. The role of cobalt in enhancement of the corrosion protection of TCPs is not yet known. Previous research in our group has studied the corrosion performance of electroplated γ-ZnNi

passivated with conventional (i.e., cobalt-containing) and cobalt-free TCPs on steel[22], and Al6061[19] substrates.

Our previous studies demonstrated that the corrosion protection mechanism of TCPs on γ-ZnNi depends on substrate interactions and that the presence of cobalt improves the performance of TCPs on non-ferrous substrates[19]. The mechanism includes oxidizing Cr(III) to Cr(VI). However, Cr(VI) contents were not measured as part of the previous study. In addition, a heat treatment step was used for the steel substrates, but not for the Al6061 substrates, which further complicated analysis of the corrosion protection mechanism.

Li and Swain[23] investigated the effect of heat treatment on TCP performance using electrochemical testing. They found that heat treatment at 100°C for 12-18 hours improved corrosion resistance through densification of the passivation, changes in the chemical nature of Cr(III), and fewer defects in the aluminum oxide. Li and Swain also found that increasing the heat treatment temperature to 155°C decreased the corrosion resistance of the coating due to cracking and delamination of the coating from dehydration and increased diffusivity through the passive layer. Hesamedini and Bund[18] deduced that heat treatment resulted in a reaction between the passivation and atmospheric O_2 and H_2O that could oxidize Cr(III) to Cr(VI) independent of the presence of Co in the passivating layer. A different study by Li and Swain[24] identified more noble intermetallic sites on the substrate as locations where O_2 can be converted to H_2O_2 by a two-electron reduction reaction which could then oxidize Cr(III) to Cr(VI). The goal of the present research was to measure the Cr(VI) content of TCP coatings on γ-

ZnNi coated Al 6061 substrates with and without heat treatments to determine the effect on corrosion performance.

2. EXPERIMENTAL PROCEDURE

2.1. SPECIMEN PREPARATION

Al6061-T6 sheets were sectioned into test panels that were 254 mm by 76 mm by 1 mm using a shear cutter. The sectioned panels were plated with a layer of electroless nickel ~5 µm thick by a commercial vendor before having electroplated γ-ZnNi (IZ-C17+, Dipsol of America) applied using the procedure summarized in Table 1. The γ-ZnNi was electroplated using a current density of 300 A/cm^2 for twenty-five minutes to produce a layer ~20 µm thick. Next, the panels were passivated with either a commercial trivalent chromium passivation (TCP; IZ-264, Dipsol of America), or a cobalt-free trivalent chromium passivation (Co-Free TCP; IZ-ASCF02, Dipsol of America). Some panels were left unpassivated to act as a control to compare the studied passivation layers against. Heat treatments chosen for the specimens were 80ºC for 30 minutes or 191ºC for 24 hours done in ambient atmosphere. The heat treatments were chosen to simulate commercially used processes for automotive components (80ºC) and low hydrogen embrittlement bakes for steel (191ºC). The procedure used to prepare panels, deposit passivations, and heat treat coatings is outlined in Table 2. All specimens were cleaned with acetone and rinsed with deionized (DI) water, then allowed to dry for twenty-four hours before testing.

Table 1. Sample cleaning and treatment for electroplating of the γ-ZnNi layer.

Step	Parameter	Material	Temperature	Time
Alkaline Cleaning	90 mL/L	523-SC, Dipsol of America	55°C	300 s
Double Rinse	-	Deionized Water	Ambient	30 s each
Surface Activation	40 wt% 60 g/L	HCl 971-SC, Dipsol of America	Ambient	60 s
Double Rinse	-	Deionized Water	Ambient	30 s each
Electroplating	300 A/cm^2	IZ-C17+, Dipsol of America	25°C	25 mins
Double Rinse	-	Deionized Water	Ambient	30 s each

Table 2. Sample treatment for application and heat treatment of passivating trivalent chromium coatings.

Step	Parameter	Material	Temperature	Time
Acid Activation	1 mL/L	HCl solution	Ambient	15 s
Double Rinse	-	Deionized Water	Ambient	30 s each
Passivation	pH 4.2 pH 4.0	IZ-264, Dipsol of America IZ-ASCF02, Dipsol of America	25°C 25°C	90 s
Drain	-	-	Ambient	25 s
Rinse	-	Deionized Water	Ambient	30 s
Hot Rinse	-	Deionized Water	71-82°C	30 s
Dry	-	-	Ambient	Until Dry
Bake	-	-	80°C 191°C	30 mins 23 hrs

2.2. CHACTERIZATION

Specimens were exposed to neutral salt spray (Cyclic Corrosion Tester, Q-Fog) as described in ASTM B117[25]. The neutral pH of the 5 wt% aqueous NaCl solution was maintained by additions of either hydrochloric acid (36.5%, Fisher Scientific) or sodium hydroxide (10.0 N, Alfa Aesar). Salt spray exposure (SSE) was performed in one week (168 hours) intervals. After removal from the chamber, test coupons were rinsed with DI

water for thirty seconds or until no visible salt remained on the surface, whichever took place first. Specimens were dried with compressed air after rinsing and had a 35 mm by 75 mm section removed for analysis. Visual inspection of test panels resulted in removal from further SSE if a majority of the panel was covered by corrosion product, otherwise panels were put back into the chamber for another 168 hours of SSE.

The amount of Cr(VI) in the passivations was measured quantitatively using a modified version of the screening boiling test for hexavalent chromium in surfaces listed by the Danish Environmental Protection Agency from IEC 62321. Three types of aqueous solutions were used in the hexavalent chromate analysis. The first was 75 wt% phosphoric acid, the second was 1,5-diphenylcarbazide indicator, and the third was Cr(VI) standards. The solutions were produced as follows:

1. 350 mL of 85 wt% phosphoric acid (Acros Organic) was added to 125 mL of DI water in a 500 mL flask and topped to 500 mL with DI water to produce 75 wt% phosphoric acid solution
2. 1.0g of 1,5-diphenylcarbazide (Certified ACS, Fisher Scientific) was added to 100 mL of acetone (HPLC-UV grade, Pharmco) with 1 drop of acetic acid (99.7%, Sigma Aldrich) and mixed until dissolved to produce the indicator solution
3. 0.113g of potassium dichromate (99%, Acros Organic) was added to 1000 mL of DI water and mixed, then 0.5, 1.0, 1.5, 2.0, or 2.5 mL of that solution were added to 450 mL of DI water and brought to 500 mL with DI water to produce the standards containing 0.04 µg/mL, 0.08 µg/mL, 0.12 µg/mL, 0.16 µg/mL, and 0.2 µg/mL of Cr(VI).

Chromate analysis was performed by placing a coating with 50 ± 5 cm^2 of exposed surface area in a beaker with 50 mL of DI water with a layer of boiling stones. The beaker was covered with a watch glass and brought to a boil for 10 minutes. After boiling the resulting solution was transferred to a sample container and filled to 50 mL with DI water and manually swirled for 15 seconds. One mL of 75 wt% phosphoric acid solution was added to the test solution and swirled for 15 seconds followed by removal of 1 mL of test solution into a 1 cm cuvette as a blank for analysis. Then, 1 mL of 1,5-diphenylcarbazide indicator solution was added to the test solution and swirled manually for 15 seconds followed by removal of 1 mL of test solution into a 1 cm cuvette for analysis. As specimens were sectioned following each SSE exposure time to produce analytical samples, only enough material was available to run each DPC test once per test condition.

UV-VIS spectrophotometry of the solutions was performed using a Thermo Scientific Genesys 10UV that was calibrated using the Cr(VI) standards described above with the calibration curve shown in the Appendix. All samples were tested immediately after preparation with a time of no longer than 20 minutes between boiling and finished analysis. For analysis, the blank was analyzed first followed by the sample. The concentration of chromate was determined by subtracting the absorbance of the blank from the sample value. Due to the amount of material required for analysis, only one sample was produced from each test specimen.

Validation of this Cr(VI) detection method was performed by taking a section of an TCP panel with no heat treatment that had 0 hours of SSE and repeating the test on the same panel to see if any Cr(VI) would be present after boiling in the first test. Results of

this test detected 0.377 µg/mL Cr(VI) on the first 10 minute boil and 0.011 µg/mL on the second boil, an amount below the limit of detection for the analytical method. If the 0.011 µg/mL is assumed to be entirely signal and not noise, then the 10 minute immersion in boiling water should recover ~97% of Cr(VI) in the TCP layers.

2.3. IMAGING

Corrosion progress and coating morphology were examined before and after SSE by imaging using a printer/scanner and digital optical microscope (KH-8700, Hirox). Computerized image analysis (ImageJ, 1.52a; National Institute of Health) was used to determine the area fraction of exposed surface covered in corrosion product or exhibiting discoloration after rinsing and drying following every interval of SSE. Area fraction was calculated by tracing corroded or discolored regions of each specimen with the polygon tool and dividing by the total exposed area. Any test panel exhibiting corrosion across the entire surface was not further analyzed.

2.4. ELECTROCHEMICAL CHARACTERIZATION

All electrochemical testing was performed using 250 mL of 0.6 M NaCl (Fisher Scientific, Granular USP/FCC) + 0.6 M $NH_4(SO_4)_2$ (Fisher Scientific, Certified ACS) electrolyte at a pH of 5.3 in a flat cell with a saturated calomel reference (SCE) electrode (+0.244 V vs. SHE at 25°C). The electrical signal was provided by a potentiostat/galvanostat (Model 273A, Princeton Applied Research) for open circuit potential (OCP) and potentiodynamic polarization (PDP). First, OCPs were measured for 7200 seconds followed by PDPs that swept from -0.3V to 0.8V vs. OCP at a rate of

0.1667 mV/second. Electrochemical tests were performed in triplicate for repeatability. Analysis of OCP and PDP data utilized CView (3.5h, Scribner Associates) software to compare results across test conditions and correlate data to corrosion performance. All electrochemical data reported are values averaged across valid collected data sets for each specimen.

3. RESULTS

3.1. APPEARANCE

The initial appearance of the test coupons varied among all experimental conditions with the greatest differences due to the heat treatment. Figure 1 shows representative test coupons before testing or SSE. The bare ZnNi specimens had a dull grey color with shiny reflective interior regions surrounded by matte edges. Specimens with a TCP coating had a darker purple-blue appearance after the 80°C heat treatment. Increasing the heat treatment to 191°C resulted in a strong brown color with some purple regions throughout. Specimens with a Co-free TCP coating showed little change in appearance between heat treatments and held a light-blue color with some purple regions.

After 168 hours of SSE, some corrosion was observed on all specimens. The unpassivated ZnNi panels were fully covered in corrosion product. The Co-free TCP heat treated at 80°C had 41 ± 7% area covered in corrosion product while the Co-free TCP at 191°C had 26 ± 10% area covered in corrosion product. The TCP specimens heat treated at 80°C exhibited 10 ± 1% of the area covered in discoloration. The TCP heat treated at 191°C had a similar amount of discoloration at 8 ± 1%.

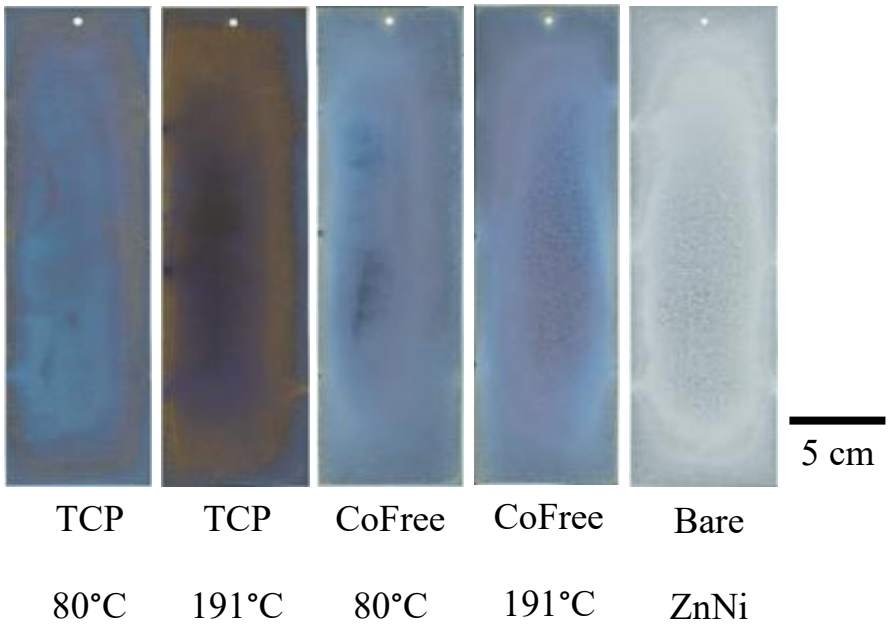

Figure 1. Visual appearance of test specimens showing the differences between heat treated passivating coatings.

After 336 hours of SSE, all specimens showed more signs of corrosion (Figure 2). For the passivated specimens, the Co-free TCP specimens heat treated at 191°C had less corrosion than the Co-free TCP specimens heat treated at 80°C with 42 ± 5% corrosion coverage compared with 55 ± 6%. The TCP specimens heat treated at 80°C showed more visible corrosion than at 168 hours SSE with 27 ± 6%. TCP specimens heat treated at 191°C exhibited 9 ± 1% corrosion coverage.

The TCP specimens retained a similar appearance after 336 hours of SSE. The TCP specimens heat treated at 80°C showed multiple streaks of color change while the TCP specimens heat treated at 191°C showed multiple scattered areas of color change. In contrast to TCP specimens, all of the Co-free TCP specimens had visible corrosion

product on the surfaces. As a result, the Co-free TCP specimens did not undergo additional SSE after 336 hours.

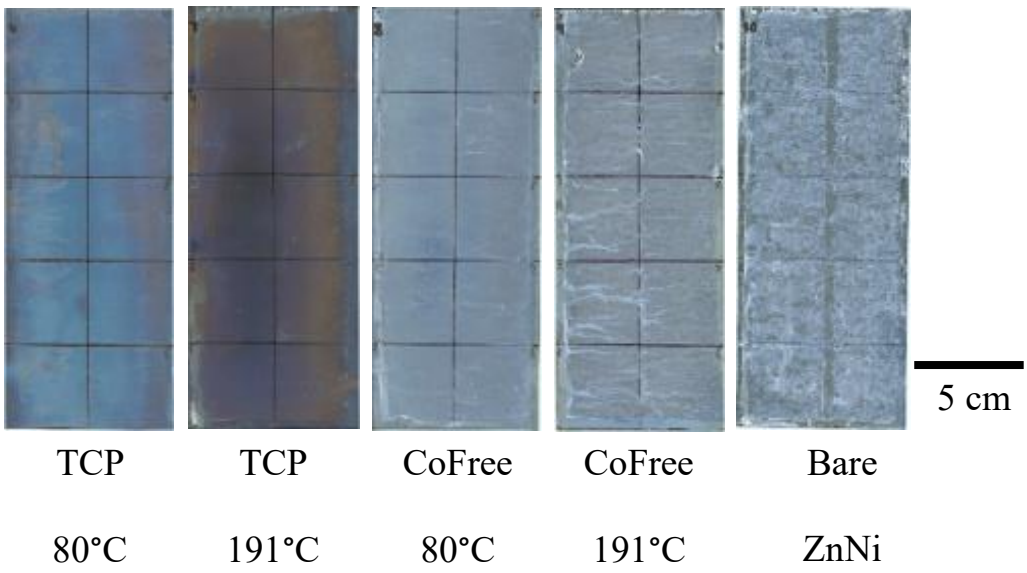

Figure 2. Test specimens after 336 hours of SSE. The marked areas were guides to section the samples for later analysis.

The TCP specimens were returned to the salt spray chamber and exposed for a total of 672 hours of SSE. After this extended time, the panels were not completely covered in corrosion product and were returned to the salt spray chamber for 1000 hours of total salt spray exposure. The TCP specimen heat treated at 80°C was removed for being nearly completely covered in discoloration at 1000 hours of SSE and the remaining samples placed back into the chamber for SSE until failure. The TCP specimens heat treated at 191°C lasted until 1359 hours of SSE before developing visible corrosion product across their entire exposed surface. After 1359 hours of SSE, there were no more specimens that resisted corrosion resulting in no further tests.

3.2. MORPHOLOGY

Optical micrographs taken prior to SSE are shown in Figure 3. The sample morphology at this scale was dominated by ZnNi features that grew from roll marks of the underlying Al 6061 substrate during electroplating. The most notable difference was that the Co-free TCP specimens had cracks through the ZnNi coating. In contrast, the TCP specimens and bare ZnNi specimens had no visible cracks. After SSE, specimens other than bare ZnNi showed localized areas of both pristine and corroded surfaces.

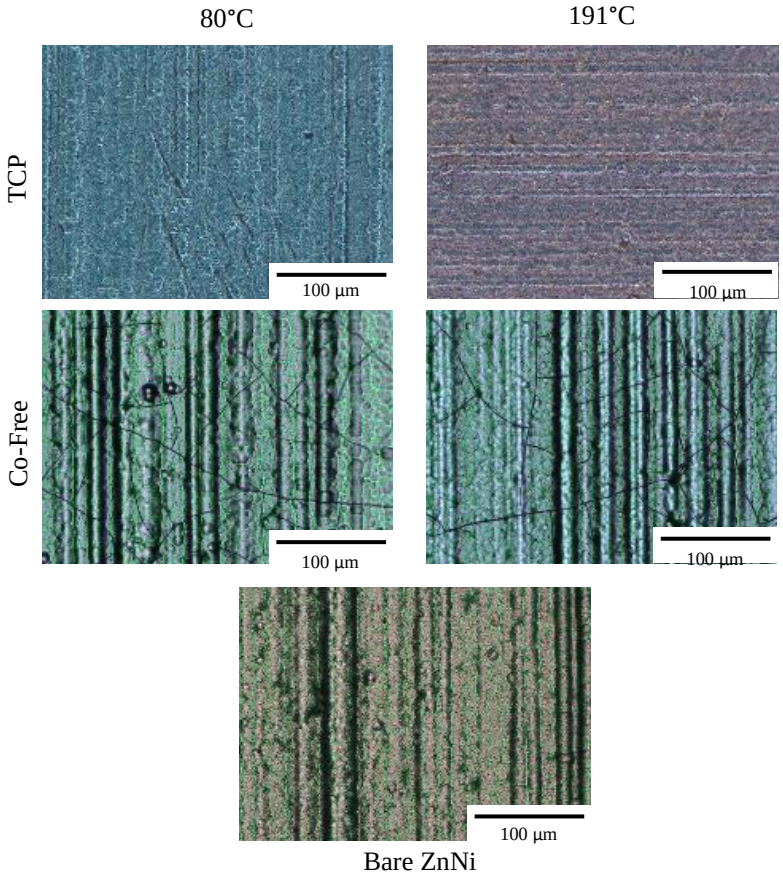

Figure 3. Optical micrographs of specimens taken at 1000X magnification prior to SSE.

Figure 4 shows micrographs of specimen regions that appear to have either corrosion product or visible color change after visual inspection after 336 hour SSE. Corroded bare ZnNi surfaces developed numerous cracks underneath the corrosion product.

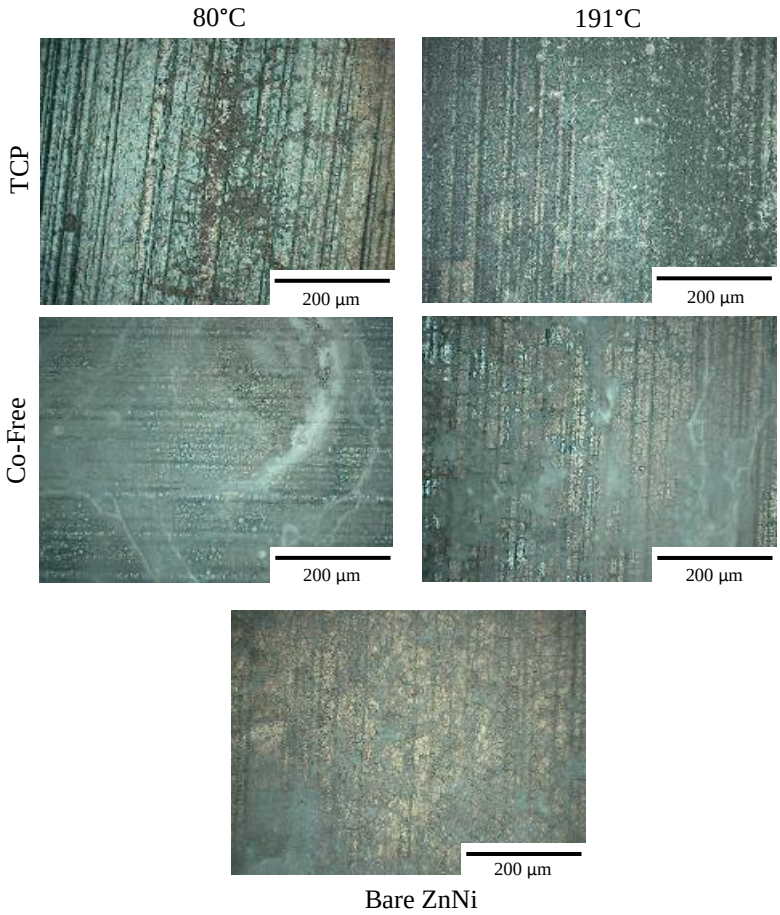

Figure 4. Optical micrographs of visibly corroded areas of specimens taken at 500X magnification after 336 hours SSE.

The heavily corroded regions of the Co-free TCP specimen heat treated at 191°C exhibited a similar appearance. Areas with cracks present sometimes had visible

corrosion product nearby as seen in most images, but pristine regions with cracks also existed on the specimens. Some instances of color change or corrosion product had no obvious flaw nearby such as the images shown for Co-free TCP specimens heat treated at 80°C that are shown in Figure 4.

3.3. ELECTROCHEMICAL CHARACTERIZATION

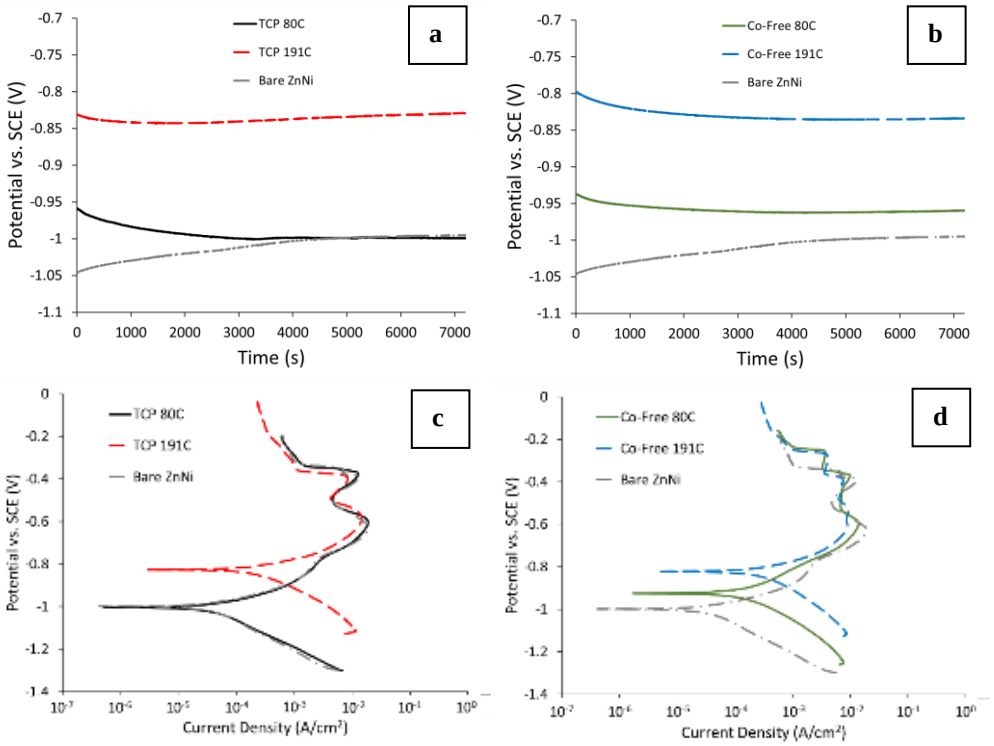

Figure 5. OCPs, and PDPs of non-corroded test specimens. a) and c) are the OCP and PDP of TCP specimens, b) and d) are the OCP and PDP of Co-free TCP specimens.

Electrochemical tests were performed on non-corroded samples to establish initial responses and for comparison with observed corrosion performance and electrochemical testing of corroded specimens. Heat treatment temperature had a significant effect on

OCP values (Figure 5). In addition, differences were noted in OCPs between TCP and Co-free TCP that were heat treated at 80°C. The most noble OCPs were for passivations heat treated at 191°C with -0.83 V for TCP and -0.84 V for Co-free TCP. The OCPs for specimens heat treated at 80°C were ~100 – 160 mV more negative with values of -0.99 V for TCP and -0.93 V for Co-free TCP.

Table 3. Tafel parameters from PDPs of test specimens.

	TCP 80°C	TCP 191°C	CoF 80°C	CoF 191°C	ZnNi
β_a (mV)	97 ± 8	71 ± 29	146 ± 2	82 ± 6	101 ± 5
β_c (mV)	172 ± 39	137 ± 56	157 ± 0	169 ± 16	222 ± 55
I_o x 10^{-5} (A/cm^2)	6.33 ± 1.73	18.4 ± 16.0	24.1 ± 0.49	20.7 ± 7.26	6.56 ± 1.41
E_o (V)	-0.99 ± 0.01	-0.83 ± 0.00	-0.93 ± 0.00	-0.84 ± 0.00	-1.00 ± 0.01
R_p (Ω/cm^2)	427 ± 51	106 ± 24	126 ± 2	121 ± 31	474 ± 42

Mirroring the results of the OCPs, clear separation was observed in the polarization curves based upon the temperature of the heat treatment as shown in Figure 5c) for TCP and Figure 5d) for Co-free. For TCP the lowest corrosion current density was measured for the 80°C heat treated specimens with an average ~6.3 x 10^{-5} A/cm^2. Higher average corrosion current densities were observed for the TCP heat treated at 191°C with ~18 x 10^{-5} A/cm^2. The Co-free TCP specimens had generally higher average corrosion current densities than the equivalent TCP specimens with ~24 x 10^{-5} A/cm^2 for heat treatment at 80°C and ~21 x 10^{-5} A/cm^2 for heat treatment at 191°C. All Tafel parameters are summarized in Table 3.

3.4. Cr(VI) MEASUREMENT

Chromate testing was performed for the TCP and Co-free TCP coatings at SSE exposure times ranging from 0 hours (as-heat treated passivations) until the point at which the panels were fully corroded to track the Cr(VI) content in the specimens. Figure 6 shows the combined results and revealed that the TCP specimens contained more Cr(VI) in the passivation layer at all times compared to the Co-free TCP specimens. The Cr(VI) content decreased as SSE time increased for both types of passivation, and both heat treatments.

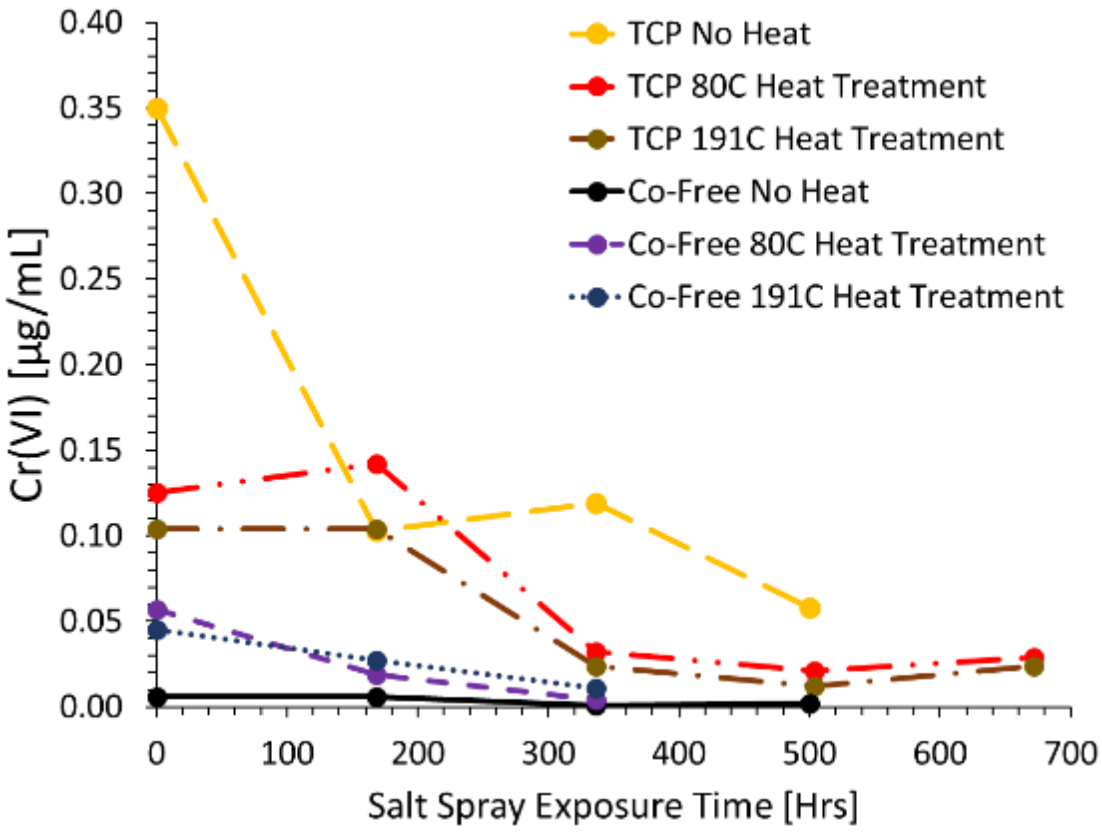

Figure 6. Cr(VI) concentrations after DPC boil test for specimens with and without heat treatment.

Chromate analysis was also performed on passivations that were deposited on γ-ZnNi coated Al6061-T6 that had not undergone heat treatment. These panels were part of a previous study of corrosion behavior[19]. The purpose of this analysis was to determine if heat treatment affected the Cr(VI) content. The levels of Cr(VI) detected (Figure 6) show that TCP specimens with no heat treatment had higher initial levels of Cr(VI) and higher Cr(VI) content was maintained throughout SSE. Heat treatment resulted in a decrease in Cr(VI) content. In contrast, Co-free TCP specimens showed an opposite trend with heat treatment as the specimen without heat treatment had Cr(VI) contents close to the margin of error for the boil test (< 0.005 μg/mL) revealing that heat treating the Co-free TCP resulted in an increase in Cr(VI) content.

4. DISCUSSION

The heat treated TCP panels had decreased corrosion resistance and the heat treated Co-free TCP panels had improved corrosion resistance compared to non-heat treated panels described in a previous study[19]. The color change associated with heat treatment of both passivations indicated that chemical or structural changes were induced by the heat treatments. The non-heat treated TCP samples exhibited little to no corrosion for up to 1000 hours of SSE while the heat treated TCP samples showed increasing discoloration and eventual corrosion product build up during SSE. Hence, heat treatment degraded the corrosion performance for TCP. Co-free TCP panels demonstrated a significant difference in appearance and improved corrosion performance after heat treatment. Heat-treated Co-free TCP specimens had mixed corroded and uncorroded

areas while non-heat treated specimens exhibited uniform corrosion after 168 hours SSE. Based on corrosion behavior, heat treatment alters the passivation layer and can either help or hinder corrosion performance.

Chromate contents of passivations showed excellent correlation to corrosion performance. Samples that had higher measured Cr(VI) contents resisted corrosion longer in SSE while samples with lowest Cr(VI) contents exhibited the greatest corrosion. Hence, the Cr(VI) content of the passivation is an important factor in determining corrosion performance. In addition, non-heat treated TCP contained the highest concentrations of Cr(VI), while the non-heat treated Co-free TCP did not contain a measurable concentration of Cr(VI). Based on that observation, the presence of Co in the TCP layer promotes formation of Cr(VI) species. Heat treating Co-free TCPs increased the Cr(VI) concentration through a thermal oxidation mechanism observed previously,[26] shown in Equation 1, and likely the same mechanism taking place in the study by Hesamedini and Bund[18]. Heat treating TCPs results in a process that reduced the Cr(VI) which has also been observed in hexavalent chromium conversion coatings (CCCs) and attributed to structural changes limiting mobility of Cr(VI)[27,28].

$$2Cr_2O_3 + 3O_2 \rightarrow 4CrO_3 \quad (1)$$

Since both thermal oxidation and reduction of Cr(VI) mobility should happen in both coatings during heat treatment, the difference in measured Cr(VI) should be caused by the difference in initial Cr(VI) concentration in both coatings. As these mechanisms compete and effect measured Cr(VI) in opposite directions, it is apparent that some equilibrium detectable concentration is reached where both mechanisms are in balance with each other. If both heat treatments were sufficient to fully oxidize the maximum

amount of Cr(III) and maximally restrict Cr(VI) mobility, then the only difference in measured Cr(VI) concentration should be due to differences in initial Cr(VI) concentration. This should make it clear that cobalt used in the deposition of TCPs results in an increase in Cr(VI) concentration prior to any subsequent treatment. The differences in appearance and corrosion coverage on the heat treated TCP specimens suggests that the 80°C heat treatment is not sufficient to fully alter the coatings.

The large difference in Cr(VI) concentrations of heat treated TCP coatings compared with non-heat treated suggests that the primary mechanism resulting in a measured concentration difference is restriction of Cr(VI) mobility for TCP. The measured Cr(VI) concentration in Co-free TCP coatings does not change as much as non-heat treated specimens, which implies that the effect of Cr(III) to Cr(VI) oxidation should only account for a small difference in corrosion performance, seen when comparing non-heat treated Co-free TCP to heat treated Co-free TCP. It follows that the difference in corrosion performance after heat treating TCP coatings must be attributed to reduction in Cr(VI) mobility as evidenced by non-heat treated TCP having no noticeable corrosion at 168 hours despite having similar measured Cr(VI) to the heat treated TCPs that exhibited some corrosion.

The cracks and defects in the coating system, such as those seen in the Co-free TCP samples in Figure 3, should affect the corrosion performance if the mechanism regarding diffusive pathways identified by Li and Swain is valid. Both the present study and a previous study done by our group[19] showed that the Co-free TCP coatings contained cracks. Further, the presence of cracks correlated with poor corrosion performance on Al6061 substrates, but prior work[22] on steel substrates heat treated at

191°C found no correlation with the presence of cracks or crack density since the Co-free TCP performed just as well as the TCP. The excellent correlation of Cr(VI) content to corrosion performance regardless of sample morphology indicates that TCP coatings exhibit enough active protection from the corrosion inhibiting mechanism of Cr(VI) to overcome the negative effects of imperfections or defects in the underlying coating.

Two effects could contribute to the differences observed between the corrosion performance of TCP and Co-free TCP passivations that were heat treated. The electrochemical data showed an increase in E_{corr} with increasing heat treatment temperature, which indicates that the passive coating became more protective of the underlying substrate after heat treatment. However, i_{corr} also increased with increasing heat treatment temperature, which indicated a greater exchange of electrons for heat treated passivations, yet they exhibited less corrosion than bare ZnNi specimens. The TCP heat treated at 191ºC showed the greatest resistance to corrosion of the heat treated specimens but also had an i_{corr} ~3 times larger than the TCP at the 80ºC heat treatment. Since the largest visual difference was observed between the 80ºC and 191ºC heat treatments on TCP and i_{corr} values for the Co-free TCP specimens showed little difference with heat treatment, the TCP i_{corr} differences must result from chemical changes influenced by the presence of cobalt in the passivation. This could be explained by CoOOH providing the brown color after oxidation during the 191ºC heat treatment. Any CoOOH present would have reacted with the acidic electrolyte during electrochemical testing to result in the increased i_{corr}. Assuming the cobalt present in the TCP layers is initially in a Co(II) valence state as $Co(OH)_2$, it would be expected that some of the

cobalt oxidizes to Co(III) to produce the mixed oxyhydroxide as seen when synthesizing cobalt nanodiscs[29].

The larger cathodic Tafel slope indicated that the passivation acted as a cathodic inhibitor. Since the cathodic Tafel slope did not change significantly with heat treatment temperature, the Cr(VI) species produced by heat treatment presumably react at cathodic sites located inside of the cracks and other diffusive pathways to form a protective chromium-containing corrosion product similar to the mechanism identified by Cho et al.[30]. This mechanism correlates with the improvement in corrosion performance for heat treated Co-free TCP compared to non-heat treated Co-free TCP. However, the greater improvement in corrosion performance on steel substrates compared to aluminum substrates suggests that another factor is influencing corrosion performance. Further research investigating interaction of the substrate with the ZnNi coating will be needed to identify the cause of this substrate dependent corrosion difference.

5. CONCLUSIONS

The effects of heat treatment and Cr(VI) content were studied for TCP and Co-free TCP coatings. Both the presence of cobalt in the passivation and heat treatment of the specimens were found to affect the Cr(VI) content of the passivating layers, which had a direct correlation to corrosion performance. A shift in open circuit potential to more positive values with heat treatment was measured, which indicated better protection of the underlying substrate. Specimens with the highest Cr(VI) contents performed the best in SSE while specimens with the lowest performed the worst. The presence of cobalt in

the as-deposited TCPs increased their Cr(VI) content, which then decreased after heat treatment. When cobalt was not present, Cr(VI) species increased after heat treatment, but not enough to match the corrosion protection for TCP coatings, which had higher Cr(VI) contents that the Co-free TCP at all test conditions. Difference in corrosion performance of TCP coatings with heat treatment was attributed to reduction in Cr(VI) mobility through dehydration of the coating.

CORRESPONDING AUTHOR

Kevin Foster, Missouri University of Science and Technology, klfmkd@mst.edu, 417-860-0460, 401 W. 16th St., Rolla, MO, 65409-1170

AUTHOR CONTRIBUTIONS

The manuscript was written through contributions of all authors. All authors have given approval to the final version of the manuscript. ‡These authors contributed equally.

FUNDING SOURCES

Authors Foster, Claypool, O'Keefe, Fahrenholtz, Nahlawi, and Almodovar received funding from the Strategic Environmental Research and Development Program (SERDP) through contract WP18-F2-1439.

ACKNOWLEDGEMENTS

The authors wish to acknowledge the guidance and support of Dr. Robin Nissan at SERDP along with Steve Gaydos and Dave Zika at Boeing.

ABBREVIATIONS

DI, deionized; SSE, salt spray exposure; TCP, trivalent chromium passivation; Co-free TCP, cobalt-free trivalent chromium passivation; OCP, open circuit potential; SHE, standard hydrogen electrode; SCE, saturated calomel electrode; PDP, potentiodynamic polarization; EIS, electrochemical impedance spectroscopy; DPC, 1,5-diphenylcarbazide

REFERENCES

1 K.H.J. Buschow, R.W. Cahn, M.C. Flemings, B. Ilschner, E.J. Kramer, and S. Mahajan: in *Encyclopedia of Materials - Science and Technology, Volumes 1-11*, Elsevier, p. 1265.

2 M.W. Kendig, A.J. Davenport, and H.S. Isaacs: *Corrosion Science*, 1993, vol. 34, pp. 41–9.

3 M. Kendig, S. Jeanjaquet, R. Addison, and J. Waldrop: *Surface and Coatings Technology*, 2001, vol. 140, pp. 58–66.

4 L. Xia, E. Akiyama, G. Frankel, and R. McCreery: *J. Electrochem. Soc.*, 2000, vol. 147, p. 2556.

5 R.R. Ray: *Interdisciplinary Toxicology*, 2016, vol. 9, pp. 55–65.

6 S. Mishra and R.N. Bharagava: *Journal of Environmental Science and Health, Part C*, 2016, vol. 34, pp. 1–32.

7 Y. Xie, S. Holmgren, D.M.K. Andrews, and M.S. Wolfe: *Environ Health Perspect*, 2017, vol. 125, pp. 181–8.

8 D. Benova, V. Hadjidekova, R. Hristova, T. Nikolova, M. Boulanova, I. Georgieva, M. Grigorova, T. Popov, T. Panev, R. Georgieva, A.T. Natarajan, F. Darroudi, and R. Nilsson: *Mutation Research/Genetic Toxicology and Environmental Mutagenesis*, 2002, vol. 514, pp. 29–38.

9 Pellerin C and Booker S M: *Environmental Health Perspectives*, 2000, vol. 108, pp. A402–7.

10 A.K. Guin, M. Bhadu, M. Sinhababu, A. Mundhara, T.K. Rout, and G. Udayabhanu: *Anti - Corrosion Methods and Materials*, 2014, vol. 61, pp. 370–9.

11 P. Visser, Y. Liu, H. Terryn, and J.M.C. Mol: *J Coat Technol Res*, 2016, vol. 13, pp. 557–66.

12 R. Berger, U. Bexell, T. Mikael Grehk, and S.-E. Hörnström: *Surface and Coatings Technology*, 2007, vol. 202, pp. 391–7.

13 Y. Guo and G.S. Frankel: *Corrosion; Houston*, DOI:http://dx.doi.org.libproxy.mst.edu/10.5006/0010-9312-68-4-3.

14 H. Kawaguchi, O. Funatsumaru, H. Sugawara, H. Sumiya, T. Iwade, T. Yamamoto, T. Koike, and R. Kashio: *SAE Int. J. Mater. Manf.*, 2016, vol. 9, pp. 833–8.

15 C. Boin: 2007, pp. 2007-01–2593.

16 N. Zaki: *Metal Finishing*, 2007, vol. 105, pp. 425-35.

17 A. Iyer, W. Willis, S. Frueh, W. Nickerson, A. Fowler, J. Barnes, L. Hagos, J. Escarsega, J. La Scala, and S.L. Suib: *Plat. Surf. Finish*, 2010, pp. 32–42.

18 S. Hesamedini and A. Bund: *Surface and Coatings Technology*, 2018, vol. 334, pp. 444–9.

19 K. Foster, J. Claypool, W.G. Fahrenholtz, M. O'Keefe, T. Nahlawi, and F. Almodovar: *ACS Appl. Mater. Interfaces*, 2021, vol. 13, pp. 4535–44.

20 S. Hesamedini, G. Ecke, and A. Bund: *J. Electrochem. Soc.*, 2018, vol. 165, pp. C657–69.

21 B. Ramezanzadeh and M.M. Attar: *Corrosion; Houston*, DOI:http://dx.doi.org.libproxy.mst.edu/10.5006/1.3676629.

22 K. Foster, J. Claypool, W.G. Fahrenholtz, M. O'Keefe, T. Nahlawi, and F. Almodovar: *Thin Solid Films*, 2021, vol. 735, p. 138894.

23 L. Li and G.M. Swain: *ACS Appl. Mater. Interfaces*, 2013, vol. 5, pp. 7923–30.

24 L. Li and G.M. Swain: *Corrosion*, 2013, vol. 69, pp. 1205–16.

25 American Society for Testing and Materials: 2019.

26 A. Apte, V. Tare, and P. Bose: *Journal of Hazardous Materials*, 2006, vol. 128, pp. 164–74.

27 V. Laget, C.S. Jeffcoate, H.S. Isaacs, and R.G. Buchheit: *J. Electrochem. Soc.*, 2003, vol. 150, p. B425.

28 V. Laget, C. Jeffcoate, H.S. Isaacs, and R.G. Buchheit: p. 13.

29 J. Yang, H. Liu, W.N. Martens, and R.L. Frost: *J. Phys. Chem. C*, 2010, vol. 114, pp. 111–9.

30 K. Cho, V. Shankar Rao, and H. Kwon: *Electrochimica Acta*, 2007, vol. 52, pp. 4449–56.

IV. XPS AND 1,5-DIPHENYLCARBAZIDE ANALYSIS OF CHROMATE CONTENT AND PERFORMANCE OF HEAT-TREATED γ-ZnNi COATED STEEL

Kevin Foster*Ξ, James ClaypoolΞ, William G.FahrenholtzΞ, Matthew O'KeefeΞ, Tarek NahlawiΛ and Felix AlmodovarΛ

Missouri University of Science & Technology Ξ
401 W. 16th St.
101 Straumanis-James Hall
Rolla, MO, 65409

Dipsol of America Λ
34005 Schoolcraft Rd.
Livonia, MI, 48150

ABSTRACT

Chromium and cobalt surface species and Cr(VI) content were determined in trivalent chromium passivations on electroplated γ-ZnNi coated steel substrates to investigate how cobalt in the passivation, an electroless nickel layer between the ZnNi and steel, and a 191°C heat treatment affect corrosion performance. Trivalent chromium passivations without cobalt exhibited primarily $Cr(OH)_3$ and Cr_2O_3 with small amounts of CrO_3 present regardless of heat treatment, electroless nickel layer presence, or salt spray exposure time. Cobalt-containing trivalent chromium passivations exhibited predominantly $Cr(OH)_3$ with greater amounts of Cr_2O_3 and less CrO_3 compared to passivations without cobalt. Analysis of cobalt species indicated that cobalt is almost entirely $Co(OH)_2$ or CoO with occasional CoOOH or Co_3O_4. Heat-treated cobalt-free trivalent chromium passivation had the lowest Cr(VI) content at all exposure times

initially containing 0.9 ± 0.6 ng/cm^2 and decreasing slightly to 0.5 ± 0.2 ng/cm^2 after 504 hours salt spray exposure. Cobalt-free trivalent chromium passivation without heat treatment and cobalt-containing trivalent chromium passivation regardless of heat-treatment had similar amounts of Cr(VI) beginning with 5.4-7.1 ng/cm^2 at 0 hours and decreasing to 1.3-2.7 ng/cm^2 after 336 hours salt spray exposure. Heat-treated trivalent chromium passivation had an increase of Cr(VI) to 13.1 ± 0.6 ng/cm^2 after 504 hours while both passivations without heat treatment remained at similar levels. Corrosion performance was found to be unaffected by the electroless nickel layer, inconsistently affected by heat treatment, and did not directly correlate with Cr(VI) content. Divalent cobalt was found to facilitate production of Cr(VI) during corrosive exposure leading to superior performance of cobalt-containing trivalent chromium passivations at exposures >336 hours.

Keywords: corrosion, trivalent chromium, x-ray photoelectron spectroscopy, diphenyl carbazide, hexavalent chromium

1. INTRODUCTION

Corrosion protection of metals is commonly achieved through the use of passivating treatments and sacrificial coatings. Hexavalent chromium is a long used passivating treatment well-known for its active corrosion inhibiting effects[1–3]. However, the environmental consequences[4], carcinogenic effects[5,6], and human toxicity[7,8] of hexavalent chromium leave it as an undesirable solution to corrosion

problems despite its excellent performance. Alternative passivations have been the subject of many research studies[9,10] and has resulted in a number of potential solutions. One of these potential solutions is trivalent chromium.

Many studies have investigated the corrosion resistance of trivalent chromium passivations (TCPs) on different substrates, most commonly steel, galvanized steel, and aluminum alloys[11–16]. TCPs commonly have cobalt added to the deposition bath to improve corrosion performance[17–19], but the exact role of cobalt has not been fully elucidated. There has been some evidence of active protection on TCPs[12,20–22] which has led to the suggestion that hexavalent chromium could be present in these trivalent passivations with an amount influenced by cobalt in the TCP. Unfortunately, attempts to find Cr(VI) in TCP coatings has not always detected a measurable amount.

Heat treatment effects on TCPs have been investigated by a few researchers on aluminum and steel alloys[21,23,24]. The first aluminum alloy study by Li and Swain investigated effects of different temperatures and different times on TCP corrosion performance and attributed changes in corrosion resistance to densification, cracking, dehydration, and chemical changes in the passive layer. The second aluminum study by Li and Swain implicated noble intermetallic sites as being areas where H_2O_2 can form from O_2 and then oxidize Cr(III) to Cr(VI). A study by Hesamedini and Bund on galvanized steel suggested that O_2 and H_2O can oxidize Cr(III) at elevated temperatures independently of cobalt content. All studies suggest that Cr(VI) is important to TCP corrosion performance and that heat treatments should be beneficial to corrosion performance via increased Cr(VI) production, although the first study by Li and Swain

cautions that too high of a heat treatment can crack the passive layer and thus reduce corrosion resistance through increased diffusivity through the passive layer.

Our group has previously investigated TCPs with and without cobalt on γ-ZnNi coated SAE 1008 steel[25] and Al6061-T6 aluminum[22] substrates to identify factors affecting the corrosion performance of TCPs. Signs of active corrosion protection, inconsistent corrosion performance results, and processing differences between the two substrates led us to run another study where the Cr(VI) content was measured on γ-ZnNi coated Al6061 substrates with and without heat treatment[26]. The results of this study indicated that the corrosion performance of TCPs correlated well with the Cr(VI) content detectable in the bulk of the passivation, cobalt-containing TCPs have higher Cr(VI) contents than cobalt-free, and heat treatments can affect the Cr(VI) content in opposite ways based on the presence of cobalt. However, the inconsistent results between the earlier steel and aluminum substrate studies and the fact that the aluminum samples could not be produced with an electroless nickel (EN) layer that is not present on the steel substrates led us to examine the same passivations on SAE 1008 steel substrates with an EN layer between the steel and the γ-ZnNi coating. We also wanted to verify the Cr(VI) measurements with XPS and investigate the type of Cr and Co species present in the passivations at different salt spray exposure (SSE) times.

The goal of this research was to investigate the chemical changes of the passive layer and Cr(VI) content after SSE under conditions of cobalt in the passivation, EN layer presence, and heat treatment on γ-ZnNi coated SAE 1008 steel substrates to determine the effect on corrosion performance.

2. EXPERIMENTAL PROCEDURE

2.1. SPECIMEN PREPARATION

SAE 1008 coupons measuring 152 mm by 76 mm by 1 mm were used as test specimens. The coupons were either plated with a layer of electroless nickel (EN) ~10 µm thick or left bare and then electroplated with γ-ZnNi (IZ-C17+, Dipsol of America) applied using the series of steps in Table 1. Electroplating of the γ-ZnNi was performed at a current density of 0.03 A/cm^2 for twenty-five minutes to plate a thickness of ~20 µm. Following ZnNi plating the panels were passivated with one of two treatments, a commercial trivalent chromium passivation (TCP; IZ-264, Dipsol of America), or a cobalt-free trivalent chromium passivation (Co-Free TCP; IZ-ASCF02, Dipsol of America). Lastly, one set of EN plated panels for each passivation and the panels with no EN layer were heat treated at 191ºC for 24 hours done in ambient atmosphere. The heat treatment is a commercially used processes for low hydrogen embrittlement bakes on steel. Table 2 outlines the procedure used for cleaning, passivating, and heat treating the relevant panels. An acetone cleaning and deionized water (DI) rinse followed by twenty-four hours of drying was used on all specimens prior to testing. The final batch of specimens was separated into six categories to describe the different experimental conditions and given shorthand identifiers as listed:

1. EN TCP 191ºC – EN-plated, IZ-264 TCP, heat-treated specimens
2. EN Co-free TCP 191ºC – EN-plated, IZ-ASCF02 TCP, heat-treated specimens
3. EN TCP no heat - EN-plated, IZ-264 TCP, no heat treatment
4. EN Co-free TCP no heat - EN-plated, IZ-ASCF02 TCP, no heat treatment

5. TCP 191ºC – IZ-264 TCP, heat-treated specimens

6. Co-free TCP 191ºC – IZ-ASCF02 TCP, heat-treated specimens

Table 1. Sample cleaning and treatment for electroplating of the γ-ZnNi layer.

Step	Parameter	Material	Temperature	Time
Alkaline Cleaning	90 mL/L	523-SC, Dipsol of America	55°C	300 s
Double Rinse	-	Deionized Water	Ambient	30 s each
Surface Activation	40 wt% HCl 60 g/L	971-SC, Dipsol of America	Ambient	60 s
Double Rinse	-	Deionized Water	Ambient	30 s each
Electroplating	0.03 A/cm^2	IZ-C17+, Dipsol of America	25°C	25 mins
Double Rinse	-	Deionized Water	Ambient	30 s each

Table 2. Sample treatment for application and heat treatment of passivating trivalent chromium coatings.

Step	Parameter	Material	Temperature	Time
Acid Activation	1 mL/L	HCl solution	Ambient	15 s
Double Rinse	-	Deionized Water	Ambient	30 s each
Passivation	pH 4.2 pH 4.0	IZ-264, Dipsol of America IZ-ASCF02, Dipsol of America	25°C 25°C	90 s
Drain	-	-	Ambient	25 s
Rinse	-	Deionized Water	Ambient	30 s
Hot Rinse	-	Deionized Water	71-82°C	30 s
Dry	-	-	Ambient	Until Dry
Bake	-	-	191°C	24 hrs

2.2. CHACTERIZATION

Neutral salt spray (Cyclic Corrosion Tester, Q-Fog) was used to test corrosion performance as described in ASTM B117[27]. The pH of the 5 wt% aqueous NaCl solution was controlled by pH adjustment through hydrochloric acid (36.5%, Fisher

Scientific) or sodium hydroxide (10.0 N, Alfa Aesar) additions. Panels remained in salt spray exposure (SSE) for one week (168 hours) intervals across a total of 4 weeks (672 hours). The test coupons were rinsed with DI water for thirty seconds, or until no visible salt remained on the surface after removal from the chamber. Drying after rinsing was done with compressed air followed by visual inspection and imaging. At each one-week interval, panels were removed from the chamber and labelled with their extent of SSE to be sectioned for further analysis while the remaining specimens were placed back into the chamber for another week.

Bulk Cr(VI) in the passivations was measured quantitatively by using 1,5-diphenylcarbazide and UV-Vis spectrophotometry on solution obtained by boiling exposed coupon surface in acidic solution to leach the hexavalent chromium. Four types of aqueous solutions were used in the hexavalent chromate analysis. The first was 75 wt% phosphoric acid, the second was 1,5-diphenylcarbazide indicator, the third was Cr(VI) standards, and the fourth was 5 wt% NaF solution. The solutions were produced as follows:

1. 350 mL of 85 wt% phosphoric acid (Acros Organic) was added to 125 mL of DI water in a 500 mL flask and topped to 500 mL with DI water to produce 75 wt% phosphoric acid solution.
2. 1.0g of 1,5-diphenylcarbazide (Certified ACS, Fisher Scientific) was added to 80 mL of acetone (HPLC-UV grade, Pharmco) with 1 drop of acetic acid (99.7%, Sigma Aldrich) then topped to 100 mL with acetone and mixed until dissolved to produce the indicator solution.

3. 0.113g of potassium dichromate (99%, Acros Organic) was added to 900 mL of DI water, topped to 1000 mL with DI water, and mixed, then 0.5, 1.0, 1.5, 2.0, or 2.5 mL of that solution were added to 450 mL of DI water and brought to 500 mL with DI water to produce the standards containing 0.04 µg/mL, 0.08 µg/mL, 0.12 µg/mL, 0.16 µg/mL, and 0.2 µg/mL of Cr(VI).
4. 5.0g of sodium fluoride (Certified ACS, Fisher Scientific) was added to 80 mL of DI water, brought to 100 mL with DI water, and then mixed thoroughly to produce the 5 wt% NaF solution.

Specimen Cr(VI) contents were analyzed by placing a section with 10 ± 1 cm^2 of exposed surface area in a 50 mL beaker with 9 mL of DI water and 1 mL of 5 wt% NaF solutions with a layer of boiling stones. The beaker was covered with a watch glass and brought to a boil for 10 minutes. After boiling the resulting solution was transferred to a sample container and filled to 10 mL with DI water and manually swirled for 15 seconds. Four drops or ~ 0.2 mL of 75 wt% phosphoric acid solution was added to the test solution and swirled for 15 seconds. 1 mL of test solution was then placed into a 1 cm cuvette as a blank for analysis. Then, 4 drops or ~0.2 mL of 1,5-diphenylcarbazide indicator solution was added to the test solution and swirled manually for 15 seconds. A 1 mL sample of test solution was then placed into a 1 cm cuvette for analysis. This process was performed in triplicate for each sample on which data was gathered which covered EN TCP 191ºC, EN Co-free TCP 191ºC, EN TCP no heat, and EN Co-free TCP no heat at SSE times of 0, 168, 336, and 504 hours.

UV-VIS spectrophotometry of the solutions was performed using a Thermo Scientific Genesys 10UV that was calibrated using the Cr(VI) standards described above.

All samples were tested immediately after preparation with a time of no longer than 20 minutes between boiling and finished analysis. For analysis, the blank was analyzed first followed by the samples. The concentration of chromate was determined by subtracting the absorbance of the blank from the sample value.

2.3. IMAGING

Corrosion progress of test specimens were examined after SSE by imaging using a printer/scanner and quantifying the corrosion coverage using computerized image analysis (ImageJ, 1.52a; National Institute of Health). The area fraction of corrosion product was determined by tracing around areas of visual corrosion product in specimen scans and calculated by dividing the traced regions by the total exposed area. The test specimens that had corrosion product across the entire surface were labelled as 100% coverage.

2.4. XPS CHARACTERIZATION

Test specimens were sectioned to produce ~1 cm^2 pieces with a shear cutter to be used for XPS analysis**.** Specimens were cleaned with a 30 second DI water rinse and allowed to dry with the test surface upside down in a glass vial laid on its side that only touched the specimen at the corners for 30 minutes. Standard specimens were powdered and were placed into glass vials shortly before testing with no cleaning done prior.

XPS data was gathered using a Thermo Fisher Scientific Nexsa using a monochromatic Al K_α 1487 eV X-ray source (6 mA, 12 kV). A charge compensation system was employed using a mixed flood of electrons and argon ions directed at the

sample surface for all specimens to neutralize the surface charge. The carbon 1s spectra from each sample was adjusted to 285.0 eV and used to charge correct every other spectra from the sample. Specimens were first sputtered for 10 seconds at 1500 eV by an argon ion beam before any spectra were taken. Survey spectra (0-1350 eV range) were then gathered with a 400 μm spot size, a 200 eV pass energy, 50 ms dwell time, and 0.5 eV step size over 2 scans. High resolution scans were then gathered on C 1s (280-298 eV), Cr 2p (569-595 eV), and Co 2p (772-812 eV) using a 400 μm spot size, a 12.5 eV pass energy, 100 ms dwell time, and 0.1 eV step size with 4 – 20 scans depending upon signal strength.

Peak fitting of the XPS data was performed using CasaXPS v2.3.23PR1.0 software with a Shirley background used for all peak fits. Line shapes were chosen by starting with a 90% Gaussian/10% Lorentzian on peak fits for the standard samples and then iterated by a 10% change towards more Lorentzian character until the fit with the smallest residual was achieved. Fitting of the Cr 2p and Co 2p spectra followed a complex series of peaks to represent the multiplet splitting of the trivalent chromium and cobalt as well as the divalent cobalt species. Previous research by Biesinger et al.[28] was used as a guide to model this multiplet peak structure with the primary peak allowed to fit at a binding energy ±0.5 eV from Biesinger et al. and subsequent peaks constrained to fixed separations from the primary peak. Full width at half max (FWHM) values were allowed to deviate ±20% on all peaks to allow for sample and machine differences. Once peak fits had been obtained from the standard samples, the results were propagated and refit to each test specimen. Component fits were done using the Marquardt-Levenberg optimization algorithm available within CasaXPS.

3. RESULTS

3.1. IMAGE ANALYSIS OF CORRODED PANELS

The amount of corrosion measured on test panels increased across all experimental conditions with increasing salt spray exposure (SSE) time, visible in Figures 2 and 3. The values in Table 3 show that Co-free TCP specimens exhibited a greater increase in corrosion coverage with increasing SSE times than either set of heat-treated TCP panels. The EN Co-free TCP no heat exhibited the least corrosion product after SSE showing only a moderate increase from 6.8 ± 1.5% at 168 hours SSE, to 26.3 ± 11.4% after 672 hours SSE. The Co-free TCP 191°C panels showed a greater increase in corrosion coverage, ranging from 4.6 ± 3.2% after 168 hours SSE, to 46.5 ± 5.8% after 672 hours SSE. The EN Co-free TCP 191°C exhibited the greatest corrosion product coverage from 13.5 ± 3.3% at 168 hours SSE to being completely covered in corrosion product after 672 hours SSE.

The TCP panels followed a different trend than the Co-free TCP panels. The EN TCP no heat panels exhibited the greatest corrosion product coverage and the heat-treated TCP panels exhibited the least corrosion product. The EN TCP no heat panels exhibited 6.0 ± 0.4% corrosion coverage at 168 hours SSE and were completely covered in corrosion product after 672 hours SSE. The TCP 191°C showed the least corrosion product with 4.4 ± 2.7% after 168 hours SSE and increasing slightly to 9.4 ± 4.3% after 672 hours SSE. The EN TCP 191°C exhibited similar amounts of corrosion product to TCP 191°C with 3.5 ± 1.7% at 168 hours SSE but exhibited a large increase in coverage and variability to 23.8 ± 22.5% after 672 hours SSE.

3.2. XPS CHEMICAL ANALYSIS

The first XPS tests were done on specimens of $K_2(CrO_4)_2$, Co_3O_4, and Cr_2O_3 to gather peak fits for species of Cr metal, CrO_3, Cr_2O_3, CoOOH, Co_3O_4, CoO, Co metal, $Cr(OH)_3$, and $Co(OH)_2$ to use as standards for analysis of test specimens when analyzing chemical shifts. Figure 4 shows the peak fits used for components on Cr 2p and Co 2p peaks in each standard specimen and later propagated to experimental specimens.

Tables 4 and 5 show the elemental quantification results of all experimental specimens for the Co-free TCP and TCP specimens. General trends are seen in both data sets with Zn and C content generally increasing and Cr generally decreasing with SSE time in both sets. Differences between the two data sets include the presence of Ca and Co in the TCP, the presence of Zr, and, in a few cases, F in the Co-free TCP. Levels of N and Cl were observed in both sets but Cl was primarily observed in the Co-free TCP coatings.

Peak fitting results of the Cr 2p spectra in the experimental specimens are displayed in Tables 6 and 7 while Table 8 contains the peak fit results for Co 2p only in the TCP specimens. Representative examples of the experimental peak fits are shown in Figures 5 and 6 for Cr 2p and Co 2p, respectively. Co-free TCP specimen peak fit results of Cr 2p exhibited primarily $Cr(OH)_3$ species at all levels of heat treatment and SSE time. The EN Co-free TCP no heat exhibited less Cr_2O_3 than the other two conditions, but all specimens had peak fits improved by adding a small amount of CrO_3 to the fit, which implies that a low level of Cr^{6+} was present in all of the coatings. The EN Co-free TCP 191°C specimen displayed a higher percentage of Cr metal species; however, the discussion will explain that this is likely differential charging of the specimens and the

amount was included in the data tables to display how much error of the peak fit area could be contributed to this factor.

The TCP specimen peak fit results for Cr 2p show a similar general trend with $Cr(OH)_3$ being the predominant species detected in the analysis. The TCP specimens also exhibited a relatively greater amount of Cr_2O_3 species than the Co-free TCP specimens. The primary difference between the two data sets comes from the amount of CrO_3 detected in the TCP specimens as the amount was generally lower and the fit was not always improved by adding CrO_3 to the peak fit. Lastly, the EN TCP no heat specimens displayed a greater amount of differential charging than the heat-treated specimens, which is indicative of a greater amount of corrosion product.

The Co 2p peak fitting results from the TCP specimens showed that most detected cobalt species were in the hydroxide and divalent oxide forms. For the heat-treated TCP specimens, the 504 and 672 hour SSE times exhibited small amounts of trivalent cobalt species, either CoOOH or Co_3O_4 and excluding the 672 hour SSE time TCP 191°C data point. For the EN TCP no heat specimens, there was not enough signal to detect the presence of cobalt from 336 to 672 hours of SSE time.

3.3. DPC CHROMIUM (VI) ANALYSIS

Chromate Measurement of Cr(VI) in test specimens via leaching with 1,5-diphenylcarbazide with increasing SSE time is shown in Figure 5. Co-free TCP 191°C showed the lowest measured Cr(VI) at all times with 0.9 ± 0.6 ng/cm^2 at 0 hours SSE and decreasing slightly to 0.5 ± 0.2 ng/cm^2 at 504 hours SSE. Both TCP conditions and the Co-free TCP no heat condition followed similar trends from 0 to 336 hours SSE with

detected amounts ranging from 5.4-7.1 ng/cm^2 at 0 hours to 1.3-2.7 ng/cm^2 at 336 hours SSE. After 504 hours of SSE the TCP no heat showed a large increase in detected Cr(VI) to 13.1 ± 0.6 ng/cm^2. The TCP 191°C exhibited a greater amount of Cr(VI) at 504 hours SSE with 2.7 ± 0.7 ng/cm^2 compared to 1.3 ± 0.4 ng/cm^2 in the Co-free TCP no heat condition after the same SSE time.

4. DISCUSSION

The heat-treated specimens of TCP and Co-free TCP, with and without the EN layer, were expected to exhibit similar corrosion behavior as the only difference between them was the presence of the EN layer. Both heat-treated Co-free TCP conditions exhibited more corrosion than EN Co-free TCP no heat specimens with the EN Co-free TCP 191°C specimens exhibiting twice as much corrosion as the Co-free TCP 191°C specimens after 336 hours SSE implying an effect from the EN layer. For TCP specimens, the heat-treated specimen performance was similar, with the exception of the EN TCP 191°C after 672 hour SSE, which showed a much larger amount of corrosion coverage and variability as a result of one-third of the panel being covered in a large streak of corrosion product while the rest of the panel had almost no corrosion product that heavily skewed the average. Previous research showed that the ZnNi coating played the role of a sacrificial coating for all conditions[22,25]. The accompanying XRD analysis of the corrosion product revealed it to be composed of zinc carbonate hydroxide hydrate ($Zn_4CO_3(OH)_6 \bullet H_2O$) and zinc chloride hydroxide hydrate ($Zn_5(OH)_8Cl_2 \bullet H_2O$) with XPS analysis of test specimens after SSE exposure showing no Ni species at the

surface. Hence, it was concluded that the observed corrosion was restricted to the ZnNi coating. Based on those results and present observations, the difference in corrosion coverage should not be affected by the presence or absence of the EN layer.

Amounts of Zr and F detected in the Co-free TCP and amounts of Ca in the TCP XPS data can be explained by differences in the passivating procedure between the two coatings. The generally higher amounts of Zn and C, and the lower amounts of Cr and Cl detected after SSE suggest that the surface exhibits some amount of the zinc carbonate hydroxide hydrate corrosion product after SSE and very little of the zinc chloride hydroxide hydrate. Elemental analysis of the panels that contained a film of corrosion product that completely covered the surface such as EN Co-free TCP 191°C and EN TCP no heat show similar proportions of O, C, Cr, and Zn and closely match several other panels after SSE. Panels with more corrosion product present are expected to have closer O, C, Cr, and Zn contents due to more complete surface coverage. The differences seen in corrosion coverage versus these ratios that indicate total corrosion coverage are likely explained by the localized nature of the visible corrosion product as compared to the 500 μm spot size sampling area used for gathering XPS spectra.

Peak fitting of Cr in all TCP and Co-free TCP specimens revealed that $Cr(OH)_3$ is the predominant form of Cr with the exception of EN TCP 191°C after 0 hours SSE and the EN TCP no heat after 168 hours of SSE. This indicates that the passive layer reacts with water from the atmosphere at the surface and the amounts of Cr oxide come from the layers just underneath this hydrated surface. As SSE time increased, less oxide formation was observed as the passivation is consumed by corrosion product growth. As a result, SSE increases the fraction of the remaining Cr that is on the exposed surface to

react with water in the atmosphere and subsequently become $Cr(OH)_3$. A couple factors confound this data as the localized nature of the corrosion product results in sampling bias showing increased amounts of Cr oxide at higher levels of SSE such as observed in the EN Co-free TCP 191°C and EN TCP no heat specimens. Differential charging of samples that contained corrosion product was a problem that could not be completely eliminated from the XPS results. The low binding energy tail that differential charging produced in the Cr spectra overlapped with the peak for Cr metal making it impossible to determine if any Cr metal was present. A peak was fit to this low binding energy tail in an attempt to estimate how much corrosion product may have been present in the sampled area by estimating how much peak area could be attributed to this tail. Specimens with greater differential charging values contained greater amounts of corrosion product in the sampled area resulting in Cr species measurements that are correspondingly less accurate. This means that the data which includes high levels of Cr metal are likely to have significant error in the amounts of other Cr species measured and should be interpreted accordingly.

Cr(VI) contents estimated from fitting the Cr peaks were greater in the Co-free TCP specimens than in the TCP specimens and was also observed in the most corroded TCP specimen. Levels of Cr(VI) detected at the surface remained relatively constant regardless of amount of corrosion product or SSE time for Co-free TCP specimens and was almost never detected at the surface of TCP specimens. These measured amounts differ from the bulk analysis by the DPC method, which showed lower levels of Cr(VI) in heat-treated Co-free TCP and similar higher levels of Cr(VI) in TCP and non-heat-treated Co-free TCP. The surface Cr(VI) in Co-free TCP was nearly constant at all conditions

despite the heat treatment differences in bulk Cr(VI), which suggests a different mechanism of action compared to TCP. Meanwhile, the higher levels of surface Cr(VI) detected after enough SSE exhibited by the most corroded TCP specimen is indicative of the corrosion resistance mechanism present.

Hexavalent chromium passivations provide corrosion protection through release of the Cr(VI) ions into water present on the surface of the specimen with subsequent reduction of Cr(VI) species to Cr(III) at corroding anodic sites. TCPs likely behave similarly releasing Cr(VI) ions into aqueous solutions that reduce at corroding sites thus explaining reports of active protection on some TCPs[12,20–22]. The corrosion performance of the Co-free TCP has been inferior to TCP in previous studies[22,25] as well as in the present study. Further, the surface Cr(VI) content in Co-free TCP panels was shown in the present study to be constant at all SSE times, but more surface Cr(VI) is detected on the heavily corroded TCP specimens. Based on these results, we posit that the difference in mechanism comes from the ability of the Cr(VI) to migrate to and reduce at corroding anodic sites. The constant surface Cr(VI) concentration on Co-free TCP derives from the Cr(VI) leaching out of the passivation and then remaining at the surface as the panel is dried, being able to adsorb to both the passivation and any corrosion product that has begun to grow. The cobalt in the TCP specimens was detected almost exclusively in a divalent state in all the panels, which would make TCP electron rich. This extra free electron concentration could facilitate reduction of the Cr(VI), which could lead to the observed depletion of Cr(VI) at the surface of the TCP. This would also explain why Cr(VI) is detected on the non-heat-treated TCP as the nearly complete coverage of the corrosion product interferes with reduction of the Cr(VI) from the

solution and is left adsorbed at the surface of the corrosion product upon drying. The large increase in bulk Cr(VI) measured via DPC seen at 504 hours SSE for the non-heat-treated specimen further suggests that more Cr(VI) is produced during SSE and as the corrosion product prevents reduction of the Cr(VI) to Cr(III) a greater amount of Cr(VI) is able to collect in the corrosion product as it grows. This production of Cr(VI) during corrosion was not observed in the Co-free TCP as the fully corroded EN Co-free TCP 191°C showed no such increase in Cr(VI) after DPC testing. This suggests that cobalt promotes production of Cr(VI) during corrosive exposure likely by donating an electron during reduction of Cr(VI) at anodic sites and later oxidizing a nearby Cr(III) to Cr(VI).

The heat treatments had opposite effects on the corrosion performance for TCP and Co-free TCP specimens. Heat-treated Co-free TCP specimens showed inconsistent results whereas heat-treated TCP had the least corrosion. Previous research[26] on passivations on aluminum substrates found that the degree of corrosion protection correlated well with the amount of measured Cr(VI), but the present data suggest that Cr(VI) content alone is not sufficient for corrosion protection. A difference between the previous work and the present work is that the previous study did not have a TCP specimen that reached a level of corrosion buildup that completely covered the exposed surface and likely had not been exposed to SSE long enough to observe the increase of Cr(VI) that accompanied the increase in corrosion product. This implies that excellent corrosion protection of TCP requires that the passivation contains a sufficient amount of bulk Cr(VI) and that Cr(VI) must be produced *in situ* to maintain the corrosion inhibition. Heat treatment may also affect an unmeasured physical aspect of the passivation that

results in more or less surface area exposed to the corrosive media, which then affects corrosion performance, but that would be a topic for a future study.

5. CONCLUSIONS

XPS and DPC analyses were performed on trivalent chromium passivated ZnNi coated steel substrates at increasing amounts of SSE time to investigate how factors such as cobalt, EN layers, and heat-treatments could affect corrosion performance. Corrosion performance of cobalt-containing and cobalt-free TCPs on ZnNi coated steel substrates was not affected by the presence of an EN layer and was inconsistently affected by heat-treatments. Cobalt-containing TCPs were found to have similar bulk Cr(VI) contents to Co-free TCPs, which did not directly correlate with SSE corrosion performance. The data suggested that divalent cobalt in the cobalt-containing TCPs facilitated production of Cr(VI) during corrosive exposure that led to improved performance over cobalt-free TCP after >336 hours SSE. The superior performance of TCP depended on a sufficient amount of Cr(VI) and included a mechanism to produce more Cr(VI) during corrosion. A future study should investigate the inconsistent heat-treatment effects with a focus on physical changes to the passivations to explain corrosion performance more fully.

Table 3. Extent of corrosion coverage in percentage of surface exhibiting visible corrosion product for Co-free TCP and TCP panels after varying SSE times.

		SSE Exposure Time							
		168 Hrs		336 Hrs		504 Hrs		672 Hrs	
Co-free TCP	**191C**	4.6	± 3.2	19.2	± 3.0	20.5	± 4.7	46.5	± 5.8
	EN 191C	13.5	± 3.3	17.9	± 2.7	49.1	± 6.7	100	-
	EN no heat	6.8	± 1.5	5.1	± 1.7	15.8	± 3.3	26.3	± 11.4
TCP	**191C**	4.4	± 2.7	9.4	± 1.1	10.4	± 1.3	9.4	± 4.3
	EN 191C	3.5	± 1.7	7.1	± 1.8	9.0	± 3.7	23.8	± 22.5
	EN no heat	6.0	± 0.4	24.1	± 7.2	54.8	± 5.0	100	-

Table 4. Elemental quantification from XPS survey spectra for Co-free TCP specimens. Element numbers are reported in atomic %.

Co-Free TCP	SSE Time(hrs)	O	C	N	Cr	Cl	Zr	Zn	F
191C	**0**	64	11	1	17	1	3	3	0
	168	53	23	2	14	1	2	5	0
	336	45	26	1	8	0	1	20	0
	504	40	34	3	8	1	2	12	0
	672	39	38	2	9	1	2	9	0
EN 191C	**0**	54	18	1	19	1	4	4	0
	168	48	20	0	9	0	0	23	0
	336	46	24	0	8	1	0	21	0
	504	42	27	2	9	0	0	20	0
	672	45	25	1	8	0	0	21	0
EN no heat	**0**	47	22	2	16	1	3	6	3
	168	39	30	2	12	1	1	16	0
	336	35	47	1	6	1	1	9	0
	504	43	28	1	8	0	0	20	0
	672	37	37	4	8	1	1	12	0

Table 5. Elemental quantification from XPS survey spectra for TCP specimens. Element numbers are reported in atomic %.

TCP	SSE Time(hrs)	O	C	N	Cr	Cl	Zn	Ca	Co
191C	**0**	55	18	0	15	2	5	3	2
	168	49	16	1	19	0	13	1	1
	336	38	41	2	9	0	8	0	0
	504	36	44	4	8	0	7	1	0
	672	39	39	3	9	1	8	0	1
EN 191C	**0**	52	14	1	19	3	6	2	3
	168	47	20	1	18	0	13	0	1
	336	42	32	1	9	0	14	1	1
	504	38	40	4	9	0	9	0	0
	672	45	27	2	9	0	17	0	0
EN no heat	**0**	46	26	2	14	0	9	1	2
	168	39	20	1	12	0	26	1	1
	336	43	31	1	8	0	16	1	0
	504	43	29	2	8	0	18	0	0
	672	43	28	2	8	0	19	0	0

Table 6. Chromium species analysis from peak fitting Cr 2p spectra in Co-free TCP specimens. Species numbers reported as % of fit area.

Co-Free TCP	SSE Time(hrs)	Diff. Charge	$Cr(OH)_3$	CrO_3	Cr_2O_3
191C	**0**	0	69	2	29
	168	0	85	3	12
	336	4	77	2	17
	504	3	91	2	4
	672	2	74	2	22
EN 191C	**0**	0	91	2	7
	168	10	66	4	20
	336	21	62	5	13
	504	7	69	2	22
	672	14	51	2	33
EN no heat	**0**	1	97	2	0
	168	4	88	1	7
	336	7	78	2	13
	504	9	89	2	0
	672	6	92	2	0

Table 7. Chromium species analysis from peak fitting Cr 2p spectra in TCP specimens. Species numbers reported as % of fit area.

TCP	SSE Time(hrs)	Diff. Charge	$Cr(OH)_3$	CrO_3	Cr_2O_3
191C	**0**	0	84	1	15
	168	1	73	0	26
	336	1	75	1	23
	504	3	77	0	20
	672	1	88	1	10
EN 191C	**0**	1	48	1	50
	168	2	55	0	53
	336	6	65	1	28
	504	1	96	0	3
	672	2	98	0	0
EN no heat	**0**	1	76	0	23
	168	11	38	0	51
	336	14	75	4	7
	504	16	68	3	14
	672	17	54	3	26

Table 8. Cobalt species analysis from peak fitting Co 2p in TCP specimens. Species numbers reported as % of fit area.

TCP	SSE Time(hrs)	$Co(OH)_2$	CoO	CoOOH	Co_3O_4
191C	**0**	88	12	0	0
	168	67	33	0	0
	336	58	42	0	0
	504	63	34	3	0
	672	40	60	0	0
EN 191C	**0**	38	62	0	0
	168	76	24	0	0
	336	63	37	0	0
	504	62	33	0	5
	672	41	51	8	0
EN no heat	**0**	76	24	0	0
	168	70	30	0	0
	336	n/a	n/a	n/a	n/a
	504	n/a	n/a	n/a	n/a
	672	n/a	n/a	n/a	n/a

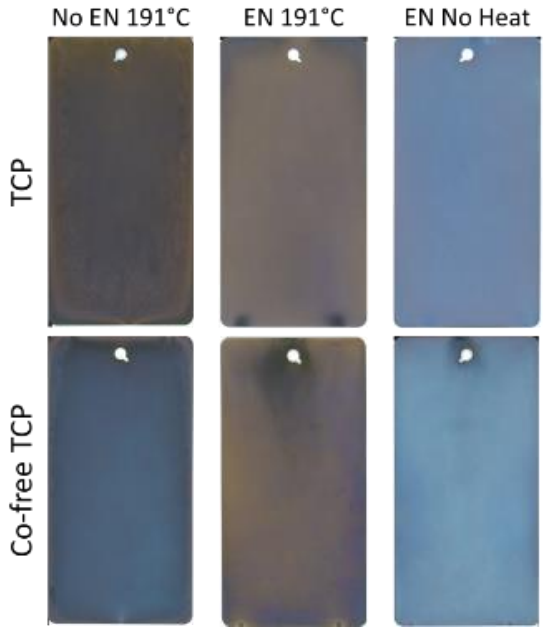

Figure 1. Pre-salt spray exposure appearance of the TCP and Co-free TCP test panels under all experimental conditions.

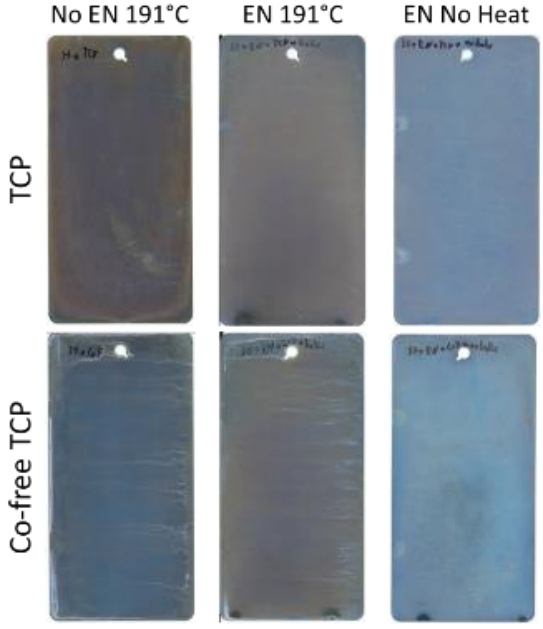

Figure 2. Corrosion product coverage on TCP and Co-free TCP panels after 168 hours of salt spray exposure.

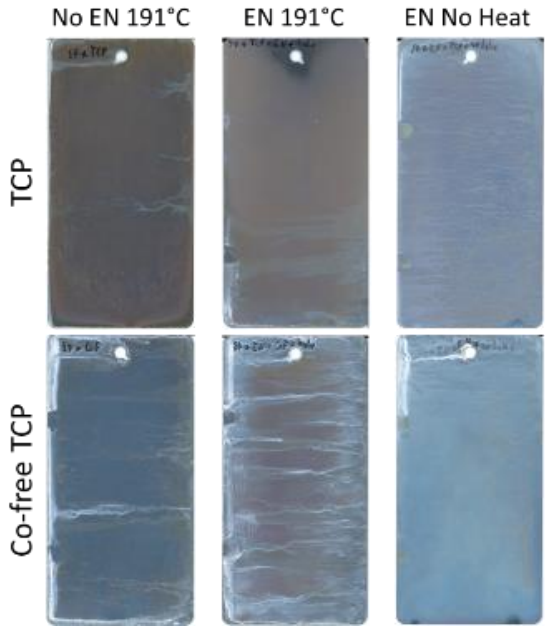

Figure 3. Corrosion product coverage on TCP and Co-free TCP panels after 672 hours of salt spray exposure.

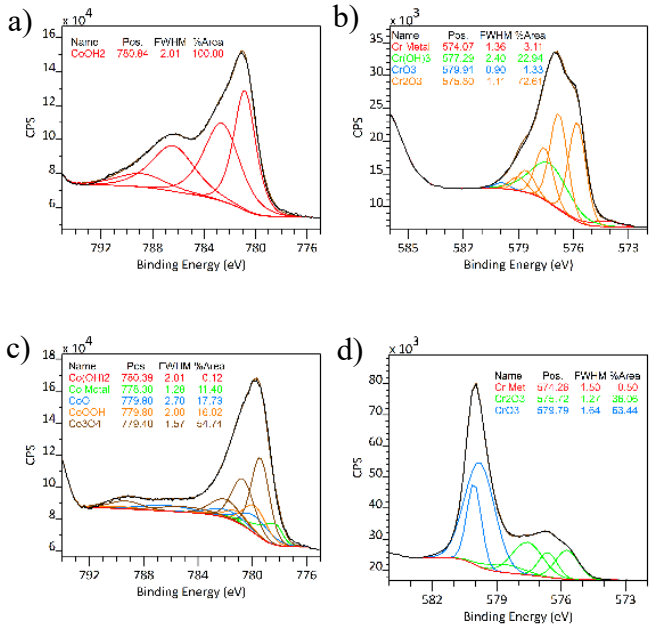

Figure 4. Peak fits used for chromium and cobalt components on known standard specimens: a) $CoOH_2$, b) Cr_2O_3, c) Co_3O_4, d) $K_2(CrO4)_2$.

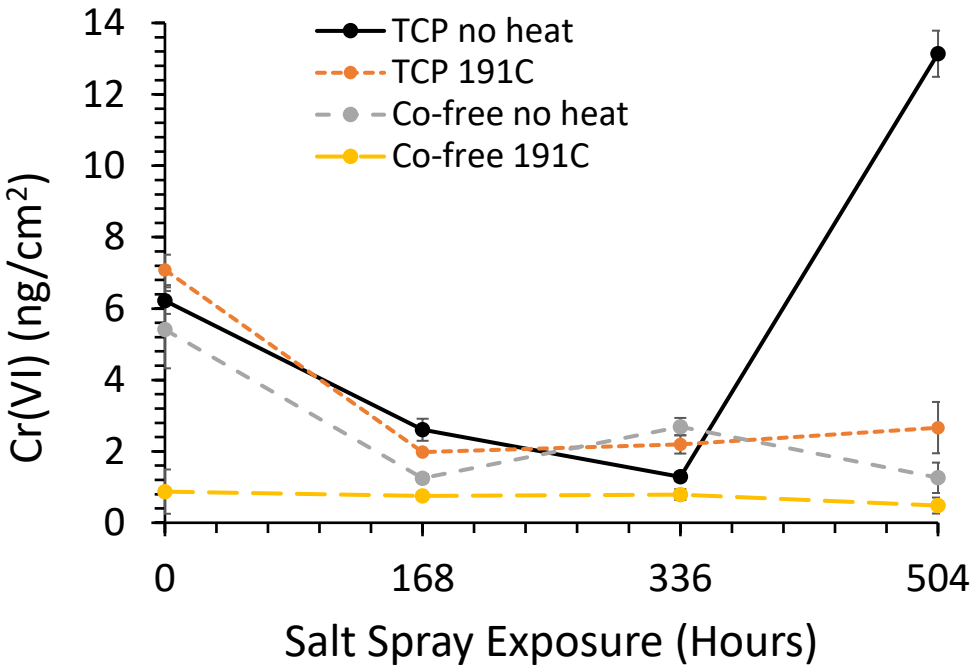

Figure 5. Measured Cr(VI) content in all test conditions from DPC analysis.

ACKNOWLEDGEMENTS

This research was funded by the Strategic Environmental Research and Development Program (SERDP) through project WP-2527. The authors wish to acknowledge the guidance and support of Dr. Robin Nissan at SERDP along with Steve Gaydos and Dave Zika at Boeing. A special thanks is extended to Brian Porter for assisting in the acquisition of the XPS data presented in this paper. Authors Foster, Claypool, O'Keefe, Fahrenholtz, Nahlawi, and Almodovar received funding from the Strategic Environmental Research and Development Program (SERDP) project WP-2527 to support work investigating alternatives to hexavalent chromium passivations on γ-ZnNi coated Al6061-T6 alloy.

REFERENCES

[1] M.W. Kendig, A.J. Davenport, H.S. Isaacs, The mechanism of corrosion inhibition by chromate conversion coatings from x-ray absorption near edge spectroscopy (Xanes), Corrosion Science. 34 (1993) 41–49. https://doi.org/10.1016/0010-938X(93)90257-H.

[2] M. Kendig, S. Jeanjaquet, R. Addison, J. Waldrop, Role of hexavalent chromium in the inhibition of corrosion of aluminum alloys, Surface and Coatings Technology. 140 (2001) 58–66. https://doi.org/10.1016/S0257-8972(01)01099-4.

[3] L. Xia, E. Akiyama, G. Frankel, R. McCreery, Storage and Release of Soluble Hexavalent Chromium from Chromate Conversion Coatings Equilibrium Aspects of Cr VI Concentration, J. Electrochem. Soc. 147 (2000) 2556. https://doi.org/10.1149/1.1393568.

[4] Y. Xie, S. Holmgren, D.M.K. Andrews, M.S. Wolfe, Evaluating the Impact of the U.S. National Toxicology Program: A Case Study on Hexavalent Chromium, Environ Health Perspect. 125 (2017) 181–188. https://doi.org/10.1289/EHP21.

[5] D. Benova, V. Hadjidekova, R. Hristova, T. Nikolova, M. Boulanova, I. Georgieva, M. Grigorova, T. Popov, T. Panev, R. Georgieva, A.T. Natarajan, F. Darroudi, R. Nilsson, Cytogenetic effects of hexavalent chromium in Bulgarian chromium platers, Mutation Research/Genetic Toxicology and Environmental Mutagenesis. 514 (2002) 29–38. https://doi.org/10.1016/S1383-5718(01)00320-5.

[6] Pellerin C, Booker S M, Reflections on hexavalent chromium: health hazards of an industrial heavyweight., Environmental Health Perspectives. 108 (2000) A402–A407. https://doi.org/10.1289/ehp.108-a402.

[7] R.R. Ray, Review article. Adverse hematological effects of hexavalent chromium: an overview, Interdisciplinary Toxicology. 9 (2016) 55–65. https://doi.org/10.1515/intox-2016-0007.

[8] S. Mishra, R.N. Bharagava, Toxic and genotoxic effects of hexavalent chromium in environment and its bioremediation strategies, Journal of Environmental Science and Health, Part C. 34 (2016) 1–32. https://doi.org/10.1080/10590501.2015.1096883.

[9] A.K. Guin, M. Bhadu, M. Sinhababu, A. Mundhara, T.K. Rout, G. Udayabhanu, Effective corrosion inhibition performance of La(NO3)3 doped sol-gel coating on galvanized steel sheet, Anti - Corrosion Methods and Materials. 61 (2014) 370–379. http://dx.doi.org.libproxy.mst.edu/10.1108/ACMM-08-2013-1292

.

[10] P. Visser, Y. Liu, H. Terryn, J.M.C. Mol, Lithium salts as leachable corrosion inhibitors and potential replacement for hexavalent chromium in organic coatings for the protection of aluminum alloys, J Coat Technol Res. 13 (2016) 557–566. https://doi.org/10.1007/s11998-016-9784-6.

[11] A.R. Di Sarli, J.D. Culcasi, C.R. Tomachuk, C.I. Elsner, J.M. Ferreira-Jr, I. Costa, A conversion layer based on trivalent chromium and cobalt for the corrosion protection of electrogalvanized steel, Surface and Coatings Technology. 258 (2014) 426–436. https://doi.org/10.1016/j.surfcoat.2014.08.057.

[12] Y. Guo, G.S. Frankel, Active Corrosion Inhibition of AA2024-T3 by Trivalent Chrome Process Treatment, Corrosion; Houston. 68 (2012). http://dx.doi.org.libproxy.mst.edu/10.5006/0010-9312-68-4-3.

[13] R. Berger, U. Bexell, T. Mikael Grehk, S.-E. Hörnström, A comparative study of the corrosion protective properties of chromium and chromium free passivation methods, Surface and Coatings Technology. 202 (2007) 391–397. https://doi.org/10.1016/j.surfcoat.2007.06.001.

[14] H. Kawaguchi, O. Funatsumaru, H. Sugawara, H. Sumiya, T. Iwade, T. Yamamoto, T. Koike, R. Kashio, Development of Trivalent Chromium Passivation for Zn Plating with High Corrosion Resistance after Heating, SAE Int. J. Mater. Manf. 9 (2016) 833–838. https://doi.org/10.4271/2016-01-0542.

[15] N. Zaki, Trivalent chrome conversion coating for zinc and zinc alloys, Metal Finishing. 105 (2007) 425–435. https://doi.org/10.1016/S0026-0576(07)80361-8.

[16] C. Boin, Black passivation films without hexavalent chromium on top of electroplated layers of zinc and zinc alloys, in: 2007: pp. 2007-01–2593. https://doi.org/10.4271/2007-01-2593.

[17] B. Ramezanzadeh, M.M. Attar, Effects of Co(II) and Ni(II) on the Surface Morphology and Anticorrosion Performance of the Steel Samples Pretreated by Cr(III) Conversion Coating, Corrosion. 68 (2012) 015008–1. https://doi.org/10.5006/1.3676629.

[18] S. Hesamedini, G. Ecke, A. Bund, Structure and formation of trivalent chromium conversion coatings containing cobalt on zinc plated steel, Journal of the Electrochemical Society: JES. 165, 2018 (2018) 657–669. https://doi.org/10.1149/2.0951810jes.

[19] A. Gardner, J. Scharf, Trivalent passivation of plated zinc and zinc alloys—alternatives to hexavalent based systems, Transactions of the IMF. 81 (2003) B107–B110. https://doi.org/10.1080/00202967.2003.11871534.

[20] A. Iyer, W. Willis, S. Frueh, W. Nickerson, A. Fowler, J. Barnes, L. Hagos, J. Escarsega, J. La Scala, S.L. Suib, Characterization of NAVAIR Trivalent Chromium Process (TCP) coatings and solutions, Plating and Surface Finishing. 97 (2010) 32–41.

[21] S. Hesamedini, A. Bund, Formation of Cr(VI) in cobalt containing Cr(III)-based treatment solution, Surface and Coatings Technology. 334 (2018) 444–449. https://doi.org/10.1016/j.surfcoat.2017.12.006.

[22] K. Foster, J. Claypool, W.G. Fahrenholtz, M. O'Keefe, T. Nahlawi, F. Almodovar, Characterization of Cobalt-Containing and Cobalt-free Trivalent Chromium Passivation Layers on γ-ZnNi-Coated Al6061-T6 Substrates, ACS Appl. Mater. Interfaces. 13 (2021) 4535–4544. https://doi.org/10.1021/acsami.0c20015.

[23] L. Li, G.M. Swain, Effects of Aging Temperature and Time on the Corrosion Protection Provided by Trivalent Chromium Process Coatings on AA2024-T3, ACS Appl. Mater. Interfaces. 5 (2013) 7923–7930. https://doi.org/10.1021/am4020023.

[24] L. Li, G.M. Swain, Formation and Structure of Trivalent Chromium Process Coatings on Aluminum Alloys 6061 and 7075, Corrosion. 69 (2013) 1205–1216. http://dx.doi.org.libproxy.mst.edu/10.5006/1041.

[25] K. Foster, J. Claypool, W.G. Fahrenholtz, M. O'Keefe, T. Nahlawi, F. Almodovar, Characterization of cobalt containing and cobalt-free trivalent chromium passivations on γ-ZnNi coated steel substrates, Thin Solid Films. 735 (2021) 138894. https://doi.org/10.1016/j.tsf.2021.138894.

[26] K. Foster, J. Claypool, W. Fahrenholtz, M. O'Keefe, T. Nahlawi, F. Almodovar, Effect of Heat Treatment on the Chromate Content and Pefformance of Trivalent Chromium Passivations on γ-ZnNi, [Submitted]. (2021).

[27] American Society for Testing and Materials, ASTMB117-19 Standard Practice for Operating Salt Spray (Fog) Apparatus, (2019). https://compass-astm-org.libproxy.mst.edu/download/B117.14142.pdf (accessed October 22, 2020).

[28] M.C. Biesinger, B.P. Payne, A.P. Grosvenor, L.W.M. Lau, A.R. Gerson, R.St.C. Smart, Resolving surface chemical states in XPS analysis of first row transition metals, oxides and hydroxides: Cr, Mn, Fe, Co and Ni, Applied Surface Science. 257 (2011) 2717–2730. https://doi.org/10.1016/j.apsusc.2010.10.051.

SECTION

3. CONCLUSIONS AND RECOMMENDATIONS

3.1. CONCLUSIONS

Divalent cobalt in TCPs significantly improves corrosion resistance on γ-ZnNi coated steel and aluminum alloys. While some variability remains in the test data, cobalt-containing passivations typically withstand 3 or more weeks of ASTM B117 salt spray exposure while remaining electrically conductive. Initially it seemed that the underlying substrate (steel vs. aluminum) could have an effect on corrosion performance, it was later revealed that the primary influencing component was the level of Cr(VI) content in the passivation. Since the amount of Cr(VI) content was positively correlated with the corrosion performance and divalent cobalt facilitated Cr(VI) production during salt spray exposure, it is clear that a TCP containing cobalt would perform better simply by increasing the Cr(VI) content. However, the specimens with the highest Cr(VI) content did not always perform as well and some cobalt-free TCP specimens, such as the ones on the initial SAE 1008 steel panels, did perform well. These results indicate that Cr(VI) content alone is not a sufficient predictor of improved corrosion performance.

The heat treatments showed contradictory results on Cr(VI) content between the two passivations, both increasing and decreasing the amounts in the different passivations. The replicatable change in OCP between heat-treated and non-heat-treated passivations clearly indicates that the passivation has been altered by the heat treatments. However, both passivations exhibited similar OCPs after heat treatment despite having

largely different amounts of Cr(VI) and no consistent differences in Cr species detected by XPS. This suggests that the heat treatments have caused a relevant change in the bulk of the passivation with little effect on the surface, caused physical changes that dominate the OCP response despite chemical differences, or had a variety of changes that by coincidence leave both passivations at the same OCP after heat treatment. The third option is highly unlikely and thus disregarded but the bulk could be studied through depth profiling of the passivation before and after heat treatment while the second has already been observed indirectly in the present research through comparison of the physical features on the first steel and aluminum samples.

While physical changes such as crack size, crack density, passivation thickness, and passivation porosity were observed, they did not correlate well with corrosion performance. In the context of heat treatments causing morphological changes to the passivations, processing parameters being different between the two passivations, and Cr(VI) content being measured separately from passivation physical features, it is clear that corrosion performance should be a function of both Cr(VI) content and physical aspects of the passivation. This combined examination of the data gathered offers insight into what is happening during corrosive exposure of the TCPs to create a model for how the TCPs protect their underlying substrate. Since the corrosion starts at localized areas and typically grows outward, it is clear that some local aspect of the coating, such as a crack, flaw, or uncovered area in a crevice, results in failure at certain points but not others. When TCPs contain cobalt and Cr(VI) content is high, Cr(VI) can leach into the corrosive aqueous solution and deposit at these sites to form a mixture of the corrosion products, zinc carbonate hydroxide hydrate ($Zn_4CO_3(OH)_6 \bullet H_2O$) and zinc chloride

hydroxide hydrate ($Zn_5(OH)_8Cl_2 \bullet H_2O$), with the Cr(III) oxide or hydroxide reduced from the Cr(VI) species. This mixture is very similar to the passivation that consists of amorphous Cr(III) oxides/hydroxides, zinc oxides/hydroxides, and small amounts of Co(II) oxides/hydroxides but has a greater molar volume from the additional carbonate, chlorine, and water present. Eventually, this mixture would grow to a thickness where it prevents the Cr(VI) from reaching the active corroding metal allowing the corrosion product to blister the nearby passivation and grow unchecked.

The EN layer on steel did not have a measurable effect on corrosion performance which helped to confirm that it was factors other than the underlying substrate that contributed to the performance differences originally observed between the steel and aluminum substrate specimens. This observation helps support the idea that the mechanism of corrosion and corrosion protection for TCP coated specimens is surface focused and depends only upon the passive film and its immediate underlying substrate (γ-ZnNi coating). While the presence of divalent cobalt in the passive films aids corrosion performance through interaction with Cr(VI), the fact that the cobalt-free TCP on the initial steel specimens withstood ASTM B117 salt spray for 1000 hours with minimal corrosion acts as a proof of concept that a superior and conductive cobalt-free TCP could be produced if the relevant physical, chemical, and processing parameters were optimized.

3.2. RECOMMENDATIONS FOR FUTURE WORK

Identifying divalent cobalt and its relation to Cr(VI) as important to corrosion performance of TCPs was important but a few aspects of the system still remain unclear.

Future work should thus focus on experiments that identify these key aspects and determine their effect on corrosion performance to create a model that can predict the time until failure of a TCP based on measurable aspects of the film. A focus on tight control of the processing and optimization of the processing parameters to produce physically and chemically consistent TCPs would help minimize the variability observed in the prior studies. Research questions that could be answered with such well controlled specimens include:

- Can cracks in the passive films be prevented by processing changes? (wetting of surface, temperature, pH, high humidity drying, etc.)
- Can an increase/decrease in γ-ZnNi surface area affect corrosion performance?
- Could other divalent dopants such as Ni(II), Mn(II), or Mg(II) behave similarly to cobalt in TCPs?
- Could corrosion performance be maintained by tetravalent dopants vs. divalent dopants without affecting conductivity?

This research did not focus much on processing changes affecting the deposition of the TCPs even though it is likely that observed cracks are a result of the passivating process. Since localized corrosion was observed in almost all cases of passivation failure, it is expected that a passive layer with no flaws would perform better than one with flaws. This is also why wetting of the chemical deposition bath solution should be investigated since there was inconclusive evidence that the deep cracks and crevices in the γ-ZnNi coating were protected by a passive layer. It is possible that some level of exposed substrate surface is necessary to facilitate reduction of Cr(VI) to Cr(III), or that

Cr(VI) protection correlates with exposed passivation surface area, both of which could be revealed by systematically examining changes to the deposition bath parameters and γ-ZnNi electroplating parameters.

This research did not conclusively identify how the divalent cobalt interacted with the Cr(VI) to improve corrosion performance which could warrant more research of its own but does leave open the possibility that similar effects can be achieved by using other catalytic divalent dopants such as Ni(II), Mn(II), and Mg(II). In a similar vein, the early test specimens had their contact resistance measured which were found to be electrically conductive as required for the intended use as passivations on electrical connectors. The present research did not examine whether the passivation was a p-type or n-type conductor which opens the possibility for tetravalent dopants to replace cobalt, but the corrosion performance impact would have to be measured. Since there is interest in making TCPs without cobalt, searching for alternatives to take the role of cobalt would be a worthwhile endeavor for future experiments.

REFERENCES

1. Bringas JE, editor. Handbook of Comparative World Steel Standards, 5th Edition. 100 Barr Harbor Drive, PO Box C700, West Conshohocken, PA 19428-2959: ASTM International; 2016 https://doi.org/10.1520/DS67D-EB

2. Bringas JE, editor. Carbon and Alloy Steels for General Use. Handbook of Comparative World Steel Standards, 5th Edition. 100 Barr Harbor Drive, PO Box C700, West Conshohocken, PA 19428-2959: ASTM International; 2016:21. https://doi.org/10.1520/DS67D-EB

3. Alloy and Temper Designation Systems for Aluminum and Aluminum Alloys. Properties and Selection: Nonferrous Alloys and Special-Purpose Materials. ASM International; 1990:15–28. https://doi.org/10.31399/asm.hb.v02.a0001058

4. Brenner A, Riddell GE. Nickel plating on steel by chemical reduction. Journal of Research of the National Bureau of Standards. 1946;37:31–34.

5. Schlesinger M, Paunovic M. Electroless Deposition of Nickel. Modern Electroplating. Hoboken, UNITED STATES: John Wiley & Sons, Incorporated; 2014:447–458.

6. Agarwala RC, Agarwala V. Electroless alloy/composite coatings: A review. Sadhana. 2003;28(3):475–493. https://doi.org/10.1007/BF02706445

7. Campbell FC. Metals Fabrication: Understanding the Basics. ASM International; 2013

8. Sriraman KR, Strauss HW, Brahimi S, et al. Tribological behavior of electrodeposited Zn, Zn–Ni, Cd and Cd–Ti coatings on low carbon steel substrates. Tribology International. 2012;56:107–120. https://doi.org/10.1016/j.triboint.2012.06.008

9. American Society for Testing and Materials. ASTMB117-19 Standard Practice for Operating Salt Spray (Fog) Apparatus. 2019.

10. Veeraraghavan B, Kim H, Haran B, Popov B. Comparison of Mechanical, Corrosion, and Hydrogen Permeation Properties of Electroless Ni-Zn-P Alloys with Electrolytic Zn-Ni and Cd Coatings. Corrosion. 2003;59(11).

11. IARC Monographs. Cadmium and Cadmium Compounds. 2011

12. Edwards JR, Prozialeck WC. Cadmium, diabetes and chronic kidney disease. Toxicology and Applied Pharmacology. 2009;238(3):289–293. https://doi.org/10.1016/j.taap.2009.03.007

13. Järup L. Cadmium overload and toxicity. Nephrol Dial Transplant. 2002;17 Suppl 2:35–39. https://doi.org/10.1093/ndt/17.suppl_2.35

14. OSHA. Medical Evaluation of Renal Effects of Cadmium Exposures. 2013

15. EPA. Aquatic Life Ambient Water Quality Criteria - Cadmium 2016. 2016

16. CDC. Lead (Pb) Toxicity: What Are U.S. Standards for Lead Levels? 2021.

17. Directive 2000/53/EC of the European Parliament and of the Council of 18 September 2000 on end-of life vehicles. Queen's Printer of Acts of Parliament; n.d.

18. Palaniappa M, Jayalakshmi M, Balasubramanian K. Effect of Zincation/Sonication on Electroplated Gold Deposited on Aluminum Substrate. J of Materi Eng and Perform. 2011;20(6):1028–1035. https://doi.org/10.1007/s11665-010-9715-0

19. The Tin Plating Process: A Step-By-Step Guide - Sharretts Plating. Sharretts Plating Company. 2015.

20. Metal Plating (Cadmium, Tin, Zinc, Nickel, Silver, Copper, & Others). n.d.

21. Whitlaw K, Egli A, Toben M. Preventing whiskers in electrodeposited tin for semiconductor lead frame applications. Circuit World. 2004;30(2):20–24. https://doi.org/10.1108/03056120410512118

22. 実日野, 賢吾平松, 典秀西田, 実平松, 仁士川崎. 硫酸浴からのZn-Co合金めっきの組成と耐食性. 表面技術. 1992;43(9):873–877. https://doi.org/10.4139/sfj.43.873

23. Mahieu J, De Wit K, De Cooman BC, De Boeck A. The properties of electrodeposited Zn-Co coatings. J of Materi Eng and Perform. 1999;8(5):561–570. https://doi.org/10.1007/s11665-999-0010-x

24. Zinc Electroplating. n.d.

25. Mason R, Neidbalson M, Klingenberg M, Khabra P, Handsy C. Update on alternatives for cadmium coatings on military electrical connectors. Metal Finishing. 2010;108(3):12–20. https://doi.org/10.1016/S0026-0576(10)00012-7

26. Ramanauskas R, Quintana P, Maldonado L, Pomés R, Pech-Canul MA. Corrosion resistance and microstructure of electrodeposited Zn and Zn alloy coatings. Surface and Coatings Technology. 1997;92(1):16–21. https://doi.org/10.1016/S0257-8972(96)03125-8

27. Hu HL, Zhu YM, Tu ZM, Liu WJ. High Anticorrosion Nano Zn-Fe Coatings by Pulse Electrodepositing. Advanced Materials Research. 2011;194–196:2209–2215. https://doi.org/10.4028/www.scientific.net/AMR.194-196.2209

28. Dubent S, Mertens MLAD, Saurat M. Electrodeposition, characterization and corrosion behaviour of tin–20wt.% zinc coatings electroplated from a non-cyanide alkaline bath. Materials Chemistry and Physics. 2010;120(2):371–380. https://doi.org/10.1016/j.matchemphys.2009.11.017

29. Shifler DA, Conrad RK, Sheetz AD. Environmental Evaluation of a Cadmium Replacement Coating for Use in a Marine Environment. NACE International; 2003

30. Rajagopalan SK. Characterization of Electrodeposited Zn-Ni Alloy Coatings As A Replacement For Electrodeposited Zn and Cd Coatings. McGill University; Montreal, Quebec, Canada; 2012

31. Okamoto H. Ni-Zn (nickel-zinc). JPE. 2003;24(3):280–281. https://doi.org/10.1361/105497103770330695

32. Bruet-Hotellaz, Bonino JP, Rousset A, Marolleau, Chauveau E. Structure of zinc–nickel alloy electrodeposits. Journal of Materials Science. 1999;34(4):881–886. https://doi.org/10.1023/A:1004553803788

33. Moonjae K, Du-hwan J, Soo Hyoun C, Hyun Tae K, Jong-Tae P, Jong Myung P. Characterization of the influence of Ni content on the corrosion resistance of electrodeposited Zn–Ni alloy coatings. Surface and Coatings Technology. 2016;288:163–170. https://doi.org/10.1016/j.surfcoat.2016.01.027

34. Tian W, Xie FQ, Wu XQ, Yang ZZ. Study on corrosion resistance of electroplating zinc–nickel alloy coatings. Surface and Interface Analysis. 2009;41(3):251–254. https://doi.org/10.1002/sia.3017

35. Girčienė O, Gudavičiūtė L, Juškėnas R, Ramanauskas R. Corrosion resistance of phosphated Zn–Ni alloy electrodeposits. Surface and Coatings Technology. 2009;203(20):3072–3077. https://doi.org/10.1016/j.surfcoat.2009.03.030

36. Alfantazi AM, Erb U. Corrosion Properties of Pulse-Plated Zinc-Nickel Alloy Coatings. Corrosion. 1996;52(11):880–888. https://doi.org/10.5006/1.3292081

37. Siitari DW, Sagiyama M, Hara T. Corrosion of Ni-Zn electrodeposited alloy. ISIJ Int. 1983;23(11):959–966. https://doi.org/10.2355/isijinternational1966.23.959

38. Müller C, Sarret M, García E. Heat-Treatment on Black-Passivated ZnNi Alloys. Journal of the Electrochemical Society. 2003;150:C212. https://doi.org/10.1149/1.1556036

39. Müller C, Sarret M, García E. Heat treatment effect on the corrosion behaviour of black passivated ZnNi alloys. Corrosion Science. 2005;47(2):307–321. https://doi.org/10.1016/j.corsci.2004.04.004

40. Fratesi R, Roventi G. Corrosion resistance of Zn-Ni alloy coatings in industrial production. Surface and Coatings Technology. 1996;82(1):158–164. https://doi.org/10.1016/0257-8972(95)02668-1

41. Oki M, Oki TK, Charles E. Chromate and Chromate–Phosphate Conversion Coatings on Aluminium. Arab J Sci Eng. 2012;37(1):59–64. https://doi.org/10.1007/s13369-011-0157-2

42. Wilcox GD. Replacing Chromates for the Passivation of Zinc Surfaces. Transactions of the IMF. 2003;81(1):B13–B15. https://doi.org/10.1080/00202967.2003.11871474

43. Ilevbare GO, Scully JR, Yuan J, Kelly RG. Inhibition of Pitting Corrosion on Aluminum Alloy 2024-T3: Effect of Soluble Chromate Additions vs Chromate Conversion Coating. Corrosion. 2000;56(3):227–242. https://doi.org/10.5006/1.3287648

44. Bellezze T, Roventi G, Fratesi R. Electrochemical study on the corrosion resistance of Cr III-based conversion layers on zinc coatings. Surface and Coatings Technology. 2002;155(2):221–230. https://doi.org/10.1016/S0257-8972(02)00047-6

45. Lu G, Ada E, Zangari G. Investigations of the effect of chromate conversion coatings on the corrosion resistance of Ni-based alloys. Electrochimica Acta. 2004;49(9–10):1461–1473. https://doi.org/10.1016/S0013-4686(03)00928-9

46. Zhu W, Li W, Mu S, Fu N, Liao Z. Comparative study on Ti/Zr/V and chromate conversion treated aluminum alloys: Anti-corrosion performance and epoxy coating adhesion properties. Applied Surface Science. 2017;405:157–168. https://doi.org/10.1016/j.apsusc.2017.02.046

47. Kendig MW, Davenport AJ, Isaacs HS. The mechanism of corrosion inhibition by chromate conversion coatings from x-ray absorption near edge spectroscopy (Xanes). Corrosion Science. 1993;34(1):41–49. https://doi.org/10.1016/0010-938X(93)90257-H

48. EPA. Toxicological review of hexavalent chromium. 1998

49. IARC. Chromium (VI) Compounds. Arsenic, Metals, Fibres, and Dusts. Vol. 100C. n.d.

50. Magalhães AAO, Margarit ICP, Mattos OR. Molybdate conversion coatings on zinc surfaces. Journal of Electroanalytical Chemistry. 2004;572(2):433–440. https://doi.org/10.1016/j.jelechem.2004.07.016

51. Cowieson DR, Scholefield AR. Passivation of tin-zinc alloy coated steel. Transactions of the IMF. 1985;63(1):56–58. https://doi.org/10.1080/00202967.1985.11870707

52. Ll L, Bw W, Gm S. Characterization and Performance of a Zr/Ti Pretreatment Conversion Coating on AA2024-T3. J Electrochem Soc. 2015;162(6):C279–C284.

53. Costa JS, Dei Agnoli R, Ferreira JZ. Corrosion behavior of a conversion coating based on zirconium and colorants on galvanized steel by electrodeposition. Comportamento da corrosão de um revestimento de conversão à base de zircônio e corantes no aço zincado por eletrodeposição. 2015.

54. Guo Y, Frankel GS. Active Corrosion Inhibition of AA2024-T3 by Trivalent Chrome Process Treatment. Corrosion. 2012;68(4):045002–1. https://doi.org/10.5006/0010-9312-68-4-3

55. Johnson DM. Zinc and Cadmium Passivating Bath. USPTO 2559878. 1951.

56. Sheu HH, Lee HB, Jian SY, Hsu CY, Lee CY. Investigation on the corrosion resistance of trivalent chromium conversion passivate on electroplated Zn–Ni alloy. Surface and Coatings Technology. 2016;305:241–248. https://doi.org/10.1016/j.surfcoat.2016.08.032

57. Qi J-T, Hashimoto T, Walton JR, Zhou X, Skeldon P, Thompson GE. Trivalent chromium conversion coating formation on aluminium. Surface and Coatings Technology. 2015;280:317–329. https://doi.org/10.1016/j.surfcoat.2015.09.024

58. Gardner A, Scharf J. High Performance Alternative to Hexavalent Chromium Passivation of Plated Zinc and Zinc Alloys. Warrendale, PA: SAE International; 2001 https://doi.org/10.4271/2001-01-0644

59. Boin C. Black passivation films without hexavalent chromium on top of electroplated layers of zinc and zinc alloys. Warrendale, PA: SAE International; 2007 https://doi.org/10.4271/2007-01-2593

60. Hesamedini S, Ecke G, Bund A. Structure and formation of trivalent chromium conversion coatings containing cobalt on zinc plated steel. Journal of the Electrochemical Society: JES. 2018;165, 2018(10):657–669. https://doi.org/10.1149/2.0951810jes

61. Hesamedini S, Bund A. Trivalent chromium conversion coatings. J Coat Technol Res. 2019;16(3):623–641. https://doi.org/10.1007/s11998-019-00210-9

62. Da Fonte J. United States Patent: 4359345 - Trivalent chromium passivate solution and process. 4359345. 1982.

63. Ramezanzadeh B, Attar MM. Effects of Co(II) and Ni(II) on the Surface Morphology and Anticorrosion Performance of the Steel Samples Pretreated by Cr(III) Conversion Coating. Corrosion. 2012;68(1):015008–1. https://doi.org/10.5006/1.3676629

64. Ramezanzadeh B, Attar MM, Farzam M. Corrosion performance of a hot-dip galvanized steel treated by different kinds of conversion coatings. Surface and Coatings Technology. 2010;205(3):874–884. https://doi.org/10.1016/j.surfcoat.2010.08.028

65. Cho K, Shankar Rao V, Kwon H. Microstructure and electrochemical characterization of trivalent chromium based conversion coating on zinc. Electrochimica Acta. 2007;52(13):4449–4456. https://doi.org/10.1016/j.electacta.2006.12.032

66. Preikschat P, DE, Jansen R, DE, Hulser P, DE. United States Patent: 6287704 - Chromate-free conversion layer and process for producing the same. 6287704. 2001.

67. Formation of Trivalent Chromium Passivation Layers. n.d.

68. Iyer A, Willis W, Frueh S, et al. Characterization of NAVAIR Trivalent Chromium Process (TCP) coatings and solutions. Plating and Surface Finishing. 2010;97(4):32–41.

69. Matzdorf C, Kane M, Green J. United States Patent: 6375726 - Corrosion resistant coatings for aluminum and aluminum alloys. 6375726. 2002.

70. Kawaguchi H, Funatsumaru O, Sugawara H, et al. Development of Trivalent Chromium Passivation for Zn Platng with High Corrosion Resistance after Heating. SAE International Journal of Materials and Manufacturing. 2016;9(3):833–838.

71. Tomachuk CR, Elsner CI, Di Sarli AR, Ferraz OB. Morphology and Corrosion Resistance of Cr(III)-based conversion treatments for electrogalvanized steel. Journal of Coatings Technology and Research. 2010;7, no. 4. https://doi.org/10.1007/s11998-009-9213-1

72. Bhatt H. Trivalent Chromium Conversion Coating for Corrosion Protection of Aluminum Surface. 2009:1–12.

73. Zaki N. Trivalent chrome conversion coating for zinc and zinc alloys. Metal Finishing. 2007;105(10):425–435. https://doi.org/10.1016/S0026-0576(07)80361-8

74. L G, A.s F, M.g I, et al. Corrosion resistance of Cr (III) based conversion layer on zinc coatings in comparison with a traditional Cr (VI) based passivation treatment. 2006.

75. Wen N-T, Lin C-S, Bai C-Y, Ger M-D. Structures and characteristics of Cr(III)-based conversion coatings on electrogalvanized steels. Surface and Coatings Technology. 2008;203(3–4):317–323. https://doi.org/10.1016/j.surfcoat.2008.09.006

76. Berger R, Bexell U, Mikael Grehk T, Hörnström S-E. A comparative study of the corrosion protective properties of chromium and chromium free passivation methods. Surface and Coatings Technology. 2007;202(2):391–397. https://doi.org/10.1016/j.surfcoat.2007.06.001

77. Di Sarli AR, Culcasi JD, Tomachuk CR, Elsner CI, Ferreira-Jr JM, Costa I. A conversion layer based on trivalent chromium and cobalt for the corrosion protection of electrogalvanized steel. Surface and Coatings Technology. 2014;258:426–436. https://doi.org/10.1016/j.surfcoat.2014.08.057

78. Li L, Swain GM. Effects of Aging Temperature and Time on the Corrosion Protection Provided by Trivalent Chromium Process Coatings on AA2024-T3. ACS Appl Mater Interfaces. 2013;5(16):7923–7930. https://doi.org/10.1021/am4020023

79. Hesamedini S, Bund A. Formation of Cr(VI) in cobalt containing Cr(III)-based treatment solution. Surface and Coatings Technology. 2018;334:444–449. https://doi.org/10.1016/j.surfcoat.2017.12.006

80. McCafferty E. Getting Started on the Basics. Introduction to Corrosion Science. New York: Springer-Verlag; 2010:13–21. https://doi.org/10.1007/978-1-4419-0455-3

81. McCafferty E. Getting Started on the Basics. Introduction to Corrosion Science. New York: Springer-Verlag; 2010:25–27. https://doi.org/10.1007/978-1-4419-0455-3

82. McCafferty E. Thermodynamics of Corrosion: Electrochemical Cells and Galvanic Corrosion. Introduction to Corrosion Science. New York: Springer-Verlag; 2010:73–89. https://doi.org/10.1007/978-1-4419-0455-3

83. LaQue FL. Chapter 6. Marine corrosion: causes and prevention. New York: Wiley; 1975

84. Popov B. Chapter 5. Corrosion Engineering. Elsevier; 2015:166–169. https://doi.org/10.1016/C2012-0-03070-0

85. Qi J, Zhang B, Wang Z, Li Y, Skeldon P, Thompson GE. Effect of an Fe(II)-modified trivalent chromium conversion process on Cr(VI) formation during coating of AA 2024 alloy. Electrochemistry Communications. 2018;92:1–4. https://doi.org/10.1016/j.elecom.2018.05.013

86. Tomachuk CR, Elsner CI, Di Sarli AR. Electrochemical characterization of chromate free conversion coatings on electrogalvanized steel. Mat Res. 2013;17(1):61–68. https://doi.org/10.1590/S1516-14392013005000179

87. Qi J, Thompson GE. Comparative studies of thin film growth on aluminium by AFM, TEM and GDOES characterization. Applied Surface Science. 2016;377:109–120. https://doi.org/10.1016/j.apsusc.2016.03.115

88. Qi J, Hashimoto T, Walton J, Zhou X, Skeldon P, Thompson GE. Formation of a Trivalent Chromium Conversion Coating on AA2024-T351 Alloy. J Electrochem Soc. 2016;163(2):C25–C35. https://doi.org/10.1149/2.0771602jes

89. Qi J, Hashimoto T, Thompson GE, Carr J. Influence of Water Immersion Post-Treatment Parameters on Trivalent Chromium Conversion Coatings Formed on AA2024-T351 Alloy. J Electrochem Soc. 2016;163(5):C131–C138. https://doi.org/10.1149/2.0221605jes

90. Dardona S, Jaworowski M. In situ spectroscopic ellipsometry studies of trivalent chromium coating on aluminum. Appl Phys Lett. 2010;97(18):181908. https://doi.org/10.1063/1.3511472

91. Li L, Swain GP, Howell A, Woodbury D, Swain GM. The Formation, Structure, Electrochemical Properties and Stability of Trivalent Chrome Process (TCP) Coatings on AA2024. J Electrochem Soc. 2011;158(9):C274. https://doi.org/10.1149/1.3607980

92. Munson CA, Swain GM. Structure and chemical composition of different variants of a commercial trivalent chromium process (TCP) coating on aluminum alloy 7075-T6. Surface and Coatings Technology. 2017;315:150–162. https://doi.org/10.1016/j.surfcoat.2017.02.018

93. Wiryawan A, Retnowati R, Burhan RYP, Syekhfani. Method of Analysis for Determination of The Chromium (Cr) Species in Water Samples by Spectrophotometry with Diphenylcarbazide. Journal of Environmental Engineering & Sustainable Technology. 2018;5(1):37–46.

94. Marczenko Z, Balcerzak M. Chromium. Analytical Spectroscopy Library. Vol. 10. Elsevier; 2000:159–166. https://doi.org/10.1016/S0926-4345(00)80081-4

95. Popov B. Chapter 5. Corrosion Engineering. Elsevier; 2015:201–202. https://doi.org/10.1016/C2012-0-03070-0

96. Popov B. Chapter 5. Corrosion Engineering. Elsevier; 2015:207–213. https://doi.org/10.1016/C2012-0-03070-0

97. Esmailzadeh S, Aliofkhazraei M, Sarlak H. Interpretation of Cyclic Potentiodynamic Polarization Test Results for Study of Corrosion Behavior of Metals: A Review. Prot Met Phys Chem Surf. 2018;54(5):976–989. https://doi.org/10.1134/S207020511805026X

98. The Kramers-Kronig Relations. Electrochemical Impedance Spectroscopy. John Wiley & Sons, Ltd; 2008:427–445. https://doi.org/10.1002/9780470381588.ch22

VITA

Kevin Lee Foster was born in Springfield, Missouri to James and Karen Foster. Kevin graduated from Nixa High School in 2008, qualifying for state competition in math team three times and placing 4th in the state competition on cybersecurity for the Future Business Leaders of America. He went to Missouri State University to achieve a Bachelor of Science degree in Psychology with a minor in biomedical science in 2013. After a change in career paths he went back to college at the Missouri University of Science and Technology to pursue a Bachelor of Science degree in ceramic engineering, obtained in 2017. An opportunity presented itself and so Kevin then pursued a Doctor of Philosophy degree in metallurgical engineering at the Missouri University of Science and Technology, which was awarded in May 2022.